Master of Science Thesis

Preliminary design of a recuperator for a gas turbine range extender application

Juan Regueiro Cueva
2018

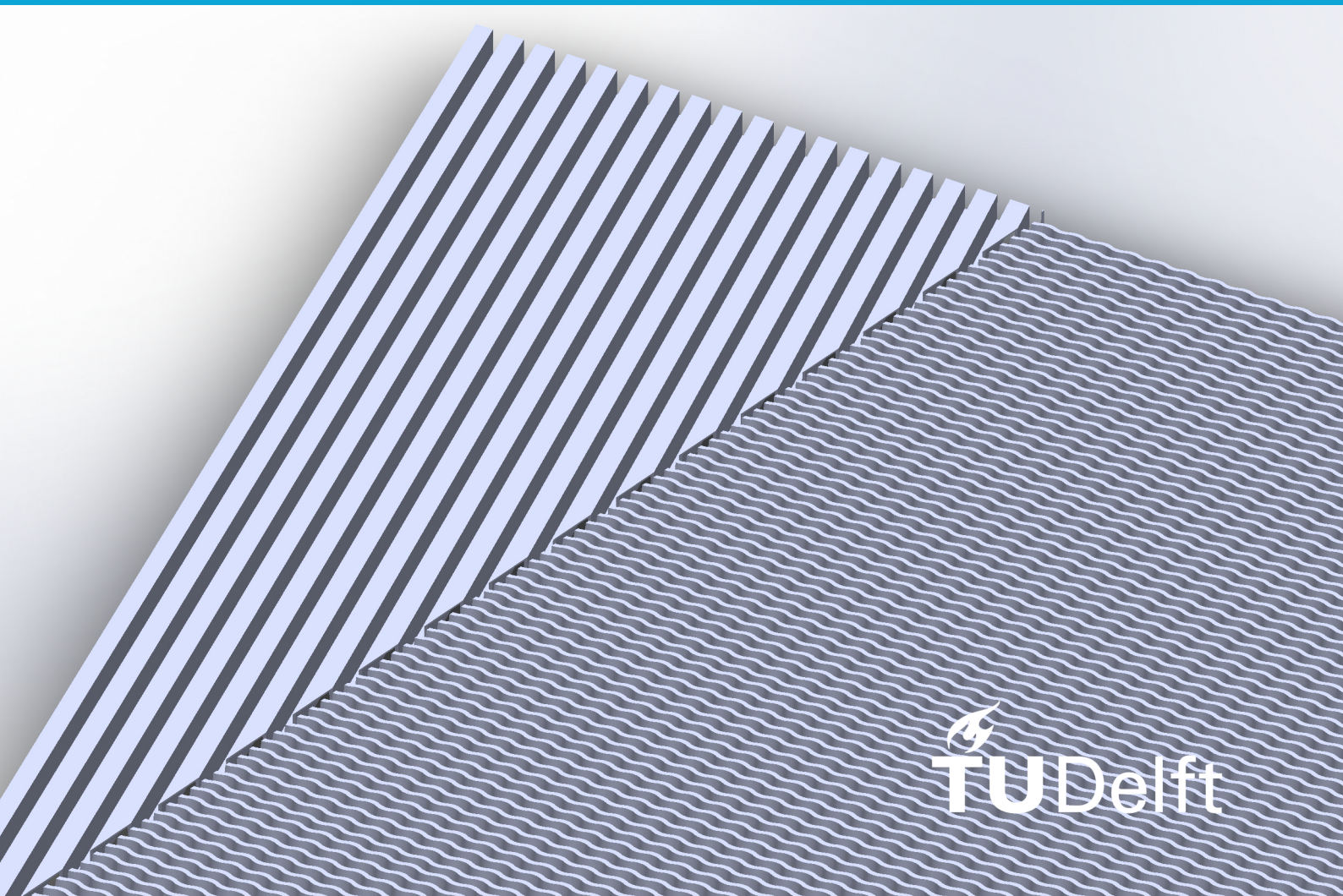

Preliminary design of a recuperator for a gas turbine range extender application

by

Juan Regueiro Cueva

to obtain the degree of Master of Science in Aerospace Engineering

at the Delft University of Technology,

to be defended publicly on Wednesday May 23, 2018 at 10:00 AM.

Student number:	4517849	
Thesis committee:	Prof. dr. ir. P. Colonna, chair	TU Delft
	Dr. ir. C. de Servi,	VITO
	Dr. ir. M. Pini,	TU Delft
	Dr. ir. F. Schrijer,	TU Delft
	Ir. R. Lammers,	Mitsubishi Turbocharger and Engine Europe

Front image shows a CAD render of a unitary plate for an annular recuperator employing cross-wavy primary surfaces.

TU Delft

Acknowledgments

As a preface to this report, I would like to acknowledge all the people that had an impact in my time at TU Delft. These years have been incredibly exciting, and I feel very grateful to have had the opportunity of accomplishing something that will have a huge impact in the rest of my life. Not only the academic aspect of this adventure has been important, but also the personal since it involved enormous changes in my life.

First I want to thank everyone that contributed to my thesis project. Dr. Carlo de Servi and Prof. Matteo Pini, my supervisors at TU Delft, have allowed me to do research in a project that was challenging. Their insight and critical feedback was invaluable throughout the last months. I would also like to thank Prof. Piero Colonna and Prof. Ferdinand Schrijer for taking the time to evaluate my work and being part of my graduation committee.

The R&D team at MTEE was the reason I am involved in this project to begin with, and I am greatly indebeted to all their support throughout my internship and thesis project. First, I want to thank Rogier Lammers for being my supervisor for the project within the company. Your insight allowed me to keep myself focused on the implications of my work within the team, allowing me to push through the most challenging periods of this thesis. Thanks to Patrick, Jaco, Rogier and Jochem who I have worked with side by side for the last months. Mark, who allowed me to tackle in this opportunity in the first place. Nikolas and Antonio for all the conversations during stressful times. The whole team has made my time at the company a very pleasant experience.

I also want to thank my friends at the university. Ioannis worked with me in some of the most stressful times during the masters. Cristina helped not to miss home so often. Sagarika, Hugo, Bruno and Jonathan throughout all those long study nights.

My family back home made all of this possible. My mother is the main reason I have had all these opportunities in life, and I am fortunate to have someone so supporting in my life. My brothers Tomás and Ander have helped me to stay motivated.

Finally I want to thank Laura, who has been with me through all of this journey. She has always been my greatest supporter and I would not be here without all of her encouragement. I owe her most of what I have accomplished in this period.

Summary

Range extended electric vehicles (REEV) are being considered as a possible solution for the electrification of passenger vehicles. The REEV concept allows to tackle challenging aspects of electric vehicle adoption such as cost and range anxiety, through the use of a prime mover which allows the implementation of smaller battery packs while still achieving increased operational range. The application of a recuperated gas turbine (GT) for REEVs shows potential in terms of power-to-weight ratio, emissions and cost. In order for the GT to achieve efficiency levels that are competitive with other prime movers, the use of a recuperated cycle becomes mandatory. Out of all the components in the recuperated GT, the recuperator plays a major role in achieving target efficiency,while being a main contributor to cost and packaging. The topology and subsequent design are key factors for the success of the concept.

First, a topology is selected based on literature research of different recuperator concepts for small gas turbines. A large number of recuperator concepts was reviewed, highlighting key features that contribute to reduction of cost and packaging while maintaining performance targets. Flow configuration, heat transfer surface type as well as material selection are some of the aspects discussed within the review of previous small gas turbine recuperators. The topology selection becomes the basis in which the models for heat exchanger design are built.

Afterwards, the development and validation of the HEX sizing model, which obtains recuperator geometry from a given set of boundary conditions and performance targets, is reviewed. A rating model was used as a basis for the development of the sizing model. Such a model uses defined HEX geometry and boundary conditions to obtain thermal duty and pressure losses. The sizing model is developed by implementing a constrained optimization routine around the rating model. The design variables are the parameters that define the HEX geometry, while the objective function to minimize is recuperator volume. A number of constraint are applied to limit the design space to concepts that are compatible with the application. Both models are validated using published experimental data from a gas turbine manufacturer. A parametric analysis using gas turbine cycle design parameters is performed, with the objective of analyzing their impact on the resulting heat exchanger geometry. The influence of heat transfer surface selection is also analyzed, by employing different experimental predictions for heat transfer and hydraulic performance. The parametric analysis shows that the heat exchanger geometry can be improved by means of cycle design parameters.

Finally, a numerical investigation of one of the experimental correlations is performed. This is done to increase confidence on the conclusions drawn from the parametric analysis as well as providing a basis for future CFD optimization of heat transfer surfaces.

Contents

List of acronyms

HEX Heat exchanger. 4, 7, 9, 15, 16, 19, 23, 25, 27, 28, 36, 39, 45, 55, 58, 60, 63

LP low pressure. 8, 9, 10, 13, 25, 35, 36, 51, 57

HP high pressure. 8, 9, 10, 13, 15, 25, 35, 36, 51, 57

GT gas turbine. 7, 10, 15, 16, 23, 39, 57, 58, 71, 77, 78

OEM Original equipment manufacturer. 1

EV electric vehicle. 1

BEV battery electric vehicle. 1

HEV hybrid electric vehicle. 77

REEV range extended electric vehicle. 1, 2, 3

PHEV plug-in hybrid electric vehicle. 1

DOE Department of Energy. 10, 25, 43, 81

CC Cross corrugated. 8, 12, 13, 20, 21, 22, 33, 51, 54, 55, 69

CU Cross undulated. 8, 22

CW Cross wavy. 8, 9, 10, 21, 22, 33, 43, 54, 55, 69

GTRE Gas Turbine Range Extender. 2, 3, 18, 78

LES Large Eddy Simulation. 20

NTU Number of exchanger heat transfer units. 28

RSAB Rekuperator Svenska AB. 12, 13

TIT turbine inlet temperature. 4, 51, 57, 60, 64, 70

TET turbine exhaust temperature. 23

PR pressure ratio. 4, 51

Nomenclature

Symbols

A_{inv}	Arc length of involute curve	m
η_c	Compressor efficiency	–
x_i	Design vector for optimization scheme	–
τ_w	Equivalent fluid shear stress at wall	Pa
f	Fanning friciton factor	–
η_o	Fin efficiency	–
G	Fluid mass velocity	kg/m^2
A_o	Free flow area	m^2
C	Heat capacity	W/K
h	Heat transfer coefficient	W/m^2K
c	Height of recuperator counterflow section	m
r_h	Hydraulic radius	m
a	Inlet length of recuperator crossflow section	m
r	Inner circle radius for involute calculation	m
L	Length of flow passage	m
b	Length of recuperator counterflow section	m
q	Local heat transfer rate	W/m^2
$\dot{m}$	Mass flow	kg/s
u	Mean flow velocity	m/s
NTU	Number of heat transfer units	–
$g_i(x)$	Optimization constraint functions	–
U	Overall heat transfer coefficient	W/m^2
V_{HEX}	Overall recuperator volume	m^3
P_{out}	Power output	kW
p	Pressure	Pa
Δp	Pressure loss	Pa
$\overline{\Delta p}$	Relative pressure loss	–
PR	Pressure ratio	–

c_p	Specific heat capacity	$J/kg\dot{K}$
η	System efficiency for gas turbine	–
T	Temperature	K
P	Temperature effectiveness	–
k_w	Thermal conductivity	$W/m\dot{K}$
A	Total heat transfer area	m^2
η_t	Turbine efficiency	–
δ_w	Wall or primary surface thickness	m
$\boldsymbol{P}$	Wetted perimeter of exchanger passages	m
x	X coordinate for involute calculation	m
y	Y coordinate for involute calculation	m
ΔT_{max}	Inlet temperature difference (ITD)	K

Subscripts

o	Outlet, outer	–
c	Cold stream	–
h	Hot stream	–
i	Inlet, flow station indicator, inner	–
m	Mean flow velocity	–

List of Figures

List of Tables

1 Introduction

1.1. Background and Motivation

Electric passenger vehicles have received increasing attention in recent years, slowly becoming a viable option for the average consumer. Several factors have contributed to the current level of adoption of electric vehicles (EVs). Efforts in the last decade to overcome some of the initial challenges of EVs such as high costs, low performance and short ranges. Thanks to air quality and climate change concerns, governments throughout the world have been promoting EV use. Common strategies are enforcing stricter legislation regarding vehicle emissions, tax subsidies for electric vehicles to reduce initial user cost and investment in infrastructure such as charging stations. Even though there is a larger number of EVs in the road operating today in comparison to 20 years ago, their numbers are still quite low compared to conventional vehicles. In 2017, the International Energy Agency [26] reported that the market share of battery electric vehicles (BEVs) and plug-in hybrid electric vehicles (PHEVs) in OECD countries was only 1.10%. Technology developments are still required in order to increase electric vehicle adoption to significant levels.

One of the main challenges for EVs adoption is the range of BEVs. Even though there has been significant improvements in battery technology in recent years, BEV performance has not yet matched conventional combustion vehicles in certain aspects [27], not meeting the expectations of certain users. The reduced range pf BEV may cause a negative effect on the adoption rate of potential adopters of fully electric powertrain technology.

Nowadays, a variety of electric powertrain concepts are being commercialized. These range from fully electric vehicles (or BEVs) to hybrid solutions, such as PHEVs and range extended electric vehicles (REEVs), which are an adaptation of the former concept. Figure 1.1 shows an overview of the different powertrain technologies that are currently available in the market. Hybrid cars are an attractive solution since they are able to reduce tailpipe emissions and increase driving range avoiding the high costs associated with high capacity batteries. The different configurations influence the required battery pack size as well as the capabilities and power output (see Figure 1.1) of the prime mover on board of the vehicle. As far as the battery pack is concerned, the BEV needs the largest unit (i.e. the most expensive) since it is the only energy source. The REEV follows, and finally the plug-in hybrid. Considering hybrid powertrain configurations, the PHEV needs a prime mover fully capable of powering the vehicle by itself, while the REEV is not required to fulfill peak power demands.

REEVs are gaining attention of automotive Original equipment manufacturers (OEMs) due to their strong advantages to other electric vehicle concepts. As mentioned before, a REEV is any plug in electric vehicle with an additional prime mover to use only when the state of charge of the main battery is approaching complete discharge. The power generated by the prime mover is used to recharge the main battery, not to drive the transmission of the vehicle. This is key difference between PHEVs/BEVs and REEVs. Such a solution, allows to mitigate customer concerns for a limited driving range of EVs while reducing the cost thanks to the smaller

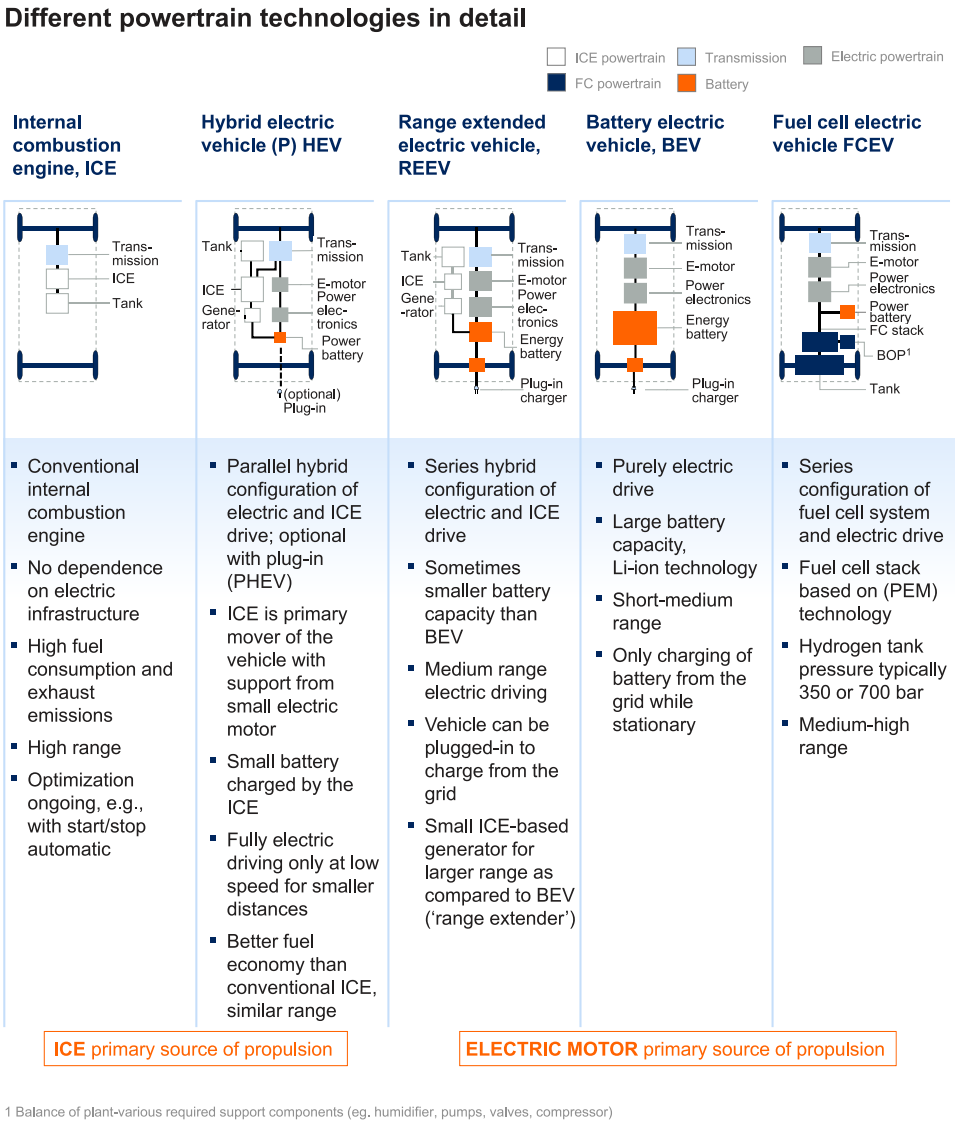

Figure 1.1: Overview of current powertrain technologies [1]

battery capacity.

For the successful implementation of a REEV concept, its prime mover needs to meet stringent requirements on cost, packaging, weight, noise, reliability and low-emissions. In principle, there are no limitations on the type of prime mover that can be adopted, as long as it is able to deliver the required power output on board of the vehicle. A large number of concepts have been investigated, each one having its own strengths and weaknesses in regards to the system requirements. Figure 1.2 shows a comparison of the four most important prime movers considered for REEV applications according to the analysis published by Coffman [2].

Micro gas turbines (usually rated in the range of 20 to 100 kW [28]) are an attractive solution for range extenders due to their high power-to-weight ratio, reliability and low emission potential. In comparison to an internal combustion engine, the reduced number of moving parts promotes lower maintenance costs [29, 30]. Moreover, a well designed pre-mixed combustor has the potential of avoiding an exhaust gas aftertreatment system. The challenges of this technology lies in achieving an efficiency level similar to that of other prime mover options (i.e. 30% [31]) are not achievable in a single-stage simple cycle Brayton cycle. For these reasons, the use of a recuperated cycle is mandatory for micro gas turbine in a range extender application.

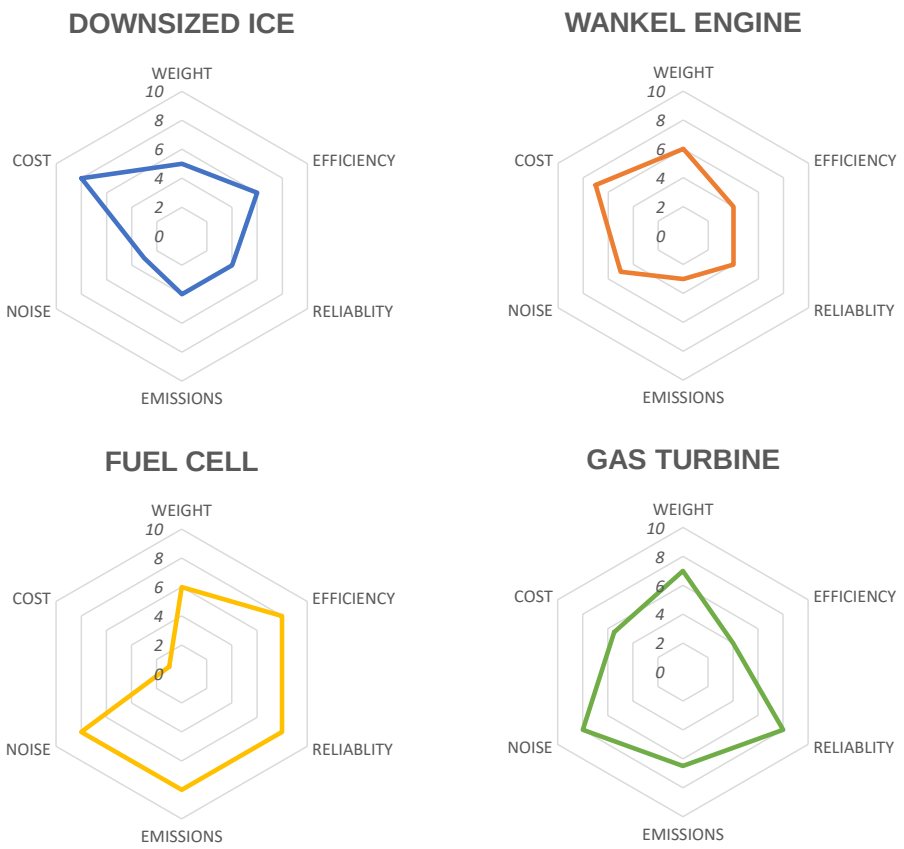

Figure 1.2: Prime mover comparison [2]

Due to their strong background in radial turbomachinery and business network in the automotive industry, MTEE has an advantageous position for developing a Gas Turbine Range Extender (GTRE). The strengths of the REEV against other electric vehicle concepts under the current emission legislation outlook, and the advantages of the micro gas turbine as a prime mover for this concepts, motivated MTEE to pursue the concept. Research efforts have identified the recuperator for the gas turbine as one of the crucial components for a successful system development.

Designing a recuperator for a GTRE poses a set of particular challenges that are not usually addressed in the design of gas turbines used for stationary power applications. REEVs do not rely on a continuous operation of the engine to charge batteries. This shifts focus from a durable, high efficiency power generator to that of a compact, low cost unit compatible with the automotive market. Still, efficiency and durability need to reach the minimum required levels in order to maintain a competitive edge against other prime movers as well as complying with emissions legislation. These aspects make the design of a gas turbine recuperator for a REEV even more complex than for stationary applications. It needs to be approached in a integral fashion taking simultaneously into consideration the impact of the recuperator characteristics on the system performance, and the constraints of the automotive environment.

1.2. Research Objectives

The objective of the research project is to assess the feasibility of a lightweight low-cost metallic recuperator for a gas turbine range extender application. The recuperator characteristics that have the largest impact on its feasibility are volume, weight and cost. While reliable measures for the first two parameters are obtained directly from a preliminary design, cost is discussed in a qualitative manner. Valuable insight towards factors affecting cost can be obtained from the characteristics of the resulting recuperator design.

The influence of different cycle design parameters on the resulting recuperator design is also investigated. Power output and system efficiency targets are fixed for the current application. The required recuperator effectiveness and mass flow are treated as dependent from the rest of the cycle parameter selections. The influence of this parameters on the feasibility of the recuperator geometry for the application is also highlighted. Changes in cycle design parameters may lead to a smaller, lighter and cheaper recuperator. Furthermore, a group of different heat transfer surface geometries were used in the analysis to understand the implications of their development and selection.

The reliability of the conclusions drawn from the research project depend on the quality of the analysis tools used. In order to increase confidence on the preliminary design, an investigation on the heat transfer surface fluid-dynamic performance using numerical simulations is also done. The goal is to provide the basis for further design optimization focused on heat transfer surface geometry.

1.2.1. Research Questions

1. Which are heat exchanger topologies suitable for the recuperator?

    - The selection of the heat exchanger topology is the first step in the development of the recuperator, which has to exhibit effectiveness, low weight as well as reliability. Since large production quantities are also required, the recuperator configuration needs to be compatible with proven manufacturing processes that can be highly automatized, an important feature for cost reduction.

2. What is the required size of the recuperator for a 30kW range extender with an efficiency of 30%?

    - The preliminary design of the recuperator will be carried out following the conventional procedure for heat exchangers. The aspects which have the largest impact on the recuperator size are expected to be the targeted power output and system efficiency as well as the Heat exchanger (HEX) topology.

3. What is the impact of gas turbine cycle parameters on the recuperator geometry?

    - In a second step, the effect of different gas turbine cycle parameters (i.e. pressure ratio (PR), turbine inlet temperature (TIT), turbomachinery efficiencies, etc.) on the recuperator will be investigated. Since the heat exchanger is one of the main contributors to the size, weight and cost of the unit, the boundary conditions of the recuperator can be altered in order improve these figures of merit, while maintaining system efficiency and power output. The insight obtained from the parametric analysis can be used to steer the gas turbine design to achieve an improved recuperator design.

4. Are the correlations used in the heat exchanger sizing reliable?

    - The preliminary design will be performed on the basis of performance correlations available in the open literature. In order to increase confidence on the reliability of the results, numerical simulations will be carried . These simulations will also represent a starting point for future work targeting a CFD based optimization of the recuperator surfaces.

1.3. Outline

Chapter 2 provides a survey on state-of-the-art recuperator technology for small gas turbines. Notably, different concepts are presented, highlighting their strengths and weaknesses in relation to the requirements of the application at hand. This chapter also describes current research developments for heat transfer surface optimization for gas-to-gas heat exchangers. Chapter 3 covers the development and the theoretical basis behind recuperator model, while Chapter 4 focuses on the validation of the same model against published data. Chapter 5 shows the influence of the different cycle parameters on the recuperator size. Chapter 6 discusses the numerical analysis of the heat transfer and pressure loss correlations used in the report. Chapter 7 provides conclusions, recommendations and suggestions for future work on this topic.

2

Literature Review

In this chapter, a review of relevant literature for the objective of this thesis project is shown. Section 2.1 covers a range of recuperator topologies and features for small gas turbines. Section 2.2 addresses the importance of different heat transfer surface geometries. Finally, Section 2.3 covers the topic of material selection for heat exchanger cores.

2.1. Small gas turbine recuperators

Recuperated Brayton cycle configurations are specially suited for small gas turbines (GTs), since they commonly adopt single-stage radial turbomachinery, limiting the pressure ratio of the system. High exhaust temperatures allow for effective heat recovery between the compressor and turbine, leading to a lower fuel consumption for a given turbine inlet temperature. Initial research on recuperators for small gas turbines can be traced back to military applications developed in the 1970's and 1980's. Previous concerns on structural integrity and leakages, which precluded their use in series production, were solved thanks to the intense research in the field [32]. Another industrial sector pursuing the development of recuperated small-scale GT was the automotive sector. Rotary matrix regenerators were the most common solution for these type of units [33]. However the development of automotive gas turbines was soon abandoned mainly to the challenges posed by poorer dynamic behavior in comparison to internal combustion engines. Leakage and cracking of the rotary ceramic matrix also played a role in this fact [34]

Recently, small recuperated gas turbines have gained relevance once more thanks to the increased interest on distributed power generation [28]. In order for small gas turbines to be competitive in the power generation market, efficiency levels above 35% need to be achieved since their main competitor at the low power output range are reciprocating diesel gensets [35]. Therefore a recuperated cycle becomes necessary, and the amount of recuperated gas turbines available nowadays in the market makes that clear. Companies such as Capstone and Ingersoll-Rand have been building small recuperated gas turbines since the mid 90's, showing a good operational record. [36].

Recuperators adopted in small gas turbines can be classified in three main categories, depending on their topology: plate-fin, primary surface and tubular heat exchangers. The latter is the concept with the longest operational history, being used from the first recuperated closed-cycle gas turbines [37]. Tubular heat exchangers show good structural properties, but are larger and heavier compared to other heat exchanger configurations. Plate-fin exchangers represented a step forward into achieving more compact units. they were originally developed in the automotive industry for applications such as radiators and oil coolers [18]. Although more compact, their structural integrity is lower than that of tubular heat exchangers mainly due to brazed joints for interface between fins and plate surfaces. Primary surface recuperators are lighter and more compact than plate-fin cHEXs thanks to the use of a single surface between hot and cold fluids, while their disadvantages are lower mechanical integrity and complex manufacturing procedures.

2.1.1. Primary surface recuperators

Primary surface recuperators are nowadays the most common compact heat exchanger architecture for small GTs due to several reasons. First, primary surface constructions preclude the effective heat transfer reduction attributed to fin efficiency. Second, weight is reduced because no brazing material is required between fins and plates. Moreover, heat transfer and pressure loss have been improved by optimizing the geometry of plates.

Three primary surface geometries are the most common in gas turbine recuperators. These geometries are referred as Cross corrugated (CC), Cross undulated (CU) and Cross wavy (CW). CC surfaces, also known as chevron plates, are built by stacking corrugated plates on top of each other. The plate corrugation usually follows a sinusoidal pattern and have a specific amplitude as well as specific spacing. These corrugated plates are stacked on top of each other at different phase angles, promoting flow mixing and increasing heat transfer. Figure 2.1a shows a diagram of a CC surface with its main geometric parameters (amplitude, spacing, phase angle) highlighted. CU surfaces differ from CC surfaces in the fact that the stacked plates do not have the same geometric pattern(see Figure 2.1b). CW surfaces use plates which exhibit a periodic pattern also in the main flow direction. They are then stacked on top of each other with a 180 degree phase shift as shown in Figure 2.1c.

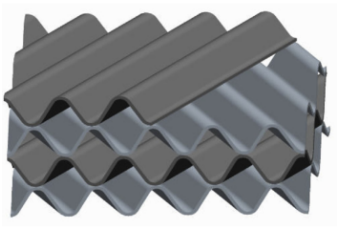

(a) Cross-corrugated surface

(b) Cross-undulated surface

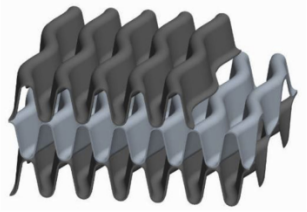

(c) Cross-wavy surface

Figure 2.1: Common primary surface geometries [3]

The recuperator built by Textron Lycoming for the AGT1500 was one of the first successful attempts in developing a reliable primary surface heat exchanger for gas turbines at high production volumes. The AGT 1500 is a 1120 kW recuperated gas turbine that powers several variants of the M1 Abrams tanks. The heat exchanger, described by Kadmabi [4], consists of a series of annular plates that are welded together in order to make a single unit. As it can be seen in the Figure 2.2, the core of plates also serve as the headers for the flow of low pressure (LP) and high pressure (HP) streams. The plates use a CW geometry, which improves heat transfer performance in primary surface heat exchangers. The flow arrangement between the two fluids is of the cross-counterflow type, with crossflow at the distributors, and a counterflow middle section (seen in Figure 2.2). The HP stream enters the heat exchanger through the triangular ducts, and exits through the oval ducts shown in Figure 2.2. The LP stream flows in a radial direction, from the inner duct towards the outer diameter of the recuperator.

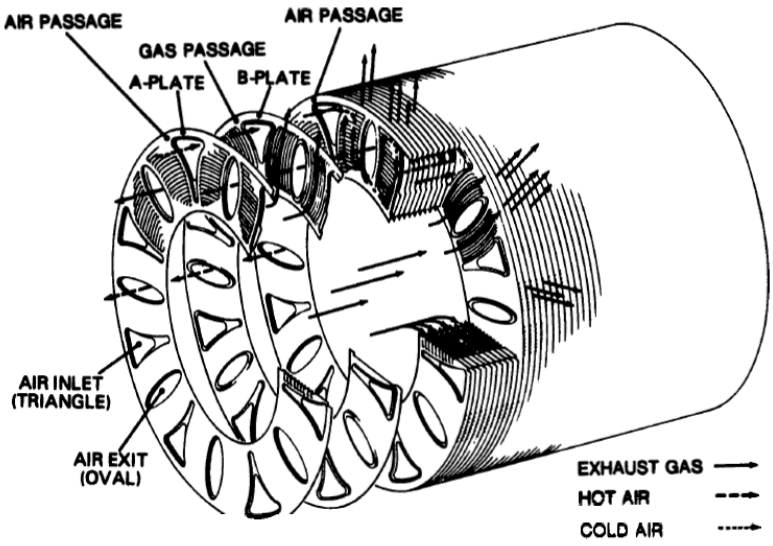

Figure 2.2: Textron Lycoming recuperator core and flow paths [4]

The reported effectiveness of the recuperator is 78% and 80% at full load and part-load respectively [38]. Pressure losses at full power are reported as 0.8% and 7% for HP and LP sides, respectively. The recuperator core is built out of Inconel 625 sheets, and the resulting weight is 195 kg. The unit has a heat transfer surface area of 84 m^2 and a volume of 0.14 m^3.

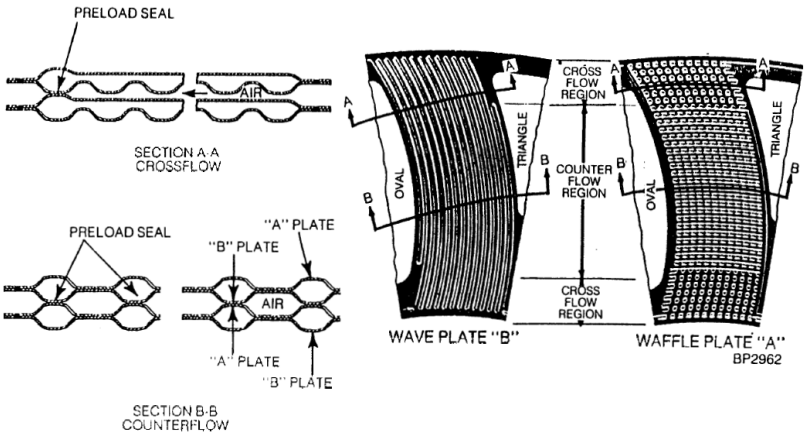

Figure 2.3: Flow arrangement of Textron Lycoming core [4]

Individual plates are manufactured by a stamping process to form the corrugations, followed by the punching of the HP stream passages. The plates are then stacked and welded along the inner and outer diameters. The last welding step is crucial, since these joints are subject to thermal stresses.

The first designs of primary surface recuperators by Solar Turbines are reported by Parsons [5]. the development of primary surface heat exchangers allowed Solar Turbines to retrofit previous recuperated gas turbines Saturn and Centaur, which adopted tubular exchangers, with a more compact HEX. The flow schematic of this concept can be seen in Figure 2.4. The HP stream enters through two separate headers, into the crossflow distributors, continues through the counterflow middle section, and then exits through another crossflow distributor to a single manifold which is connected to the combustor. The primary surface counterflow section is comprised of a CW pattern. According to the research done by the Solar Turbines under a research contract awarded by the US Navy, primary surface recuperators are superior in several aspects compared to other exchanger topologies like plate-fin and tubular. For the same application, the report states that a primary surface recuperator has a 24% lower weight and 65% lower volume than a plate-fin concept. Fur-

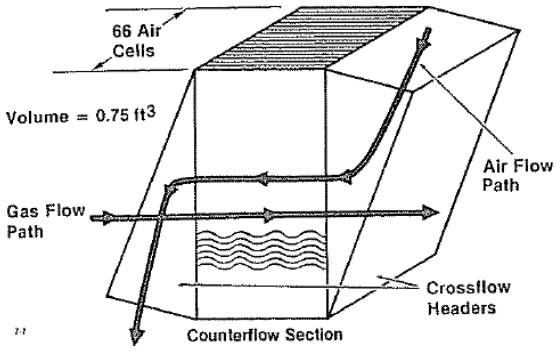

Figure 2.4: Flow schematic for standard Solar Turbine recuperator [5]

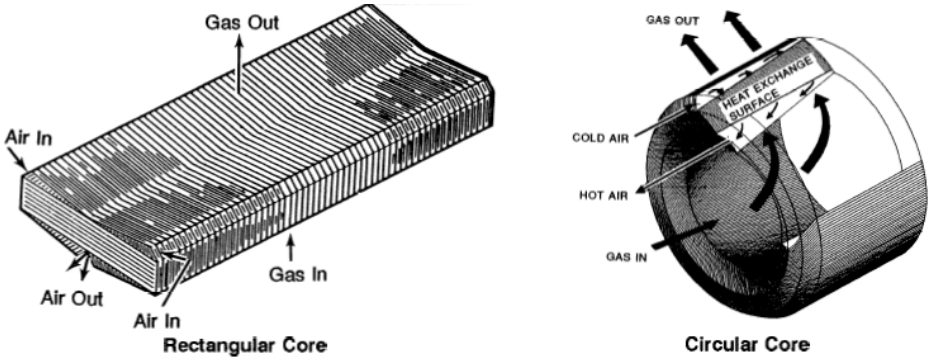

Figure 2.5: Rectangular and annular configurations of Solar Turbine recuperator [6]

thermore, according to the same report, the unit price of a plate-fin unit is 4.4 times higher. [6].

The reported effectiveness of this recuperator concept is 93% for the 950 kW Saturn and 94% for the 2700 kW Centaur. Both units have a low pressure losses, around 1% and 3%, for HP and LP sides respectively. The recuperator cores are built of stainless steel, which would suggest that their lower LP temperatures than the original AGT1500, which used Inconel 625. Another feature of this concept is the flexibility in the flow arrangement using the same core geometry. For Solar turbines, the recuperator is built in a rectangular shape, and then mounted on top of the turbomachinery. The same core geometry was rearranged for the AGT 1500, which required an annular arrangement. Shorter cores were arranged in a ring, and the manifolding was modified in order to match the layout. Both configurations can be seen in Figure 2.5.

Manufacturing is similar to other primary surface recuperators. According to the aforementioned report, the welding process is highly automated to achieve high volume production. The recuperator design reduces thermal stresses by carefully selecting weld locations. It is also claimed that installed units in the AGT 1500 have gathered more than 37,000 hours without reporting any major issues.

Capstone Turbines are one of the most successful manufacturers of small scale gas turbines. In a 2002 publication [7], their manufacturing and operating experience of small GTs with a power output below 100 kW is discussed. The first design Capstone developed for this power range used brazed assemblies (shown in Figure 2.6), which resulted in high manufacturing costs as well as reliability challenges. The following design iteration (shown in Figure 2.7), was sourced to Solar Turbines and used a fully welded assembly. This design change resulted in lower costs and increased durability.

Their smallest unit, the 30 kW C30, features an annular recuperator with 86% effectiveness and an overall pressure drop of 3.5% for both HP and LP streams combined. The complete recuperator is built out of stainless steel 347 since the turbine exhaust temperature 600 ^{o}C.

The manufacturing procedure [8], uses simple modular elements (i.e. unit cells) which are stacked and

Figure 2.6: Brazed annular Capstone recuperator ‘ [7]

Figure 2.7: Capstone complete assembly for 200 kW microturbine [8]

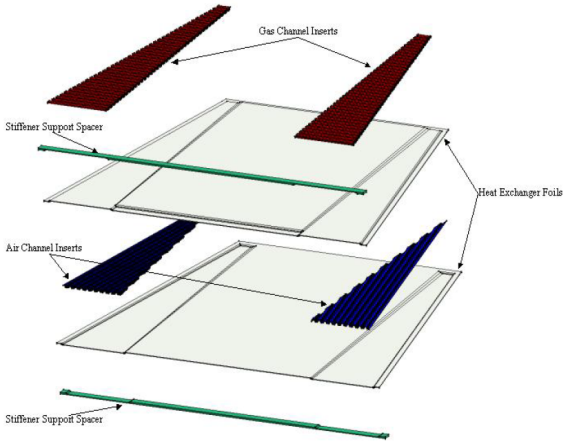

Figure 2.8: Capstone unit cell components [8]

welded in the final annular setup. The unit cells, shown in Figure 2.8, are constructed out of two metallic plates with a CW pattern in the counterflow section. The inlet and outlet distributors have a cross-flow arrangement, with inserts that increase surface area and provide structural support. The cells are welded, leaving the air inlet and outlet at the ends of the inner diameter. A strength of this design is the minimum amount of manifolding needed and the ease of integration with the turbomachinery, which reduces pressure losses. Capstone proved the flexibility of their concept, by successfully scaling the small power output versions to a 200 kW concept. Currently a two-stage, high efficiency 370 kW concept is being developed under Department of Energy (DOE) funding [39]

A recuperator concept developed by Rolls-Royce for stationary power gas turbines [9] features a primary surface architecture. The key feature of this concept is, arguably,the low-cost manufacturing process. The recuperator is constructed by wrapping a formed foil in a continuous manner, reducing the cost related to manufacturing and increasing resistance to thermal stresses. The foils are previously formed to have the desired geometry and stamped to build the required air passages. An overview of the manufacturing process is shown in Figure 2.9, as well as a unit section depicting the flow paths. The construction has also added flexibility, since an extra row of fins can be added to the rolling process in order to increase heat transfer surface at the gas side. Reference [9] states that a prototype has been subject to severe testing, derived from the WR21 intercooled recuperated engine program, for several weeks without any sign of damage. No figures for effectiveness of pressure losses were reported.

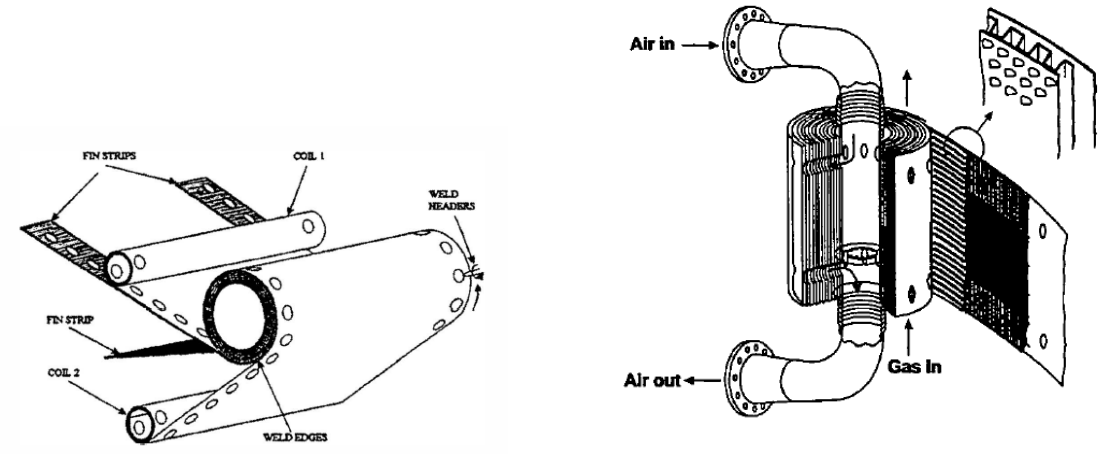

(a) Manufacturing process (b) Recuperator section

Figure 2.9: Rolls-Royce wrapped recuperator concept [9]

ACTE [10] developed a spiral primary surface recuperator for small gas turbine applications, shown in Figure 2.10. This design was created with the objective of achieving high reliability, compactness and low cost. The recuperator has cross-flow inlet headers and a main counterflow section, similar to other concepts previously described. The initial design used triangular corrugations, but further research [40] determined that the implementation of a CC geometry would greatly improve the performance of the unit. With the implementation of the CC surfaces, effectiveness was increased from 86% to 89%, the recuperator weight was reduced by 43% and pressure losses were kept 5%. This shows that the implementation of surface geometry optimization can have significant benefits.

Figure 2.10: ACTE wrapped annular recuperator [10]

The manufacturing process of the ACTE recuperator is similar to highly automated proposals discussed previously. Thin foil is continuously fed through rollers that form the corrugations in the core. Afterwards, two welding operations are done: in the first, the edges of the two sheets are welded and in the second one flat spots are welded between both sheets to increase the pressure resistance of the recuperator. Finally, the sheets are straightened and then coiled into a final unit. The authors state that the spot weld in the flat surfaces, requires a high degree of accuracy to avoid any weld attempts in areas were there is no contact between two plates. Once the core is constructed, openings have to be spark eroded and manifolding subsequently welded. This manufacturing process has the advantage of high automation potential, but suffers from the complexity required by the high precision automatic welding and spark erosion.

In the mid 1990's Rekuperator Svenska AB (RSAB) developed a prototype for hybrid vehicles equipped

with small recuperated gas turbines for Volvo [11]. This recuperator also features welded primary plates for form unitary cells. These unitary cells are then stacked and welded by the edges to obtain the recuperator core. The flow configuration uses crossflow distributors with main counterflow sections. By using a different number of unitary cells, variants for different applications could be easily developed.

Figure 2.11: RSAB prototype for 100kW microturbine [11]

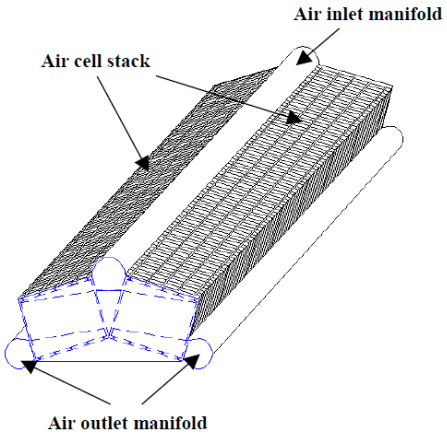

Figure 2.12: RSAB core for 300 kW microturbine [11]

RSAB built a prototype for a 100kW microturbine, as shown in Figure 2.11, which fulfills the performance requirements of 89% effectiveness and 4.5% of total pressure losses. A concept for a larger powerplant using the same cell geometry is shown in Figure 2.12. These two designs are an example of the different number of unitary plates to fulfill the requirements of different applications.

A low cost recuperator concept for stationary and automotive vehicular applications was developed by Forster and Kleeman [41] and later modified by McDonald [12] to improve its suitability for automated manufacturing methods. According to McDonald, this concept is one of the most promising for a successful low-cost high efficient recuperated gas turbine. The recuperator core is built out of a thin foil which is stamped to form a CC pattern. The foil is then folded to obtain counterflow passages with low hydraulic diameters. During the folding process, two thick strips are added to each side of the foil to provide enough material for weld operation. Finally, cover plates are added to create individual channels, leaving open sections at the edges that function as inlet and outlet headers. The resulting geometry, as well as a description of the flow path within the recuperator are shown in Figure 2.13.

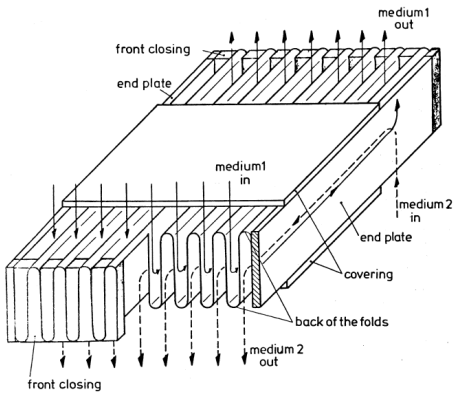

Figure 2.13: Parts and flow configuration of unit cell for low cost PSR [12]

Forster and Kleeman report an effectiveness of 84% for a metallic recuperator prototype tested in a 450 kW vehicular gas turbine, with HP and LP stream pressure losses of 0.3% and 4.5%, respectively. This concept was

built out of 12 individual matrices with a volume of approximately 8 liters. The 12 matrices are placed in a V-shaped arrangement that, according to the authors, simplifies the construction of headers and manifolding. McDonald proposed an improvement to the matrix arrangement, which consists of a single annular matrix that reduces the overall unit volume. The recuperator uses a chrome-nickel alloy to handle the high temperatures of the specific application. As part of the development efforts, a ceramic matrix was also constructed with the aim of investigating its potential for future high temperature applications.

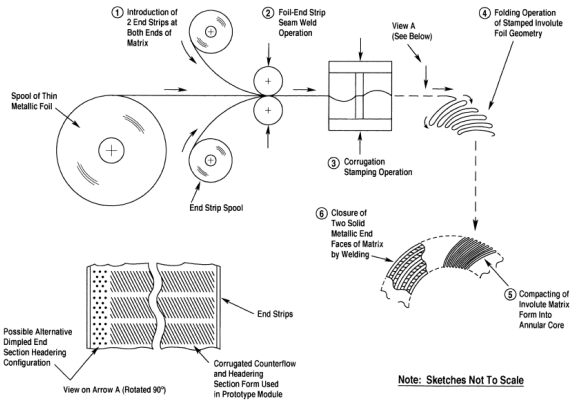

Figure 2.14: Manufacturing steps for low-cost primary surface recuperator [12]

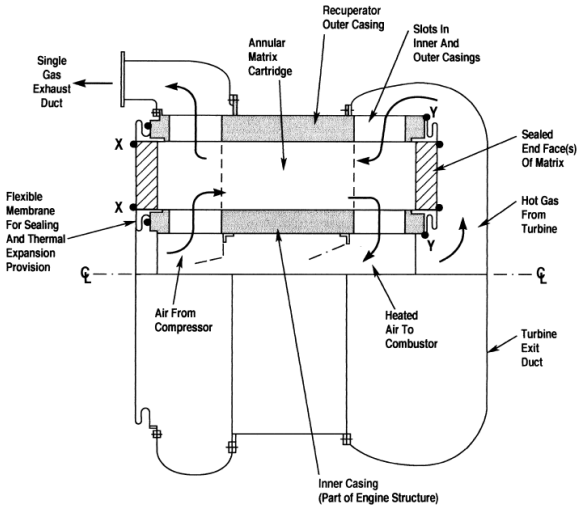

Figure 2.15: Cartridge layout for low cost PSR [12]

The highly automated manufacturing process, makes this concept attractive for large production volumes. Figure 2.14 shows McDonald's proposal for manufacturing the recuperator in the newly proposed annular layout, which only consists of 5 parts, the thin foil and the four end strips. It can be argued that all of the steps shown in Figure 2.14 can be automated when the specific machinery and tooling is developed. All of the recuperator joints are welded, thus there is no need for costly brazing operations. Another benefit of this annular configuration, is that it improves system integration and assembly. The resulting matrix (see Figure 2.15) that can be slid into a previously manufactured enclosure and then welded in 4 spots that allow for simple disassembly afterwards. In addition these benefits, the author claims that this configuration reduces thermal stresses by allowing the matrix to expand in the axial direction of flow.

2.1.2. Plate-fin recuperators

In plate-fin (or extended surface) HEXs fins are placed between plates that separate hot and cold fluids. These heat exchangers are commonly used in gas-gas configurations. The extended surfaces improve the performance of the heat exchangers by increasing the effective surface area in contact with the fluids, which can be increased up to 12 times [18]. Fins are commonly brazed to the parting plates, which results in higher weight. Another disadvantage with respect to the latter is that the increase in surface comes with a penalty: the effective temperature difference between fluids is reduced due to the temperature gradient occurring in the fins. This performance reduction is accounted for by the concept of fin efficiency (described in Section 3.2.5).

Ingersoll-Rand has developed a plate-fin recuperator design for application in small GT [13]. The main challenge to address with this design are high operating temperatures of the application as well as high recuperator costs, an aspect that has hampered their widespread application. The recuperator has a counterflow configuration in its main section with crossflow distributors. The heat exchanger is constructed using a number of unitary cells (seen in Figure 2.16). These cells are built out of two stamped parting plates, an air fin segment with distribution headers and two fin segments for the gas side plate. The perimeter of the two parting plates is welded, closing of the HP stream. The unit plates are then stacked, and then welded only by the circular headers, avoiding a rigid connection between the unit cells. This allows to minimize the internal thermal stresses during operation.

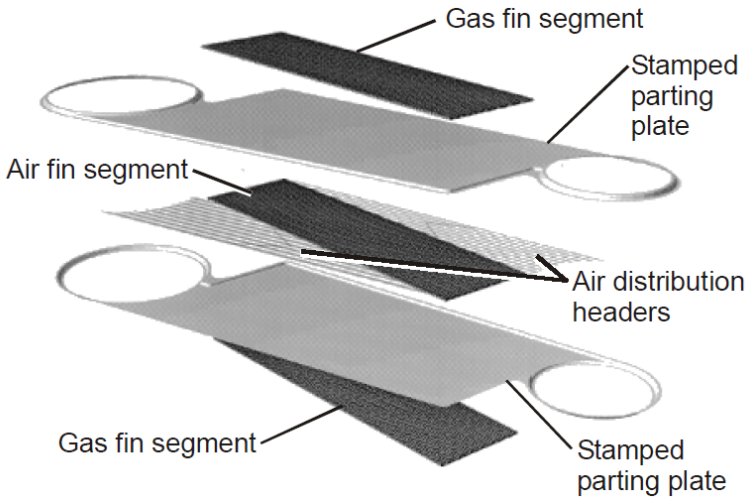

Figure 2.16: Components of Ingersoll Rand's plate-fin unitary cell [13]

2.1.3. Tubular recuperators

Even though tubular HEXs show higher structural integrity in comparison to primary surface and plate-fin concepts, their lower heat transfer performance leads to bulky recuperators. For this reason, tubular HEXs are not commonly seen in low power output applications. Still, their simpler construction and potential low-cost has lead some researchers to investigate their applicability to the small GT segment by proposing updates to the traditional topologies.

Proeschel proposed a recuperator concept, Proe 90, based on a tubular architecture [14]. The intention was to build a recuperator that had effectiveness levels above 90% and was simple enough to be manufactured using basic techniques, lowering costs. In addition to making manufacturing simpler, the tubular topology allows the heat exchanger to withstand higher thermal stresses. Figure 2.17 shows one of the concentric tubular assemblies, built out of three tubes and a central rod. The tubes have holes that connect with the manifolding, which result in a purely counterflow configuration. All of these parts can be assembled by welding or brazing. The author claims that the use of a complete laminar flow regime reduces pressure losses and avoids the need of turbulence promoters to enhance heat transfer.

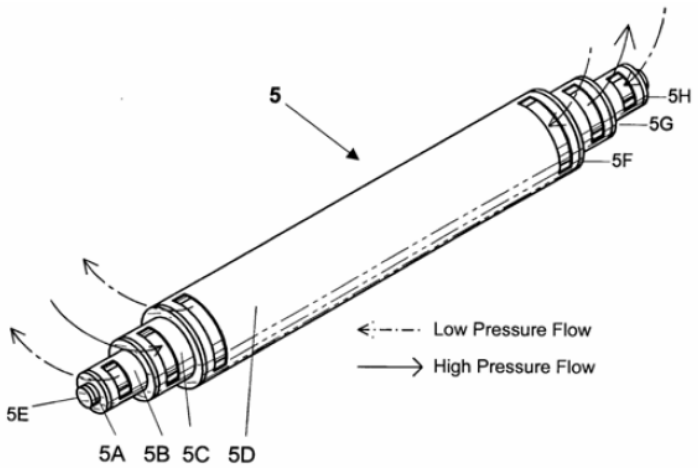

Figure 2.17: Proe 90 concentric tube assembly [14]

The author performed a design study for a 30 kW Ericsson afterburning generator with a mass flow of 0.13 kg\s and an effectiveness target of 95.3%, resulted in a unit of 454 kg. This is a considerably large unit, but it is important to point that recuperator size grows exponentially as effectiveness approaches ideality. Changing effectiveness to a value of 85%, shortened the recuperator length from 127 cm to 40 cm. The same performance modification is achieved by reducing the number of concentric tube assemblies from 257 to approximately 60. These changes would reduce weight proportionally to 77% (102 kg). The unit weight is still considerable, but its structural integrity compared to primary surface concepts could justify this aspect.

A coiled pipe-in-pipe recuperator was analyzed by Clay [15] as a possible low-cost solution for recuperated microturbines. Figure 2.18 shows the proposed design which uses two concentric pipes coiled, leaving a void where the rest of the gas turbine components are placed. The strength of this construction is its potential for reducing costs. A preliminary design for a 1 kW gas turbine application was carried out. The results of this concept were unsatisfactory for the application, since the predicted thermal performance was too low. To obtain high effectiveness levels, long tubes were needed, which resulted in high pressure losses. Further research considers the use of internal tube features to increase heat transfer, but this will likely increase the cost of the concept.

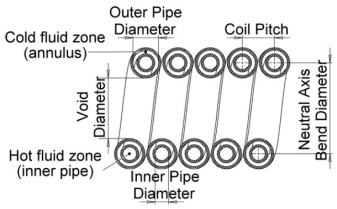

Figure 2.18: Proposed layout for a coiled double pipe recuperator [15]

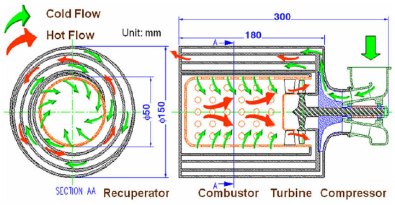

Figure 2.19: Proposed Swiss-Roll recuperator with outlined turbomachinery [16]

Shih and Huang presented a coiled recuperator concept denominated as Swiss-Roll [42]. The recuperator is built out of two plates (schematic seen in Figure 2.19) that are spirally wrapped resulting in a counterflow configuration in the radial direction. Even though the concept may seem attractive due its simplicity, it is not suited for high effectiveness due to the high pressure losses caused by the long flow path needed. For an effectiveness of 85%, the authors estimated pressure losses close to 30%, which would implementing this concept in a microturbine application. The authors suggest investigating the adoption of heat enhancement techniques which would increasing the cost and complexity of the design.

2.1.4. Summary of heat exchanger configuration features

The survey of different heat exchanger designs for small gas turbines allows to identify a number of design choices compatible with the requirements of the GTRE recuperator. These aspects are outlined below:

Flow configuration

All of the recuperator concepts reviewed feature a predominant counterflow configuration, which is obvious from their effectiveness values. A counterflow configuration maximizes the temperature difference between both streams at fixed inlet conditions, leading to smaller heat transfer area required. This is in line with the requirements for a GTRE recuperator. The only drawback of this configuration is the construction of headers. A common solution also observed in the reviewed concepts is the use of crossflow distributors, which reduces the challenges of a fully counterflow configuration.

Heat transfer surface type

Successful heat exchanger concepts for gas turbines have been built using all of these three heat transfer surface types. From the reviewed concepts, the primary surface construction shows a two main strengths for a GTRE application:

- Lower weight resulting from the use of thin primary plates and the lack of secondary surfaces. Additionally welded primary plates avoid the weight penalty of brazing material used in plate-fin constructions.
- High volume production potential when using a continuous stock of metal sheet that is welded. This process has been demonstrated successfully.

2.2. Heat transfer and pressure drop characteristics

An important aspect of heat exchanger research is the development and characterization of different heat transfer surface geometry. The key mechanisms that define heat exchanger performance are heat transfer and pressure losses. The goal of recuperator design is to maximize heat transfer while maintaining a low pressure losses. A higher thermal performance implies a larger amount of heat recovered from turbine exhaust flow, while lower pressure losses (better hydraulic performance) allow to extract more work from the turbine. Both of these aspects lead to higher efficiencies of the recuperated gas turbine cycle and a more compact system, which is key for the success of a gas turbine range extender.

Characterization of heat transfer surface geometry focuses on predicting the heat transfer and pressure loss performance as a function of flow conditions by means of numerical or experimental studies. The results of these investigations are, generally, analyzed using non-dimensional parameters such as Nusselt number, Colburn, and Fanning factors. Nusselt number is defined as:

$$Nu = \frac{hd_h}{k_f} \tag{2.1}$$

where h, d_h and k_f are the heat transfer coefficient, hydraulic diameter and the thermal conductivity of the fluid, respectively. The Nusselt number indicates the ratio of convective to conductive heat transfer occurring in the fluid. The Colburn factor is defined as:

$$j = \frac{Nu}{RePr^{1/3}} \tag{2.2}$$

By using the Colburn factor, heat transfer coefficients that were obtained for a specific fluid, e.g. water, can be extrapolated to another working medium such as air.

The Fanning factor is a common non-dimensional expression for the pressure loss in an internal flow. It is the ratio of wall shear stress τ_w to the flow kinetic energy per unit volume. It is defined as:

$$f = \frac{\tau_w}{\rho u_m^2/2} \tag{2.3}$$

where u is the mean flow velocity in the channel. Pressure loss performance can also be reported using the Darcy friction factor, which is exactly four times the Fanning friction factor. These expresions allow to estimate the heat transfer and pressure loss performance of the heat exchanger by correlating them to flow conditions such as velocity, temperature and fluid composition. The use of non-dimensional correlations becomes useful when performing a preliminary design of an HEX, since numerical simulations are not feasible due to their large computational burden.

Heat transfer surface performance predictions can be obtained using an experimental setup as well as numerical simulations. Experimental analysis is usually more reliable, but usually costly and more time consuming. In addition, detailed flow characteristics like velocity and temperature distributions are difficult to obtain by experiments. For this reason, numerical simulations are an attractive alternative since they allow to analyze a large number of geometries and flow conditions with smaller investments in time and equipment. Special attention has to be devoted to selecting suitable boundary conditions, proper grid definition as well as turbulence model selection (as noted by [43]).

Plain fins and other complex geometries have been used in order to improve the performance of heat exchangers. One of the mechanisms for increasing heat transfer surface is to increase the effective heat transfer area. Another alternative is to increase the heat transfer coefficient by means of modifying flow patterns. Figure 2.20 shows how different channel geometries influence flow behavior in order to increase heat transfer. Examples of modifying flow behavior can be seen in both extended and primary surface constructions.

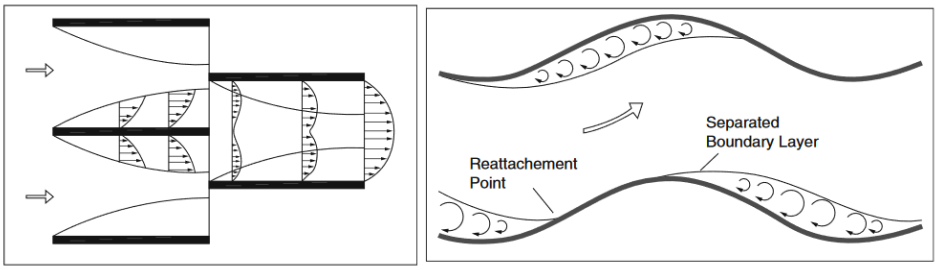

Figure 2.20: Heat transfer improvement mechanisms in offset-strip fins and wavy fins [17]

Offset-strip fins, increase heat transfer by creating fresh boundary layers at the leading edge of each offset strip. Wavy channels promote mixing and force boundary layer separation and reattachment.

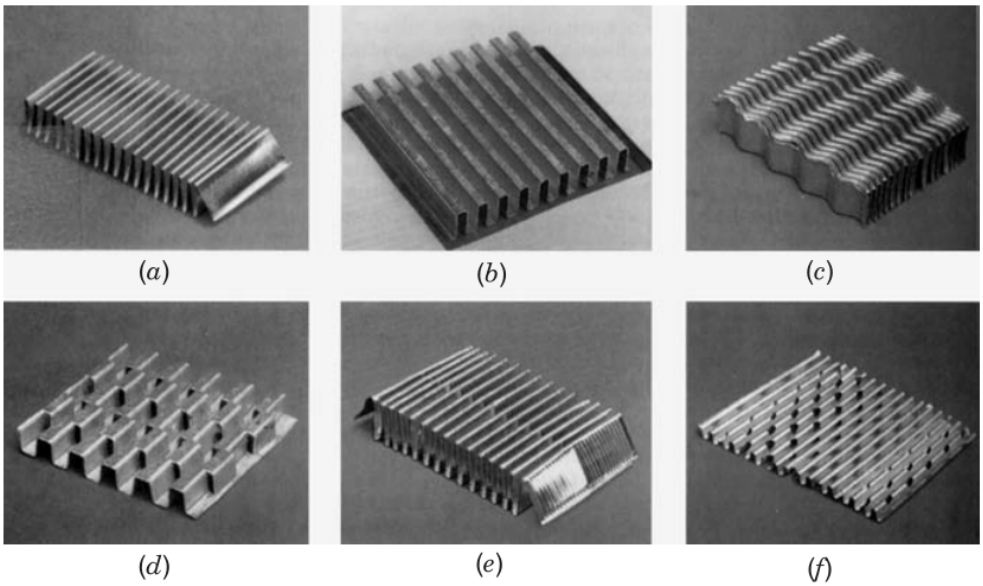

Figure 2.21: Corrugated fin geometries for plate-fin heat exchangers: (a) plain triangular fin; (b) plain rectangular fin; (c) wavy fin (d) offset strip fin; (e) multilouver fin; (f) perforated fin. [18]

Several types of fin geometries exist for increasing heat exchanger thermal and hydraulic performance. For instance, Figure 2.21 shows different geometries that have been used in plate-fin heat exchangers. Furthermore, parameters of the same base geometry such as pitch P (spacing between periodic fin corrugations) and fin height H can be varied to optimize performance

Cross corrugated surfaces have been the subject of different experimental and numerical studies aimed at characterizing their thermal and fluid-dynamic performance. The studies that are more relevant for the application at hand focus on geometries operating at low Reynolds numbers ($Re < 1000$). Stasiek and Ciofalo [44, 45] researched CC surface performance in an experimental setup, and later simulated the same flow conditions using a numerical model. Local Nu was measured using liquid crystal thermography and static pressure was measured along the passage using pressure tapings. Three different pitch-to-height ratios P/H were analyzed at several plate angles ranging from 30 to 79 degrees. The last parameter refers to the angle between the corrugation patterns of top and bottom plates. Their measurements sufficiently agreed with the data of similar experimental setups from other publications. The analysis reveals that Nu decreases with higher pitch to height ratios, while f increases. They also observed that an increasing plate phase angle has a positive effect on Nu and a negative effect in f.

The experimental work was validated using numerical analysis which employed different turbulence models. Simulations were run using no turbulence models (laminar assumptions), standard $k-\varepsilon$ with wall

function, low Reynolds $k-\varepsilon$ formulation as well as Large Eddy Simulation (LES). The flow was modeled as periodic, by setting equal velocity and temperature profiles at inlet and exit of the periodic surface. All models with the experimental data below $Re = 1000$. The results calculated with the laminar and standard $k-\varepsilon$ models exhibit an increasingly different trend above $Re = 3000$, suggesting flow transition at these conditions. For the turbulent regime, the low-Re model shows good agreement with the experimental data, while the LESs have good predictions in the complete Re range of interest.

Utriainen [23] compared the results published by Stasiek and Ciofalo, with two other experiments available in literature [46, 47] that used the same CC geometry. These investigations used similar Re numbers, plate phase angle and P/H ratios. The author stated that the results obtained by Stasiek and Ciofalo were the median of the set of experiments and analyzed, and deemed them suitable for use in recuperator sizing. Cross-undulated, the cross-corrugated variant with different corrugation profiles on top and bottom plates, has also been subject to research. Stasiek [48] used an experimental setup to characterize the thermal and hydraulic performance of this type of surfaces. By means of liquid crystal thermography, six different plate geometries at 4 different inclination angles were tested. The influence of Reynolds number as well as geometric characteristics such as pitch-to-height ratio was also analyzed. The experiments showed that the inclination angle between both plates had the largest impact on the flow behavior.

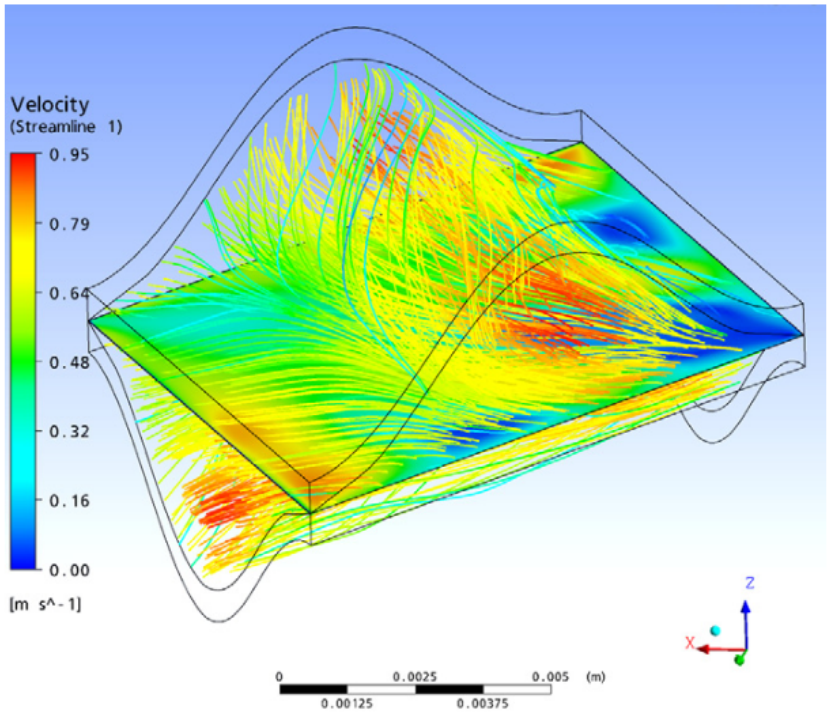

Figure 2.22: Velocity streamlines obtained by means of CFD in a CC section [19]

CW are a HEX surface geometry that used successfully in gas turbine recuperator concepts such as Capstone [7] and Solar Turbines [5]. Utriainen [20] performed a numerical investigation of seven different CW cross-wavy ducts with a rounded profile. The geometries had different wave profiles, as well as pitch to height ratios, while the hydraulic diameter of all the surfaces was kept constant. The flow was simulated as periodic unitary cell (common with this type of analysis in heat transfer surface). The researcher worked on numerical simulations for cross-wavy surfaces, but using a trapezoidal cross section, instead of a rounded section [49]. Figures 2.23 and 2.24 show the difference between rounded and trapezoidal profiles of cross-wavy ducts. Both publications reported a significant performance improvement in comparison to standard rectangular channels.

Novel heat transfer surface geometries have appeared recently, mainly due to higher reliability of numerical experiments as well as the availability of new techniques such as additive manufacturing. Wang [3] presented an overview of current developments in primary surfaces. Novel surface concepts recently proposed are shown in Figures 2.25 and 2.26. The advantage of this new geometries is that vortices and impingement

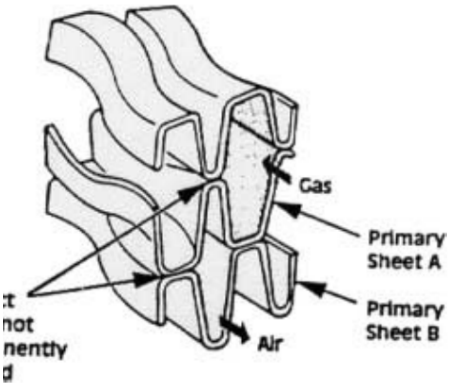

Figure 2.23: Trapezoidal cross-wavy primary surface [20]

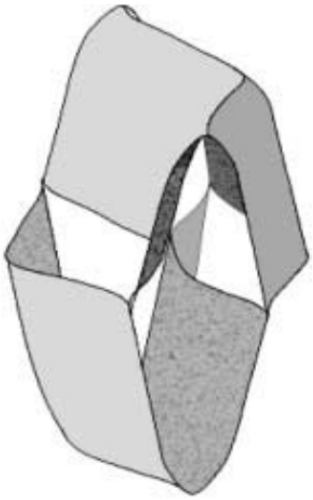

Figure 2.24: Rounded cross-wavy primary surface [20]

areas are increased, improving heat transfer significantly. For example, Figure 2.27 shows the streamlines of a primary surface with secondary corrugations out of phase. These out of phase corrugations cause an impingement zone that increases heat transfer. It is reported that this geometry has a 10% higher heat transfer in comparison to the equivalent CC surface without the additional secondary corrugation pattern.

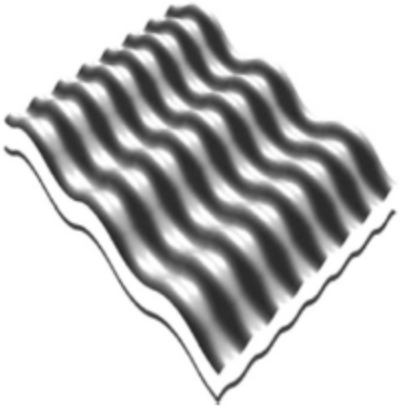

Figure 2.25: Double wave primary surface [3]

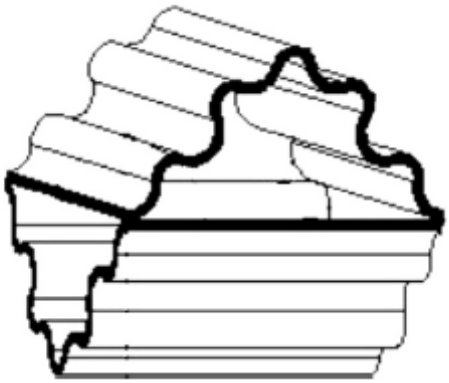

Figure 2.26: Cross corrugated surface with additional corrugations [3]

Research has also focused on comparing the performance of different primary surface geometries for gas turbine applications. Utriainen published an evaluation of the performance of different primary surface geometries [23]. A selection of different primary surface geometries (based on a previous study from the same author [50]) and an offset strip plate fin were used to do a preliminary sizing study based on a concept 50 kW microturbine using a recuperator with a fixed 85% effectiveness. Data for CC surfaces and offset strip plate fin were obtained in an experimental setup while CU and CW are a product of numerical simulations. The CC surfaces employed had different phase angles between the two plates as well as P/H ratios. The CW surfaces had different phase angles between plates. By doing a preliminary sizing exercise, an initial estimation of the recuperator dimensions can be achieved. Weight calculations were done by assuming a plate thickness of 0.08 mm. CC surfaces show the best performance out of the whole group. Plate-fin has a poor performance even though there is no consideration for the brazing material in the core weight. CC surfaces were identifies as the best performing family.

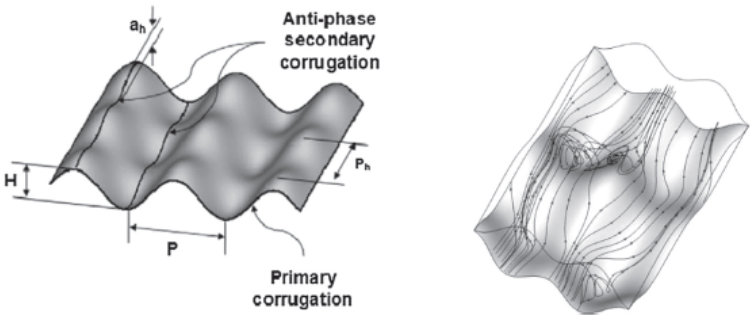

Figure 2.27: Modified primary surface with secondary corrugations [3]

In a similar comparison exercise, Traverso and Massardo [51] developed an optimization procedure for compact heat exchangers sizing and then applied it to compare the performance of different heat transfer surfaces. CC, CW, CU and plate fin surfaces were used. In comparison to Utriainen [23], a much larger selection of plate-fin geometries was used, as well as a larger selection of CW surfaces. Recuperator volume and weight were obtained for three different gas turbines with power outputs of 50, 100 and 500kW. The results of this study reinforce the superiority of primary surfaces over plate-fin, even when using a large selection of plate-fin configurations and selecting the best performer. It was noted that the three different power ratings did not affect the conclusion regarding which surfaces show better performance.

2.3. Material selection

A brief overview of the impact of material selection in the construction of recuperators for small gas turbines is needed in order to understand some key trade-offs in the reported parametric analysis. Structural behavior is a challenging aspect of recuperator design for small gas turbines. From the point of view of the GT cycle, high turbine inlet temperatures are desirable since they result in higher system efficiencies. But important structural challenges arise from the high temperatures. The higher thermal stresses in the recuperator may lead to a design that requires higher grade materials, making the gas turbine incompatible with the requirements of a low-cost application.

McDonald [21] has discussed the issue of interaction of gas turbine performance and recuperator material selection. Figure 2.28 shows the influence of different gas turbine design parameters like turbine inlet temperature and compressor pressure ratio on the turbine exhaust temperature, which mainly determines the required recuperator core material.

Figure 2.28 shows approximate temperature limits of several common materials for recuperator construction. The operating temperature limits range from 675 ^{o}C for the stainless steel 347 up to 900 ^{o}C for the Haynes 214 alloy. Capstone Turbine [52] has researched new materials for their 65 kW recuperated variant. Even though the geometry of the recuperator is the same es the one used for the 30 kW variant, the increased temperatures required to avoid stainless steel constructions. Capstone's C65 has been built using Haynes 120 since 2005. At these high operating temperatures, not only thermal stresses become an issue but corrosion due to water content in the combustion gases becomes a major challenge. Advanced alloys like the Haynes 120 and 214 can withstand these adverse operating conditions, but its cost is approximately nine times compared to the SS347 [21]. McDonald has also suggested the possibility of using a bi-metallic core which uses high grade alloys for the hottest sections of the HEX, and uses lower grade stainless steel for the rest. This allows to reach higher turbine exhaust temperature (TET) while keeping material costs low.

The development of ceramics has gained traction in recent years, specially in aerospace applications where cost is of less importance. Grady [53] outlined the development of a fully non-metallic GT built using additive manufacturing. This shows that ceramic matrix composites are a nowadays a reality for demanding applications such as aircraft propulsion. Rodgers and McDonald [28] describe a concept for a small GT that uses ceramics to manufacture the turbine wheel as well as the recuperator. The authors state that ceramic

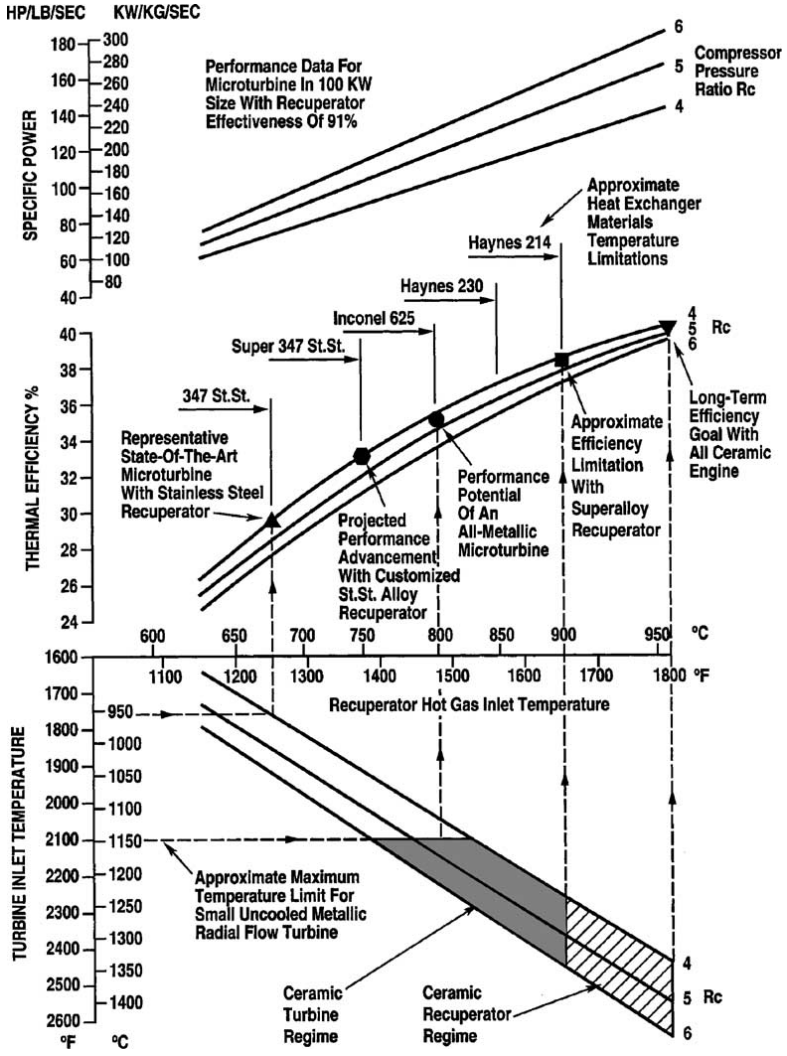

Figure 2.28: Effect of recuperator temperature limitations on microturbine performance [21]

components are a good solution for the structural challenges faced by components operating at high temperatures. They also highlight the fact that the manufacturing processes for ceramic recuperators allow for the construction of channels with much lower hydraulic diameters which resulting in smaller units. It remains to be seen if ceramic matrix manufacturing will fulfill the cost and reliability requirements of the automotive market.

3

Methodology-Model development

This chapter covers the methodology used for the development of the heat exchanger performance models. Section 3.1 addresses the motivation behind the selection of the heat exchanger topology. Section 3.2 describes the development of a rating model for the heat exchanger. Finally 3.3, covers the development of the sizing model starting from the rating model.

3.1. Configuration selection

The first step in the preliminary design of the recuperator is the choice of the heat exchanger topology. An annular configuration with finned crosflow headers and a main primary surface counterflow section were selected. The recuperator designs as well as the heat transfer surface geometries reviewed in Section 2.1.4 were used to motivate the topology selection. This reasoning is outlined below:

- A primary surface construction results in a compact and lightweight layout, due to its higher performance in comparison to plate-fin topologies. Packaging is one of the main challenges of the range extender application.
- Primary surfaces can be built by welding, which allows a high level of automation that benefits the costs of the unit. The automotive market commonly employs high quantity, low cost concepts.
- The annular configuration allows to reduce the amount of manifolding by placing the inlet of HP and LP streams close the outlets of compressor and turbine, respectively.

A well documented example of this type of construction is Capstone Turbine's recuperator concept used in several of their units. Figure 3.1 shows an example of the selected configuration. The figure shows how the complete assembly is made using unitary plates, as well as the flow configuration within this plates. The HP stream flows through the small inlet located in the radial direction. The plates are curved in order to maintain the same spacing throughout the complete HEX. The HP outlet is located on the other end of the unit cell, following a radial orientation. The LP stream flows in the axial direction. This results in three distinguishable sections, with different flow arrangements (highlighted by the flow arrows in Figure 3.1).

Finally, the selection of this topology as a starting point was also motivated by the available data needed for model validation. Capstone has published detailed geometric and performance data in a report for a DOE funded development project [8]. The document contains details on the recuperator thermal and hydraulic performance, with pressure losses for each stream, recuperator effectiveness, detailed geometry as well as boundary conditions such as mass flow, temperatures and pressures. These figures are stated for a number of test geometries, which allows to have a larger number of cases for model validation. This level of detail in recuperator data was not found in any of the other concepts that were presented in Section 2.1.

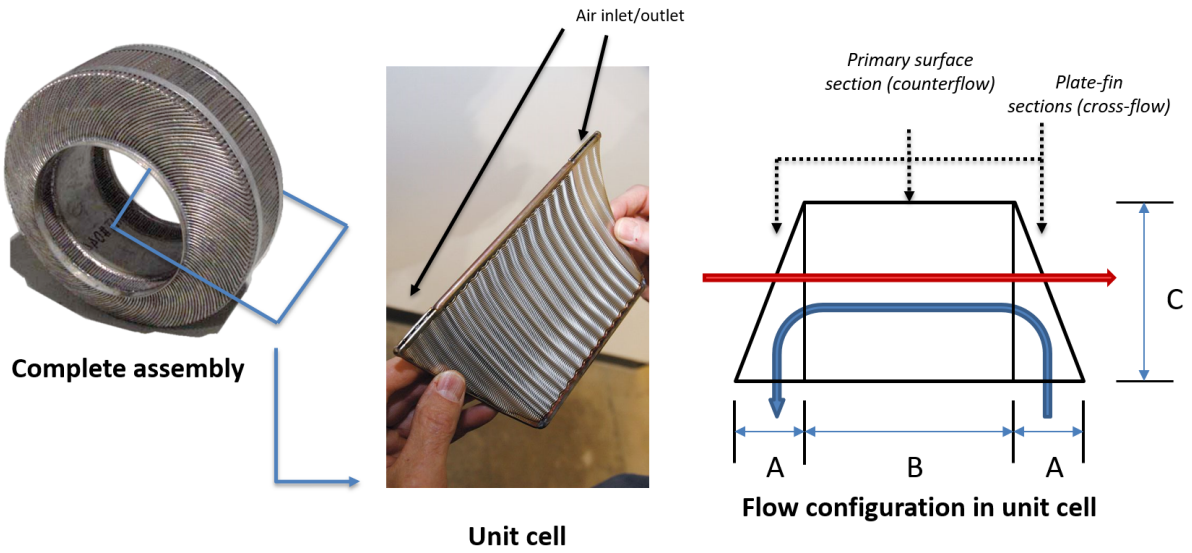

Figure 3.1: Selected configuration for preliminary sizing model base in Capstone

3.2. Rating model

To perform the preliminary design of the recuperator for the application at hand a simplified rating model for the HEX topology described above was developed. This model was validated against performance data published Capstone Turbine [8]. Rating and sizing refer to different setting of a heat exchanger design problem. A rating exercise occurs when the operating conditions of the heat exchanger as well as its detailed geometry are known. This information is used in order to estimate the thermal and hydraulic performance of the heat exchanger, in other words the expected pressure losses and effectiveness. On the other hand, a sizing procedure starts with known boundary conditions and target recuperator performance. The objective of the exercise is to obtain a recuperator geometry that will provide the desired performance.

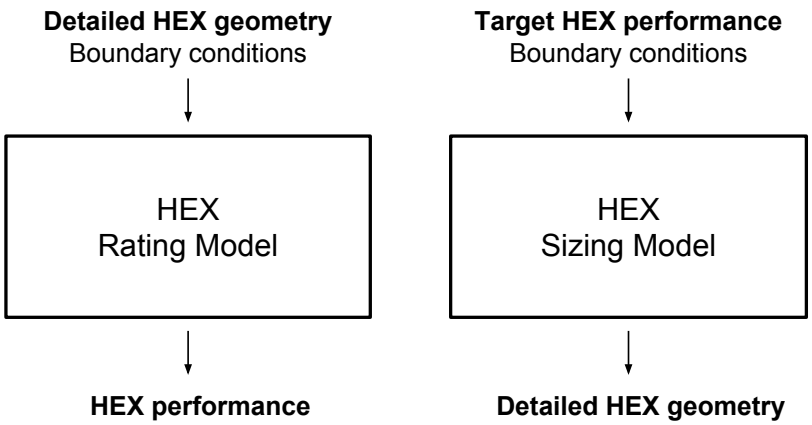

Figure 3.2: Input and output comparison for heat exchanger rating and sizing procedures

3.2.1. Thermal design theory

In order to understand the sizing and rating methodologies that will be later addressed, a brief overview of the thermal design theory of heat exchangers is presented. Before describing the rating model for this recuperator, it is useful to introduce first the assumptions used during this derivaiton:

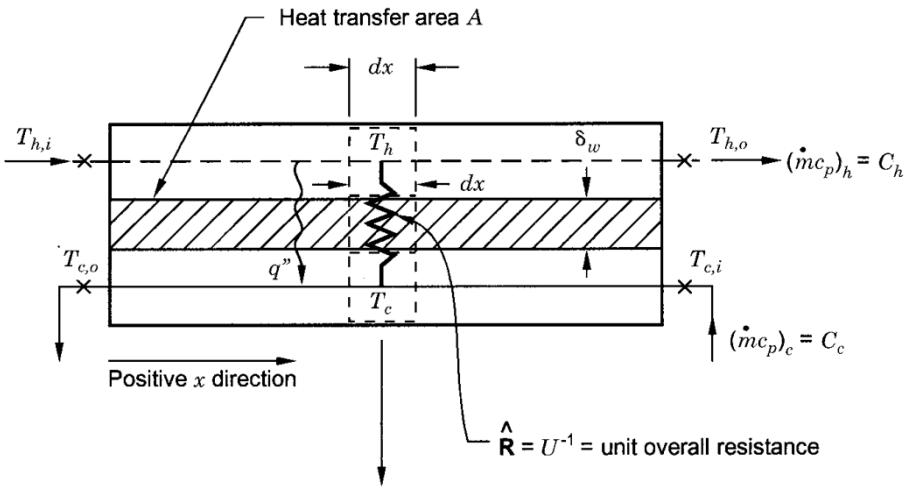

Figure 3.3: Diagram of thermal circuit in a heat exchanger [18]

- The heat exchanger operates in steady state conditions.
- There are no heat losses to or from the surroundings (i.e. the heat exchanger is adiabatic).
- There are no thermal energy sources or sinks in the walls and fluids.
- The wall resistance is distributed uniformly in the entire heat exchanger.
- The effects of longitudinal heat conduction are negligible.
- Average fluid properties are used and assumed constant throughout the HEX sections.

Figure 3.3 shows the thermal circuit in a section of a heat exchanger. The thermal circuit consists of two fluid flows, the high temperature T_h and low temperature T_c streams. Each stream has an inlet temperature $T_{c,i}$, $T_{h,i}$ and an outlet temperature $T_{c,o}$, $T_{h,o}$ and a heat transfer surface area A . The so called thermal resistance, comprised by the circuit of hot stream convect. Assuming the global heat transfer coefficient constant along the HEX or a portion of it, the heat flux between the cold and hot stream reads:

$$q = U(T_h - T_c)_{local} \tag{3.1}$$

Where the overall heat transfer coefficient U is defined as:

$$U = \frac{1}{(\eta_f hA)_c} + \frac{\delta_w}{k_w A_w} + \frac{1}{(\eta_f hA)_h} \tag{3.2}$$

h_c and h_h refer to the hot and cold heat transfer coefficients, while δ_w, k_w and A_w refer to the wall thickness, wall thermal conductivity and wall area. η_f refers to fin efficiency, a concept that comes into play when extended surfaces are used. This formulation of U does not take into account additional thermal resistance attributed to fouling. When the heat exchanger uses a primary surface these efficiencies are equal to one. The definition of fin efficiency is discussed in detail on Section 3.2.5. The change in temperature in both fluids is dependent on the heat transfered dq, the fluid's specific heat c_p and the mass flow $\dot{m}$ going through each stream:

$$dq = -(\dot{m}c_p)_h dT_h dA = -(\dot{m}c_p)_c dT_c dA \tag{3.3}$$

The complete set of dependent and independent variables and parameters can be summarized as:

$$\underbrace{T_{h,o}, T_{c,o}, Q, U}_{\text{dependent variables}} = \underbrace{\phi(\underbrace{T_{h,i}, T_{c,i}, C_h, C_c}_{\text{operating condition variables}}, \underbrace{\text{Surface geometry}, A, \text{flow arrangement}}_{\text{design variables}})}_{\text{independent variables and parameters}} \tag{3.4}$$

The dependent variables are the thermal duty Q and the outlet temperatures of both the hot and cold streams $T_{c,o}, T_{h,o}$ and the independent variables are the inlet temperatures of the hot and cold streams $T_{c,i}, T_{h,i}$ as well as the heat capacity of each stream C_h,C_c. Design variables are the overall heat transfer coefficient U, the compete heat transfer area A and the flow arrangement of the heat exchanger. The selection of the best set of design parameters for the required design is the challenge of heat exchanger design. An important part of heat exchanger development is to modify surface geometry to maximize U for given operating conditions or even increase Awhile keeping the overall volume footprint the same.

3.2.2. P-NTU method

For all the heat exchanger modeling performed in this research project, the P-NTU method was used. The reason behind this choice is the simplicity of implementing this model in a network of heat exchangers, which is the case for the selected recuperator configuration. The P-NTU methodology states that the total heat transfered in the heat exchanger is:

$$q = P_1 C_1 \Delta T_{max} = P_2 C_2 \Delta T_{max} \tag{3.5}$$

where C_i is the heat capacity of each heat exchanger stream, ΔT_{max} is the inlet temperature difference between both streams ($T_{h,i} - T_{c,i}$), while P known as the temperature effectiveness. It is important to understand the difference between effectiveness and temperature effectiveness. The concept of temperature effectiveness is defined as the ratio temperature change for each stream and the maximum temperature difference in the HEX. Note that the subscripts 1 and 2 refer to each side of the heat exchanger and refer to the cold and hot exchanger sides (subscripts c and h respectively).

$$P_1 = \frac{T_{1,o} - T_{1,i}}{T_{2,i} - T_{1,i}} \quad P_2 = \frac{T_{2,o} - T_{2,i}}{T_{2,i} - T_{1,i}} \tag{3.6}$$

Through means of non-dimensional analysis, it can be shown P is only a function of NTU_i , the heat capacity ratio R_i and flow arrangement [18]. R_i refers to the the ratio of the heat capacity for the current stream by the heat capacity of the other stream.

$$P_i = \phi(NTU_i, R_i, \text{flow arrangement}) \tag{3.7}$$

Number of exchanger heat transfer units (NTU) is defined as the ratio of the overall thermal conductance UA to the heat capacity rate C_i. What NTU defines is the non-dimensional heat transfer size or thermal size of the heat exchanger, and it is a common parameter to describe and compare the performance of exchangers for the same application.

$$\text{NTU}_i = \frac{UA}{C_i} \tag{3.8}$$

Since dimensional analysis proves that the temperature effectiveness P only depends on the three parameters shown in Equation 3.7 , expressions for predicting temperature effectiveness can be obtained for fixed flow arrangements like counterflow, parallel flow, cross flow, etc. Figures 3.4 and 3.5 show heat exchanger temperature effectiveness P plotted as a function of NTU for different values of R. From this comparison,

some important conclusions can be drawn. As mentioned before, flow arrangement plays a mayor role in the performance of heat exchangers. The temperature distribution in the counterflow flow configuration allows to achieve higher effectiveness for a given NTU and R levels than, for example, a cross flow construction. It is also evident that R has a large impact on the resulting effectiveness. This becomes less relevant for recuperator applications since the heat capacity of both flows is similar. Finally, it can be observed that the behavior of effectiveness vs NTU is not linear, and small increases in effectiveness closer to the 90% range require a large increase in NTU values.

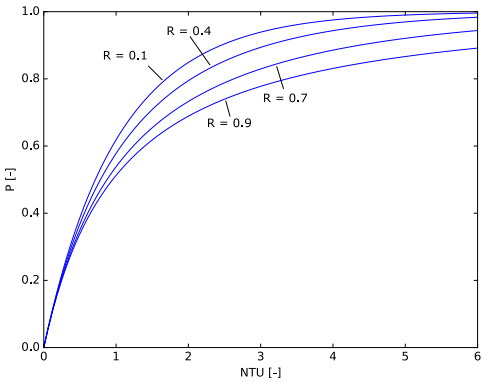

Figure 3.4: Temperature effectiveness as a function of the number of transfer units for various values of capacity ratio for a counter-flow heat exchanger [22]

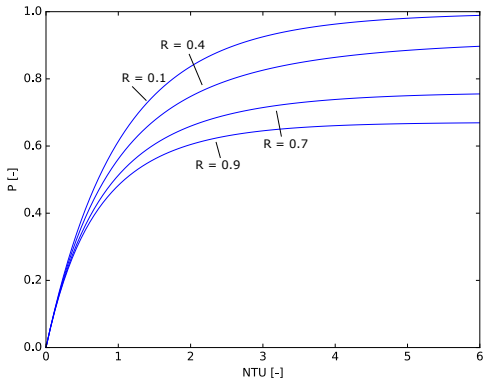

Figure 3.5: Temperature effectiveness as a function of the number of transfer units for various values of capacity ratio for a cross-flow heat exchanger with both fluids unmixed [22]

By calculating U and defining the heat transfer area A and flow arrangement, the effectiveness of the heat exchanger can be calculated. This means that if the boundary conditions of the heat exchanger as well as the geometry are defined, the thermal duty and the properties of both streams can be obtained.

3.2.3. Pressure loss estimation

Pressure losses in heat exchangers are also a design target, since they have a direct impact on the system that surrounds the unit. In case of the recuperated gas turbine cycle, pressure losses will have a negative impact on the system by increasing the power required by the compressor as well as reducing the amount of power than can be extracted from the turbine. Therefore, proper estimation of the pressure losses in the recuperator is needed in order to understand the performance of the whole system.

Before outlining the theory behind pressure loss estimation in heat exchangers, a series of assumptions need to be stated. These assumptions are:

- Flow is steady and isothermal, and fluid properties are time independent.
- Fluid density is only dependent on the local temperature.
- The pressure at a point in the fluid is independent of direction. When shear stress is present, it is assumed as the average of normal stresses at the point.
- Body forces are only caused by gravity.
- Bernoulli equation is only valid along a streamline.
- Friction factor is considered as constant with passage flow length.

Pressure loss throughout the heat exchanger can be separated in three main components: entrance pressure losses, core pressure losses (related to momentum and friction losses) and exit pressure recovery (seen in

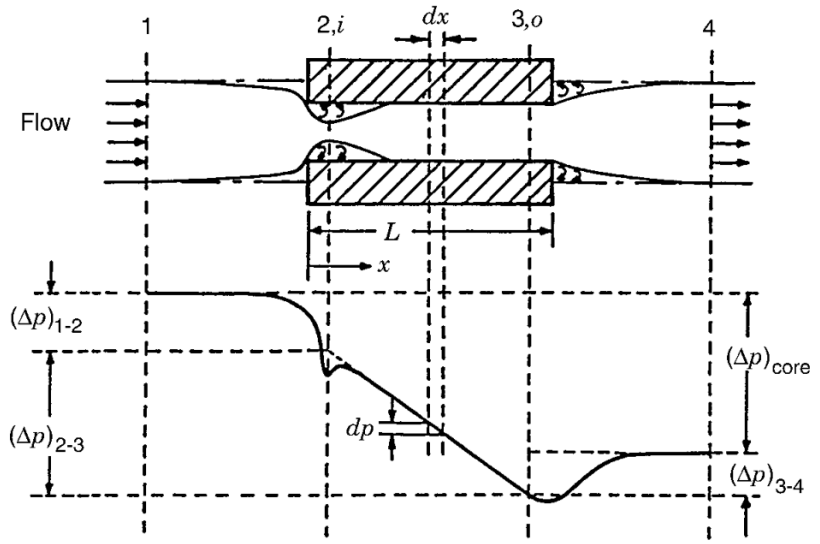

Figure 3.6: Pressure losses occurring through an exchanger unit [18]

Figure 3.6). The relative magnitude of each components depends on the flow conditions and heat exchanger geometry, but usually pressure losses occurring at the core are the largest contribution.

Core entrance pressure losses are driven by two mechanisms occurring at the inlet of the heat exchanger: the pressure drop due to the area change and the pressure losses related to the flow expanding after the sudden area contraction. The pressure loss at the entrance caused by an area change for an incompressible fluid, is given by Bernoulli:

$$p_1 - p'_2 = \rho_i \left(u_2^2 - u_1^2\right) \tag{3.9}$$

where ρ_i is the the fluid density at the core inlet, and $p_2^{'}$ the static pressure as if only the area change losses would be taken into account. By introducing the continuity equation, and the concepts of free-flow/frontal area ratio $\sigma = \frac{A_{o,2}}{A_{o,1}}$, and core mass velocity $G = \rho_i u_2$, the pressure drop can be expressed as:

$$p_1 - p'_2 = \frac{G^2}{2\rho_i}(1-\sigma^2) \tag{3.10}$$

The second pressure loss $\Delta p_{loss,exp}$ occurring at the inlet is caused by the free expansion of the flow following a sudden contraction. These losses are taken into account by the contraction loss coefficient K_c, which is dependent on the area ratio σ as well as Reynolds number and geometry type (i.e. square or triangular surface profiles). These contraction coefficients are available in the form of tables in open literature (for example Kays and London [54]).

$$\Delta p_{loss,exp} = K_c \frac{G^2}{2\rho_i} \tag{3.11}$$

By adding the contribution of these two phenomena, the resulting pressure losses at the core entrance, shown in the first section of Figure 3.6 are:

$$p_1 - p_2 = \frac{G^2}{2\rho_i}(1-\sigma^2+K_c) \tag{3.12}$$

The same phenomena applies to the core exit phenomena (in this case pressure increases), with the only difference being the change in area ratios and the use of the expansion coefficient K_e instead of the contraction coefficient K_c. The resulting expression for the core exit losses, seen in the third section of Figure 3.6 is:

$$p_4 - p_3 = \frac{G^2}{2\rho_i}(1 - \sigma^2 - K_e) \tag{3.13}$$

The most important contributor to the pressure changes in the exchanger is the core itself, where losses due to momentum changes and friction occur. Figure 3.7 shows the force and momentum terms affecting a differential element (also shown in the middle section of Figure 3.6). From the differential element diagram, the inlet and outlet momentum terms can be seen, as well as the pressure surfaces acting in the inlet and outlet faces as well as the shear force acting on the complete element perimeter $\boldsymbol{P}$.

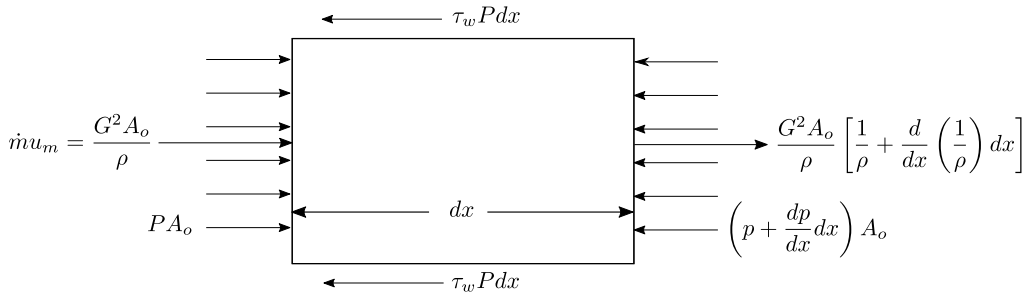

Figure 3.7: Force and momentum rate terms for a differential element of a heat exchanger core [18]

By applying Newton's second law on the differential element, we arrive to the following relationship:

$$G^2 A_o\left[\frac{1}{\rho} + \frac{d}{dx}\left(\frac{1}{\rho}\right)\right]dx - G^2 A_o = pA_o - \left(p + \frac{dp}{dx}dx\right) - \tau_w P dx \tag{3.14}$$

Arranging and simplifying:

$$-\frac{dp}{dx} = G^2\frac{d}{dx}\left(\frac{1}{\rho}\right) + \tau_w\frac{P}{A_o} \tag{3.15}$$

By using the Fanning friction factor f (introduced in Section 2.2), the concept of hydraulic radius $r_h = \frac{Ao}{P}$, and rearranging the terms we obtain:

$$-\frac{dp}{dx} = G^2\left(-\frac{2}{\rho^2}\frac{d\rho}{dx} + f\frac{1}{\rho r_h}\right) \tag{3.16}$$

By integrating Equation 3.16 from $x = 0$ (where $\rho = \rho_i, p = p_2$) to $x = L$ (where $\rho = \rho_o, p = p_3$), we obtain an expression for the pressure loss at the core:

$$p_2 - p_3 = \frac{G^2}{2\rho_i}\left[2\left(\frac{\rho_i}{\rho} - 1\right) + f\frac{L}{r_h}\rho_i\left(\frac{1}{\rho}\right)_m\right] \tag{3.17}$$

3.2.4. Heat exchanger cell method

The rating model of the recuperator was developed according to the cell method [**?**]. This method allows to model a network of heat exchangers by defining a linear system of equations based on aforementioned

P-NTU method relationships. Each heat exchanger in the network has its own independent surface area as well as overall heat transfer coefficient U.

The heat exchanger network selected to model the chosen topology is shown in Figure 3.8. The network consists of three heat exchangers: unit 1 operating in a crossflow configuration, unit 2 operating as a counterflow configuration, and unit 3 also a crossflow configuration. Each unit has its independent heat transfer surface area A_i and its independent overall heat transfer coefficient U_i. Hot and cold streams are noted by the subscripts h and c respectively. For each stream we can identify 4 different temperatures, one at the inlet od each heat exchanger and the final one at the outlet of the recuperator.

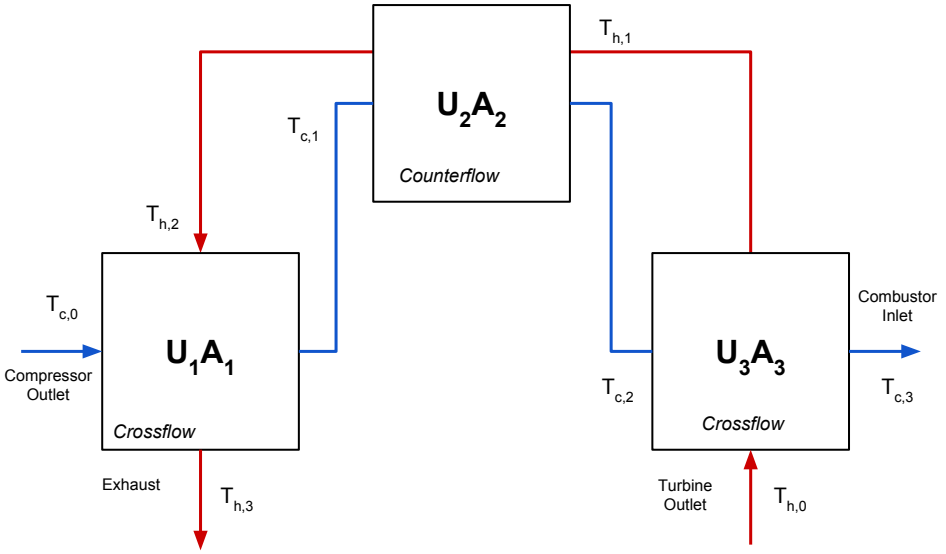

Figure 3.8: Heat exchanger network for the selected configuration

The only temperatures known are the compressor outlet temperature $T_{c,0}$ (cold stream flow going into the first unit U_1A_1) and the turbine outlet temperature $T_{h,0}$(hot stream flow going into the third unit U_3A_3). By using the concept of dimensionless temperature difference, we can obtain a total of $2n$ equations (n equations for each stream), with n being the number of cells in the heat exchanger network.

Following, the nomenclature in Figure 3.8, the equations for the cold and hot streams:

$$P_{c,1} = \frac{T_{c,1} - \boldsymbol{T_{c,0}}}{T_{h,2} - \boldsymbol{T_{c,0}}} \tag{3.18}$$

$$P_{c,2} = \frac{T_{c,2} - T_{c,1}}{T_{h,1} - T_{c,1}} \tag{3.19}$$

$$P_{c,3} = \frac{T_{c,3} - T_{c,2}}{\boldsymbol{T_{h,0}} - T_{c,2}} \tag{3.20}$$

$$P_{h,1} = \frac{\boldsymbol{T_{h,0}} - T_{h,1}}{T_{h,2} - \boldsymbol{T_{c,0}}} \tag{3.21}$$

$$P_{h,2} = \frac{T_{h,1} - T_{h,2}}{T_{h,1} - T_{c,1}} \tag{3.22}$$

$$P_{h,3} = \frac{T_{h,2} - T_{h,3}}{\boldsymbol{T_{h,0}} - T_{c,2}} \tag{3.23}$$

Note that the temperatures highlighted in bold, are known. Subsequently a system with six equations and six unknowns is obtained, since the dimensionless temperature value can be obtained from heat exchanger characteristics such as U, A and R.

While the heat exchanger geometry is know beforehand when performing a rating exercise, this is not the case for U and R due to their dependence of the fluid properties. Since fluid properties are dependent in temperature, an iterative solution procedure needs to be adopted. Initial guesses for the overall heat transfer coefficient U as well as the thermal capacity ratio R are used in order to calculate the first iteration. When the first iteration is completed, all the network temperatures are known, and new properties are obtained. New fluid properties lead to an updated U value, and updated network temperatures. The iteration is complete when convergence occurs in all of the temperatures in the network.

3.2.5. Estimation of overall heat transfer coefficient U

Obtaining a reliable estimate of the overall heat transfer coefficient U is a key step in building an accurate heat exchanger rating model. Recalling the definition of U:

$$U = \frac{1}{(\eta_f hA)_c} + \frac{\delta_w}{k_w A_w} + \frac{1}{(\eta_f hA)_h} \tag{3.24}$$

The key steps to calculate the overall heat transfer coefficient are:

- Obtain heat transfer coefficients h for cold and hot streams.
- In the case of extended heat transfer surfaces, obtain fin efficiency η_f
- Obtain conduction resistance given the geometry (δ_w,A_w) and thermal conductivity of the wall (k_w).

The heat transfer coefficient h is obtained by means of heat transfer correlations for the specific type of surface present on each side of the recuperator. These heat transfer correlations are usually obtained analytically for laminar flow in simple geometries (i.e. circular ducts) or obtained experimentally for more complex flow conditions and geometries such as the primary surfaces discussed in Section 2.2. Figure 3.9 shows an example of the Nusselt number behavior of several different CC and CW surfaces against Reynolds number.

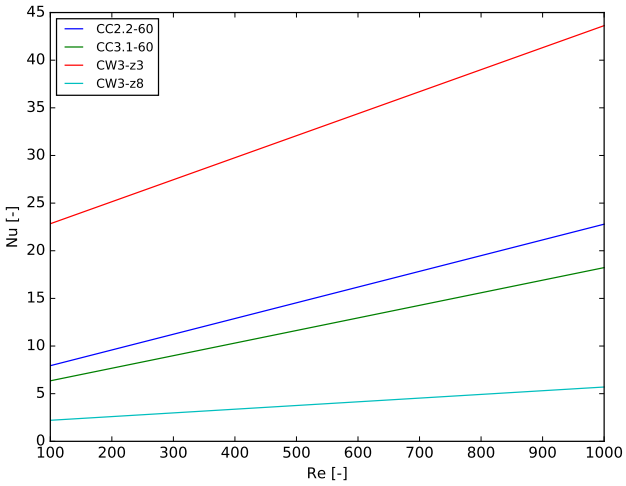

Figure 3.9: Nusselt number behavior vs Reynolds number for a number of CC and CW surfaces [23]

The effect of fin efficiency is also taken into account in the crossflow plate-fin sections of the heat exchanger configuration. While extended surfaces increase the effective heat transfer surface area and the heat transfer rate, the actual heat transfer coefficient is reduced due to the effects of conduction through the fin. This is essentially caused by the increasing temperature (i.e. temperature difference reduction) in the span if the fin (see Figure 3.11). The effects of the temperature gradient occurring in the fin are captured in a concept known as fin efficiency, and it is modeled by means of a thin fin idealization (shown in Figure 3.10).

The thin fin temperature distribution is described by the second order, linear, homogeneous ordinary differential equation shown below:

$$\frac{d^2\theta}{dx^2} + \frac{d(lnA_{k,x})}{dx}\frac{d\theta}{dx} - m^2\theta = 0 \tag{3.25}$$

where the distribution of $\theta(x)$ is:

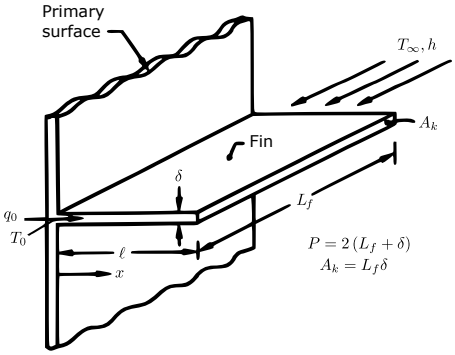

Figure 3.10: Straight thin fin [18]

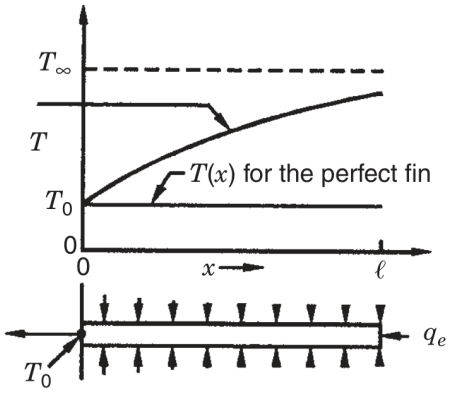

Figure 3.11: Temperature distribution comparison for a heating fin [18]

$$\theta(x) = T(x) - T_\infty \tag{3.26}$$

m is known as fin parameter and is defined as $m^2 = hP/k_f A_{k,x}$. This fin parameter will have a distinct definition for specific fin geometries.

Equation 3.26 can be solved by using different boundary conditions to define the temperature or heat transfer at the tip. By obtaining the temperature distribution throughout the fin, the actual heat transfer occurring in the fin can be calculated. The ratio of the actual heat transfer and the ideal heat transfer throughout the fin is called fin efficiency:

$$\eta_f = \frac{q_0}{q_{max}} \tag{3.27}$$

The definition of the boundary conditions for Equation 3.25 will affect the resulting expression for the fin efficiency. The most common boundary condition used for plate-fin surfaces is the adiabatic fin tip [18], which results in the following definition of the fin efficiency:

$$\eta_f = \frac{\tanh m\ell}{m\ell} \tag{3.28}$$

In the selected heat exchanger configuration, plain fins with rectangular cross sections were used. m and ℓ are defined in Equations 3.29 and 3.30, where b is the height of the plain fin. Figure 3.12 shows the relevant geometric features of a rectangular fin geometry.

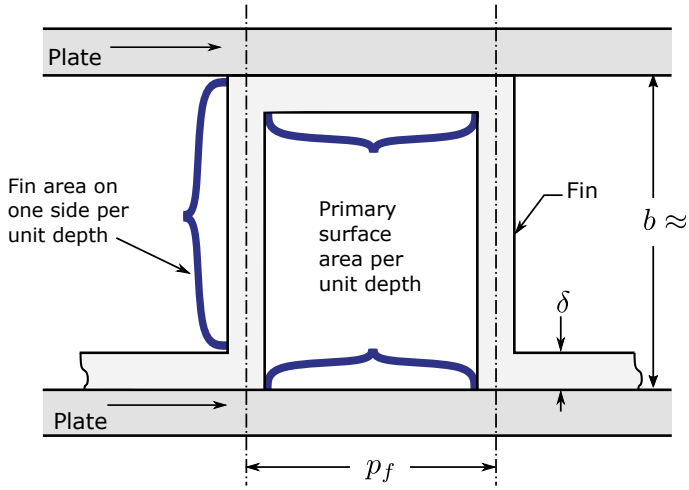

$$m = \left[\frac{2h}{k_f \delta}\left(1 + \frac{\delta}{L_f}\right)\right]^{1/2} \tag{3.29}$$

$$\ell = \frac{b}{2} - \delta \tag{3.30}$$

Figure 3.12: Rectangular fin geometric features

Finally the effect of the conductivity k_w of the heat exchanger walls needs to be taken into account to obtain the overall heat transfer coefficient. Different materials have a different thermal conductivity behavior, and they are dependent mainly on the temperature of the material. As mentioned in Section 2.3, material selection is dependent on the inlet temperature of the LP stream of the heat exchanger. The selection of the thermal conductivity value in the model was done assuming a maximum temperature of 700 ^{o}C for SS347. When the LP stream inlet temperature is above this limit, the properties of Inconel 625 are used. The thermal conductivity curves where obtained from open literature [24, 25, 55] The value of the thermal conductivity was set as a function of the average temperature of HP and LP. Further implications of material temperature limitations are addressed on Section 5.2.4.

3.2.6. Overview of the calculation procedure

An outline of the rating algorithm used to obtain heat exchanger performance is shown in Figure 3.13. The rating algorithm begins with the estimation of the total heat transfer area of the heat exchanger. The dimensions of the unitary cells are known, as well as the inner diameter of the recuperator, which determines the number of unitary plates used. The height of the primary surface corrugations determines the thickness of each unitary cell.

In order to perform the cell method calculations, an initial assumption for the overall heat transfer coefficient U for each of the heat exchanger sections is needed. This assumption is based on usual ranges for primary and extended surface gas-to-gas heat exchangers. Inlet temperatures are used in order to obtain the heat capacity ratios C_c and C_h for the initial iteration. Once U, A and C are known for each heat exchanger section, the cell method is used to calculate the resulting stream temperatures at each station.

After the first iteration of the cell method is completed, new fluid properties are obtained using the now known temperatures. These fluid properties as well as the pressure loss correlations for the different geometries are used to obtain pressure losses. Consequently, the new fluid properties are used to recalculate the overall heat transfer coefficient U.

This iteration continues until U values reach a certain tolerance value for each section in the heat exchanger. Finally the heat exchanger thermal duty, pressure losses and outlet temperatures are obtained, along with the secondary the geometric characteristics such as number of plates and inner/outer diameters. These secondary geometric characteristics will play an important role when dealing with the sizing procedure.

3.3. Sizing model

The main objective of the research project is to obtain GT turbine recuperator size from given flow boundary conditions, pressure loss and effectiveness targets. In order to do so, a sizing model needs to be developed. Sizing problems are more difficult compared to rating problems, since the geometry of a HEX involves many design parameters, whose definition is not unique. This means that different solutions to the heat exchanger design problem do exist. It is the task of the designer to identify the best one for the application under consideration.

To this purpose, the sizing problem of the recuperator is formulated as a constrained optimization problem where the objective function to minimize is the HEX volume, while the main constraints are the maximum pressure drop in the hot and cold streams combined, and the prescribed effectiveness. This formulation allows to find the smallest recuperator in the delimited design space that fulfills the required performance.

Naturally, the results of a sizing model built using a constrained optimization problem will be highly dependent on the selection of design variable bounds and constraint values. When requirements of an application become more detailed the design space can be reduced to obtain recuperator geometries that are more significant for the gas turbine at hand.

Special attention has to be placed on the pressure loss measure that is used within the optimization problem. Generally, when a fixed heat transfer surface is used (i.e. no changes to D_h), independent pressure losses for the HP and LP streams in a counterflow configuration are not feasible. For this reason, the sum of pressure losses in both circuits is used as the performance parameter. This assumption is reasonable at this stage of the design process, since the overall pressure losses in the HEX impact the system efficiency by reducing the power output of the turbine.

Geometry parametrization

In order to implement the optimization routine, the heat exchanger main geometry was parametrized using 4 design variables, shown in Figure 3.14. The design variables used are:

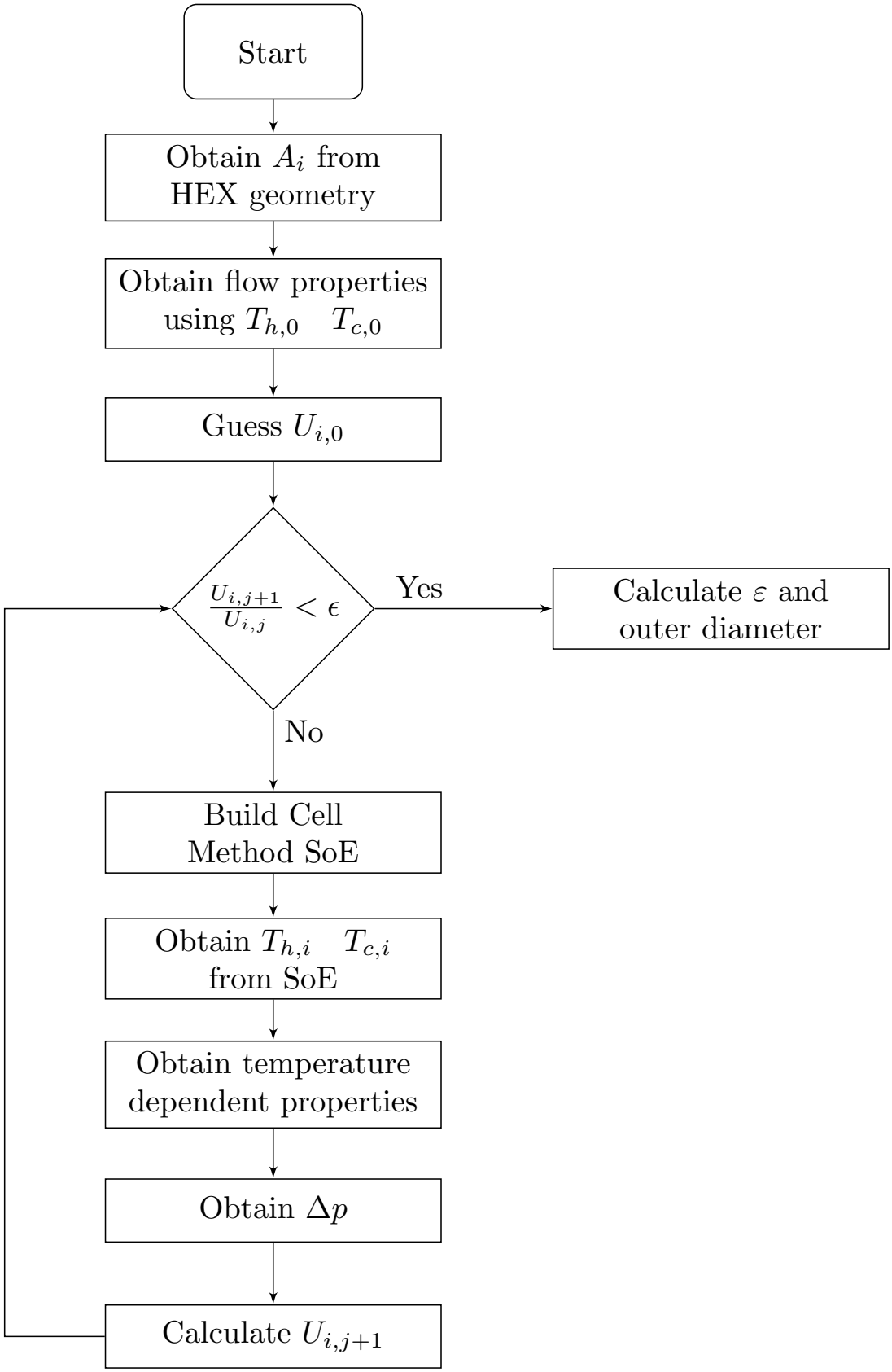

Figure 3.13: Flow diagram for rating algorithm

- x_1 - Recuperator overall length
- x_2 - Unit cell aspect ratio (b/c)
- x_3 - Unit cell height
- x_4 - Recuperator inner diameter

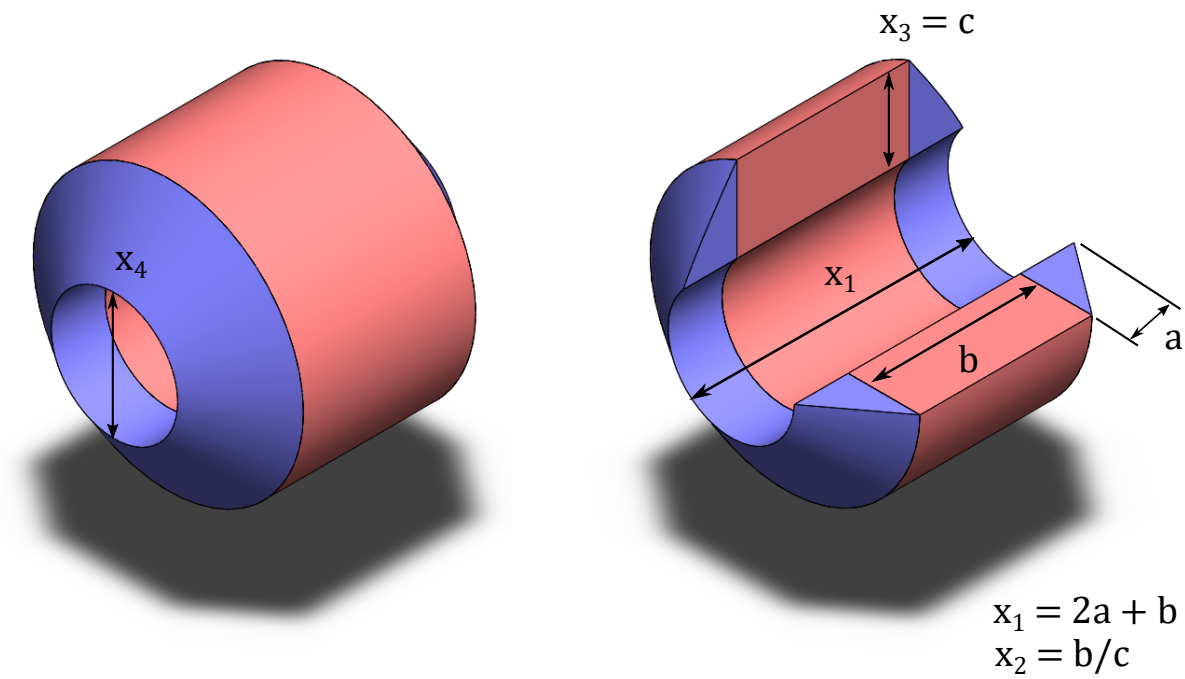

Figure 3.14: Annular heat exchanger geometry parametrization

The crossflow sections are taken as symmetric (also the case for the reference configuration) to improve manufacturing costs of the unit by reducing the number of unique parts.

Objective function

The recuperator volume was chosen as the objective function to minimize in the optimization procedure. Packaging constraints for the range extender concept are one of the most important challenges, and the recuperator is one of the main contributors to the overall unit volume. In addition to that, the weight of the unit is directly related on the resulting volume, specially when using heat transfer surfaces of similar geometric characteristics as well as a constant metal sheet thickness. Furthermore, the volume of the recuperator provides a meaningful relative measure of the unit cost. On a highly automated manufacturing process, unit costs would be close to 1.5 times the material cost [12].

The objective function reads:

$$\textbf{min} \quad f(x) \quad V_{\text{HEX}} = d_i(2a+b)(d_o - d_i) \tag{3.31}$$

where d_i and d_o are the inner and outer diameter of the annulus, respectively. Special attention needs to be placed on translating the plate height c, to the dimension $d_o - d_i$ since the annular construction features curved plates. The assumptions made to obtain the curve profile are shown in Appendix A.

Constraints

The selected set of equality and inequality constraints were formulated as follows:

$$g_1(x) = \varepsilon_{opt} = \varepsilon_{target} \tag{3.32}$$
$$g_2(x) = \Delta p_{opt} = \Delta p_{target} \tag{3.33}$$
$$g_3(x) = d_{o,opt} \leq d_{o,target} \tag{3.34}$$
$$g_4(x) = 0.15 \leq \left(\frac{a}{c}\right)_{opt} \leq 0.45 \tag{3.35}$$

Equations 3.32-35 represent the equality constraints for effectiveness and pressure losses. These constraints are formulated by means of equality constraints to ensure that the parameters used in the GT cycle (described in Section 5.1.1) are consistent in both models.The target pressure loss is defined as the total relative pressure loss of the HEX, thus:

$$\Delta p_{target} = \frac{\Delta p_c}{p_{c,in}} + \frac{\Delta p_h}{p_{h,in}} \tag{3.36}$$

Additional constraints, Equations 3.34, 3.35, related to the recuperator dimensions are introduced in the optimization procedure. The first one (Equation 3.34) is the resulting outer diameter of the recuperator. This dimension is important for the range extender packaging constraints, since low recuperator volume does not necessarily result in a feasible design. As the recuperator is placed around the combustion chamber, a unit that has a large frontal area and a short axial length may not be able to fit in the volume allocated for a range extender.

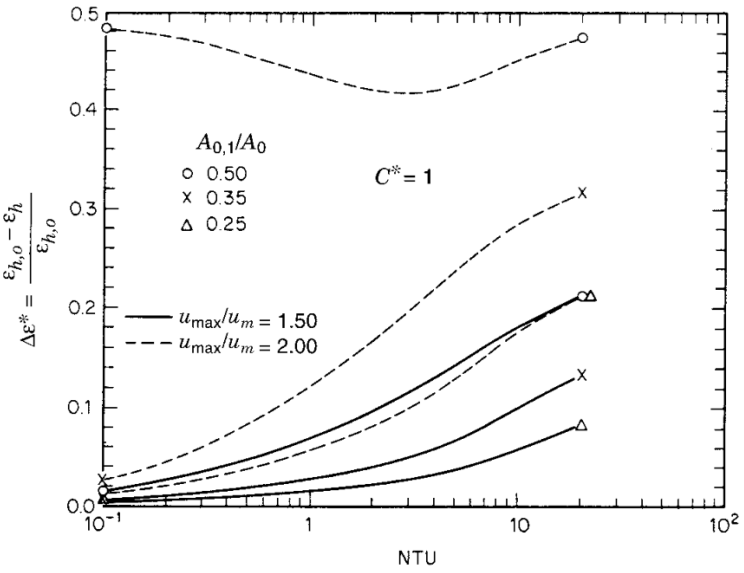

Figure 3.15: Impact of flow maldistribution on heat exchanger effectiveness [18]

Constrain $g_4(x)$ (Equation 3.35) concerns to the ratio between the width, a, and the height, c, of the crossflow sections of the exchanger . The aim of this constraint is to prevent the onset of flow distribution issues, which could significantly lower the actual recuperator performance. Since the optimization routine has the objective of reducing exchanger volume for a given performance, the crossflow section tends to be reduced in size, reducing the a/c ratio. One of the basic assumptions used in heat exchanger thermal design theory is the fact that the fluid is distributed uniformly throughout the heat transfer surfaces. Flow maldistribution can have a considerable impact on the effectiveness of the designed recuperator.

Figure 3.15 shows the performance deterioration as a function of NTU for a counterflow exchanger. The impact was obtained by dividing the exchanger in two subunits, and distributing flow to these two units by different amounts. The data was obtained for different amounts of maldistribution (25%, 35% and 50%) as well as two velocity ratios (1.5 and 2) u_{max}/u_{mean}. It is difficult to predict flow distribution issues when designing a heat exchanger at a system level, but the use of this constraint should prevent the onset of such a kind of problems if the admissible ratio is properly tuned. a/c ratio constrained between of 0.75 and 1.25 as a starting point, but further analysis is needed in order to obtain a proper geometric relationship for this two dimensions as a function of other operating parameters.

The values for the constraints and design variable bounds will be modified depending on the application for which a recuperator is being modeled. This difference will become clear when comparing the setup for the sizing model validation (200 kW application, discussed in Section 4.2.1) and the setup for the 30kW recuperator application discussed in Section 5.1.2. It is also important to stress the fact that the optimization routine is not being employed throughout the complete design space. The constrained optimization problem is only being used to obtain the set of design parameters that leads to the most compact recuperator for a given set of boundary conditions. In other words, the gas turbine cycle design is not being optimized in order to find an optimal solution for a given power output and system efficiency.

Sizing Model Workflow

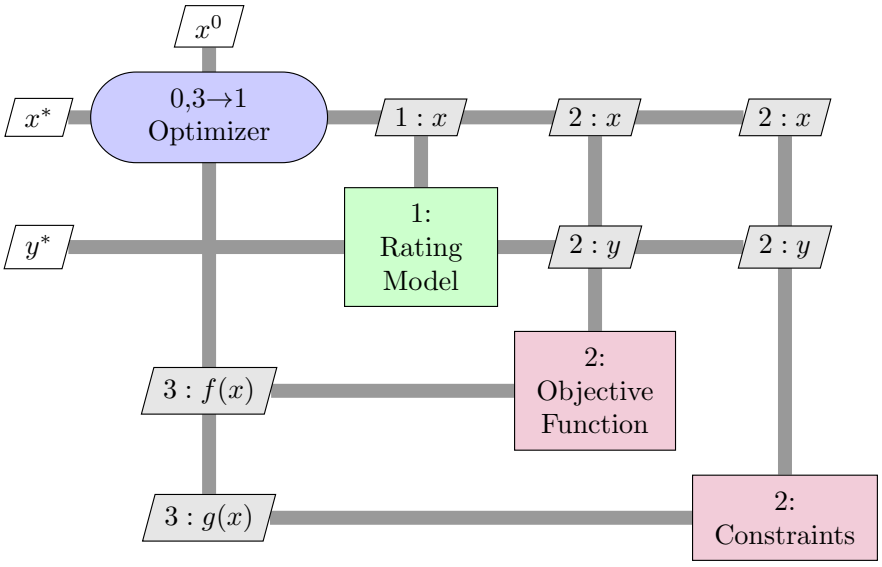

Figure 3.16: Design Structure Matrix for the Sizing Model

Figure 3.16 shows the workflow of the proposed sizing model. The diagram was built using the Design Structure Matrix conventions proposed by Lambe and Martins [56]. The model is built out of 4 main components: the optimizer, the rating model described in Section 3.2, the objective function and the constraints. The optimization method used is the gradient based on the Sequential Least Squares Programming implemented by Dieter Kraft [57]. This optimization scheme is available in the `SciPy` package [58] in Python. The low computational cost of the thermal design calculations allows for the use of this optimization scheme, which requires a large number of evaluations in order to obtain gradient data.

The element that contains all of the thermal and hydraulic calculations is the rating model, which used geometric data and boundary conditions to obtain recuperator performance. This recuperator performance, as well as the generated geometric data is used to evaluate the constraints $g(x)$, as well as the objective function $f(x)$. The order of execution is noted in the design structure matrix by the numbers that are above each of the blocks in Figure 3.16. The first step is to run the rating model with the initial design vector x^0, then the data that is generated is used in the objective and constraints functions. The value of these functions is

then fed returned the optimizer, to verify the feasibility of the current design vector. A local optimum is found when the optimality conditions are fulfilled, and the optimum design vector x^* along with the dependent variables at the optimum state y^* are stored.

4

Model validation

The current chapter covers the validation procedure for both heat exchanger models using published data. Section 4.1 shows the validation performed for the rating model, while Section 4.2 shows the validation for the sizing model.

A model validation was performed for both the heat exchanger rating and sizing models. The data used for verifying the rating and sizing models was published by Capstone Turbine as part of their development efforts for a 200 kW microturbine [8]. This project was funded by the DOE, and the published report contains detailed data about different recuperator geometries tested for this application. The validation procedure consists of two steps: performing rating calculations with the geometric data that is provided in the report to understand the differences in predicted performance, and perform a sizing procedure with the target performance and compare the resulting geometry with the reference dimensions. Heat exchanger characteristics such as exact primary surface geometry and plate-fin fin density are not stated in the report, adding a degree of uncertainty to the validation efforts. These shortcomings are addressed in the process.

4.1. Rating model validation

The first step in the rating model validation is to properly determine the boundary conditions at which the recuperator is operating. The heat exchanger was designed for the 200 kW Capstone microturbine. The design point operating conditions are shown in Table 4.1. The mass flow, the pressure ratio, the compressor outlet and turbine outlet temperatures will be used as boundary conditions for the recuperator. Of note is the difference between the actual gas turbine cycle power output (138 kW) and the 200 kW development target.

Table 4.2 shows the set of geometric parameters available for the model validation. The dimensions include the height C and length B of the counterflow section, the length A for the crossflow section, the number of unitary plates, the fin/primary surface spacing, as well as the inner and outer diameters. 20 different test cases (i.e. unique sets of dimensions and performance) in total were analyzed for validation purposes. A complete overview of the data used for model validation is available in Appendix B. The report also provides specific values for effectiveness and overall pressure loss, without describing the distribution of the losses on hot and cold sides.

The only information available regarding the heat transfer surface geometry besides the fin/primary surface spacing, is the type of primary surface (CW) as well as the fact that the hot side geometry fin spacing is twice the cold side geometry (seen in Figure 4.1). The height of the corrugations H was not specified, but it was obtained using the provided data of number of unitary plates, plate thickness and inner diameter. The amplitude and frequency of the waviness of the CW surface is not reported. For the crossflow section of the recuperator a fixed rectangular fin geometry was assumed, using the same height of the primary surface corrugations. The fin height was assumed equal to the fin spacing (i.e. square fins).

Table 4.1: Gas turbine design point operating conditions

Parameter [unit]	**Symbol**	**Value**
Power [kW]	P	138
Efficiency [-]	η	0.366
Mass flow [kg/s]	$\dot{m}$	0.981
Pressure ratio [-]	PR	3.58
Compressor efficiency [-]	η_c	0.815
Compressor outlet temperature [K]	T_3	443.59
Combustor inlet temperature [K]	T_4	918.15
Turbine inlet temperature [K]	T_5	1227.59
Turbine efficiency [-]	η_t	0.853
Turbine exit temperature [K]	T_{55}	950.92
Exhaust temperature [K]	T_6	524.82
Recuperator effectiveness [-]	ε	0.92
Recuperator pressure losses [-]	Δp_{HEX}	0.0192

Table 4.2: Sample geometric parameters used for rating model validation

No. of plates	**Fins/Meter [-]**	**C [m]**	**B [m]**	**A [m]**	**ID [m]**	**OD [m]**
223	511.8	0.265	0.222	0.041	0.448	0.800

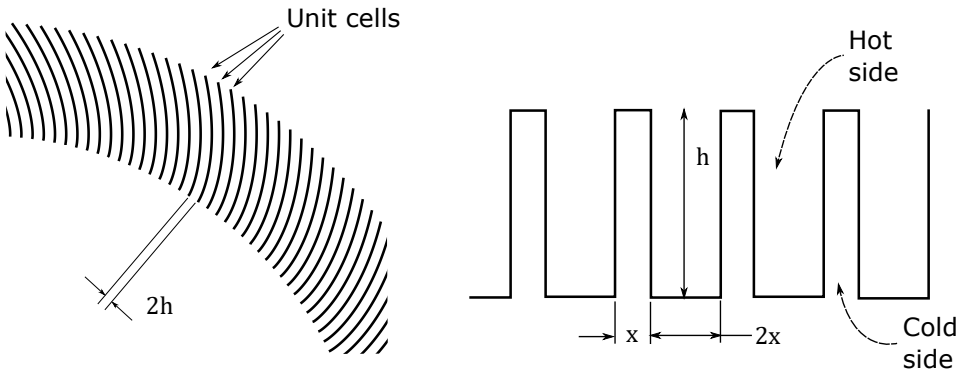

Figure 4.1: Geometric features available for model validation

In order to account for the lack of detailed information regarding the heat transfer surface geometries, the validation exercise was done using seven different published correlations for cross wavy surfaces, published by two different authors. The majority of correlations used come from the work of Utriainen [20], which carried out a numerical study to understand the impact of the waviness shape in surface performance. The six different geometries have the same frontal geometry (rounded, pitch-to-height ratio of 0.61). The differences lie in the period and amplitude of the waves in the axial direction. The remaining correlation used was published by Ting [59]. The pitch-to-height ratio of the researched geometry was 0.82. The pitch-to-height ratio of the available data in Capstone's report varies from 0.62 to 0.86 due to the fact that the fin spacing varies while the fin height is kept constant.

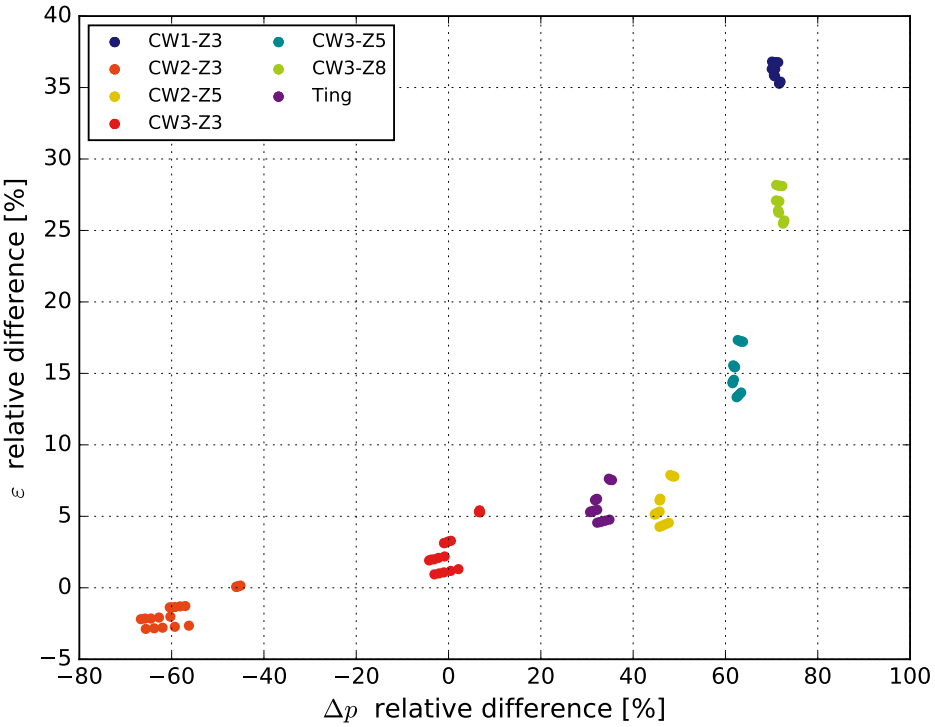

Figure 4.2: Relative difference for ε and Δp (Reference - model)/Reference

Figure 4.2 shows the resulting differences between the reported Capstone data with the performance predicted by the rating model. The 24 test cases are analyzed with the seven different heat transfer and pressure loss correlations. The effectiveness error ranges from -2 up to 32% approximately for all surface geometries. The error for both parameters was obtained by subtracting the calculated value from the reference data. Regarding the pressure losses, the errors in prediction range from -1.5% to 1.5% in absolute terms.

The heat transfer surface CW3-Z3 from Utriainen appears to have the most accurate recuperator performance prediction. The average relative differences in effectiveness and pressure loss are 2.7% and -2% respectively. The fact that this is the geometry that results in smaller errors is notable, since it shows the best performance in terms if j/f ratio on the study performed by Utriainen [23]. This supports the idea that the geometry implemented by Capstone has undergone sufficient analysis and optimization.

Figure 4.2 shows how the performance prediction error varies throughout the 20 test cases. Further analysis was done in order to understand possible root causes for the errors observed when data of a single surface geometry is observed. Figures 4.3 and 4.4 show the relative effectiveness errors plotted against unitary plate dimensions A and C. A clear correlation is seen between the error in effectiveness prediction and the dimension A. This is a sign that the accuracy of the sizing model's effectiveness is dependent on the ratio of crossflow area vs counterflow area. One possible cause for this is that the real flow orientation deviates slightly from an ideal cross-flow orientation (illustrated in Figure 4.5). In fact, as the air inlet for the cross-flow section moves towards the external part of the recuperator, the flow configuration between the hot and cold fluids becomes more and more of the counterflow type. The direction of the trend in Figure 4.3, seems to support this claim. This effect is not captured by the analytical models used in the rating procedure.

Overall, the rating model predictions have the required level of accuracy for the objective of this research project. The resulting effectiveness is constantly under predicted. This means that the model will provide a conservative estimate of the recuperator size. This is definitively acceptable in a conceptual study like the one at hand.

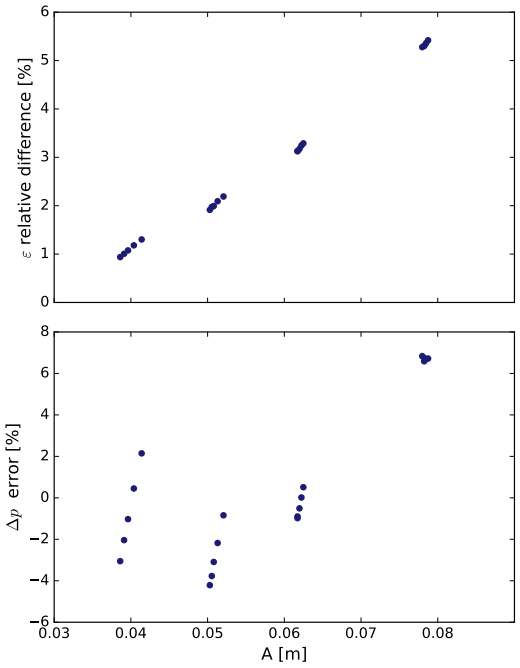

Figure 4.3: Effectiveness and pressure loss relative errors vs dimension A

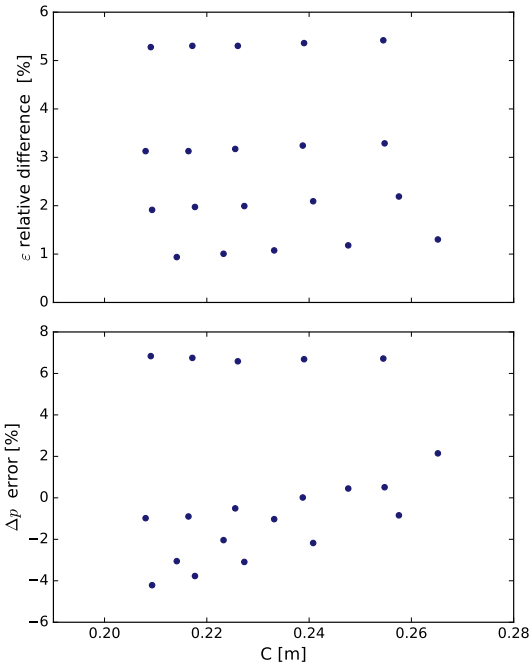

Figure 4.4: Effectiveness and pressure loss relative errors vs dimension C

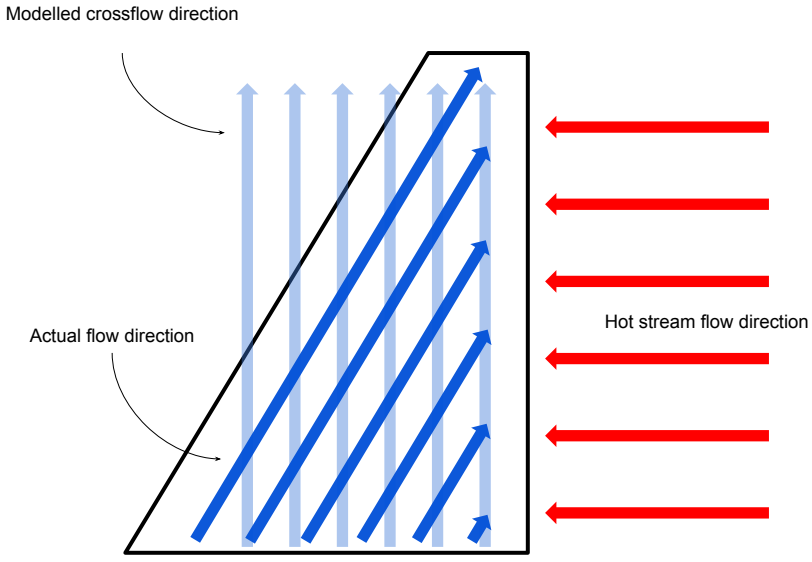

Figure 4.5: Difference between actual flow direction and modeled flow direction at headers

Finally, the validation of the rating model reinforces the idea that different geometries (like the sample used for validating this model, listed in Appendix B) can result in the same HEX performance. This idea is presented in the introduction of Section 3.3 and will become important for the rest of the analysis presented.

Table 4.3: Selection of design variable bounds and constraints for the sizing model validation

Design variable	Initial Value	Lower/Upper Bounds
HEX Length (x_1)	0.32	[0.20, 0.35]
C/B Ratio (x_2)	1.2	[1,1.5]
C (x_3)	0.3	[0.2,1.2]
Inner Diameter (x_4)	0.25	[0.2,0.30]
Maximum OD (from g_3)		0.35

4.2. Sizing model validation

4.2.1. Setup of sizing model validation

The validation for the sizing model was done by using the operating conditions of the Capstone recuperator reference before [8]. The boundary conditions and target performance are used to obtain heat exchanger geometries that are later on compared to the reference data. A key aspect to obtain meaningful results is the definitions of proper lower and upper bounds for the design variables as well as design constraints. These are:

- The outer diameter of the recuperator should be lower than 0.8 m.
- The aspect ratio C/B of the counterflow plate should be lower than 1.5.
- The recuperator length should not exceed 0.36 m.

Subsequently, design variable bounds and the values for the constraints to be applied in the sizing model for the 200 kW application are:

The aspect ratio C/B of the counterflow plate as well as the overall length were limited by defining bounds for design variables x_1 and x_2. The limit on the outer diameter conditions was met by using the inequality constraint $g_3(x)$ seen in Equation 3.34.

There is no specific mention of a constraint for the ratio of dimensions A/C , but the reported geometries indicate that a minimum ratio needs to be met in order to ensure proper flow distribution. For the purpose of this model validation, the admissible range for the A/C ratio was set from 0.15 to 0.45. Clearly this assumption has a large impact on the resulting geometries, and further work needs to be done when developing new applications to ensure proper flow distribution and compatibility with the layout of the turbomachinery.

4.2.2. Results of sizing model validation

Table 4.4 shows the comparison between the reference data and the dimensions obtained using the sizing model. The sizing model performed correctly, providing a recuperator geometry that fulfills the required effectiveness and pressure losses within the defined design space boundaries and constraints.

The generated recuperator volume is 6.59% larger than the reference model. This is consistent with the results from the sizing methodology validation, since the effectiveness was underpredicted. Figures 4.6 and 4.7 show the comparison of a unitary plate as well as the front view of the annular recuperator. From the comparison it can be observed that the crossflow headers have similar dimensions, while the overall length of the recuperator is similar. The front view clearly illustrates that the outer as well as the inner diameter are slightly smaller.

The constraint of the A/C dimension ratio is active, making the crossflow section as small as possible within the feasible design space. This is an indication that the resulting recuperator volume is highly sensitive to this parameter, and special attention needs to be placed in determining the factors that drive the required

Table 4.4: Geometric parameters for reference recuperator and sizing model results

Parameter	Reference	Sizing model
A [m]	0.041	0.037
B [m]	0.222	0.251
C [m]	0.265	0.251
OD [m]	0.800	0.779
ID [m]	0.448	0.424
Length [m]	0.305	0.327
C/B [-]	1.193	1
Volume [m^3]	0.090	0.097
Number of plates	223	212
Overall volume difference		+6.59%

size of the header inlets. The only variable in the design vector that is bounded is the C/B ratio at a value of 1. This limit was set for validation purposes only since the report does not state any lower boundary for this parameter.

Another important difference is the lower number of plates that is required. The sizing model geometry has 212 unitary cell plates, against the reference design, which has 223 plates. The difference in 11 plates comes from the fact that the sizing model results in a smaller diameter. The report states reasoning behind the selection of the inner diameter, but given the layout of the system, it is clear that it has to be large enough to accommodate the combustor. Since the heat transfer surface characteristics are kept constant, the thickness of each plate is also kept constant. The reduced number of plates could also be a subject of interest from the perspective of manufacturing costs.

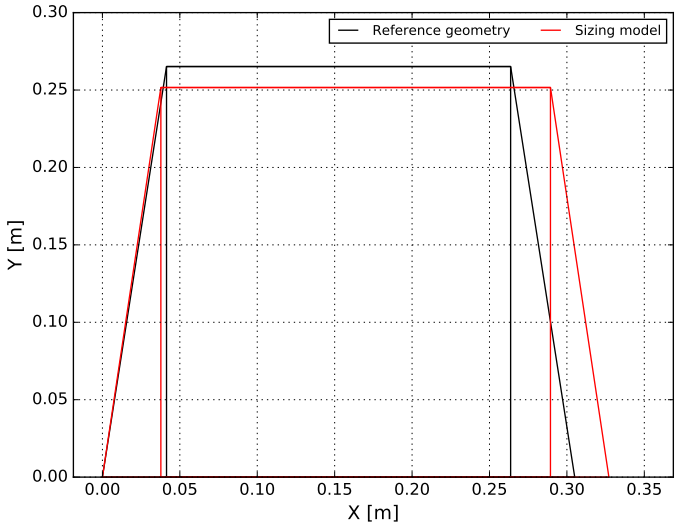

Figure 4.6: Comparison of unitary plate geometry between reference data and sizing model results

The comparison between the generated design and the reference data shows that the sizing model provides accurate results consistent with the conclusions drawn from the rating model validation. This is a sign that the implementation of the optimization scheme around the heat exchanger rating calculations was done correctly. Furthermore, when using this approach special care has to be put when defining the design vector bounds, the constraints as well as the initial guess for the design vector. As discussed before, the results are highly dependent on how the constraints are defined. Detailed analysis of the complete system (component layout, packaging, manufacturing, etc.) is required to obtain feasible designs by means of this methodology.

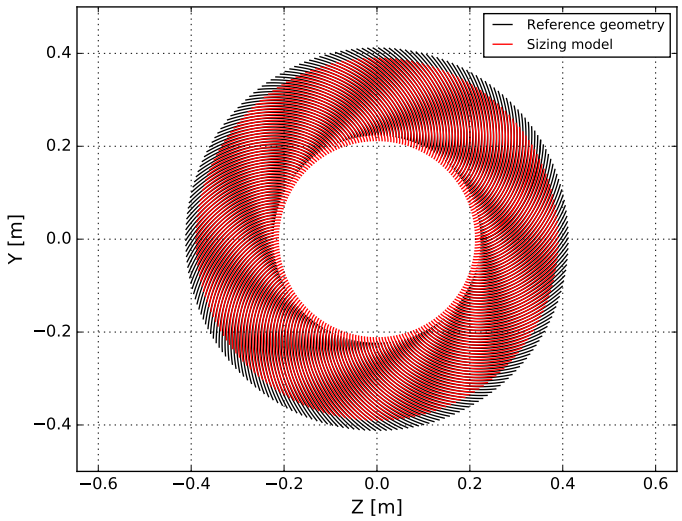

Figure 4.7: Comparison of recuperator front view between reference data and sizing model results

5

Parametric study

The following chapter covers the parametric study done to understand the impact of the design parameters of the gas turbine cycle on the recuperator dimensions. Notably, TIT, PR, turbomachinery component efficiencies, and allowable overall pressure losses in the recuperator. The influence of these design variables will be evaluated in terms of recuperator volume, weight and cost. The chapter starts with the description of the gas turbine model and then continues reviewing the explored design space. Afterwards the results of the analysis are discussed. These are organized in two different sections:the first one analyzes the impact of the different cycle parameters on the recuperator size for a given heat transfer surface of th CC type; the second one compares the impact on the recuperator design of different types of heat transfer surfaces.

5.1. Parametric study overview

5.1.1. Gas turbine cycle modeling

In order to relate the changes in gas turbine design parameters to heat exchanger dimensions, a recuperated turbine cycle is defined. The input parameters for the definition of recuperated Brayton cycle calculations target efficiency and power output, while the output of interest includes mass flow, temperature and pressure for both HP and LP streams as well as recuperator effectiveness. The change in design parameters of the gas turbine cycle has an impact on the design specifications of the heat exchanger, which will in turn affect the recuperator dimensions based on the sizing methodology.

The assumptions for the gas turbine cycle calculations are the following:

- The working fluid behaves like an ideal gas throughout the process. The working fluid before the combustion chamber is air, and the working fluid after the combustion process is treated as exhaust gases. The properties for both working fluids are assumed as temperature dependent only (consistent with the thermal design calculations).
- All calculations are done at design point operation, meaning the system is at steady state with constant component behavior.
- Pressure losses throughout the system as well as component efficiencies are maintained constant, regardless of design specifications for each component.
- There are not heat losses from any component of the system to the ambient (i.e. adiabatic).

The temperature-entropy diagram for the recuperated cycle and a schematic of the components and stations are shown in Figure 5.1.

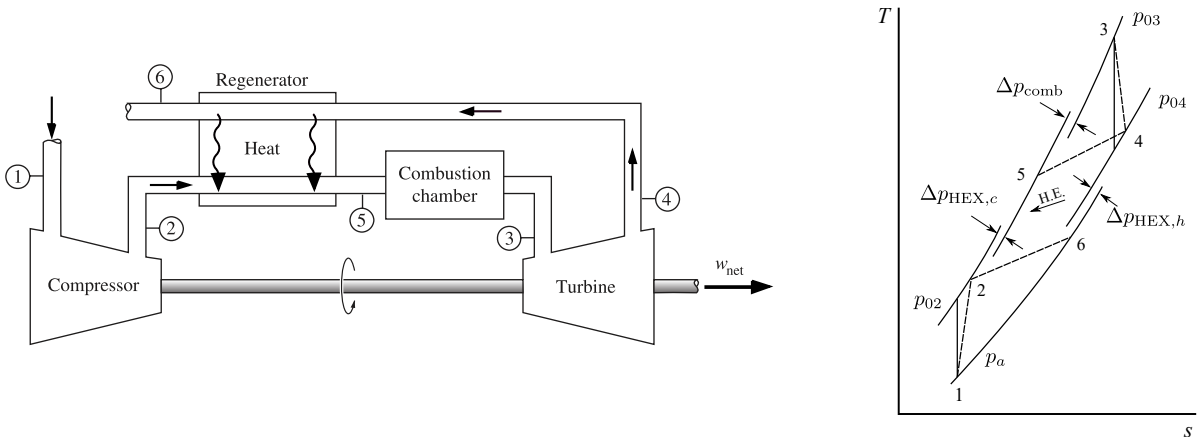

Figure 5.1: Recuperated Brayton cycle

The processes occurring in the recuperated cycle, with the corresponding compressible flow relations[1], are listed below:

1-2 Working fluid is compressed through the compressor.

$$T_2 = T_1 + T_1 \left[PR_c^{\left(\frac{\gamma-1}{\gamma}\right)/\eta_{comp}} \right] \tag{5.1}$$

$$p_2 = p_1 PR_c \tag{5.2}$$

2-5 Working fluid flows through cold side of the recuperator, increasing temperature and losing pressure.

$$T_5 = T_2 + \varepsilon \frac{\dot{m}_4 c_{p_{4,6}}}{\dot{m}_2 c_{p_{2,5}}} (T_4 - T_2) \tag{5.3}$$

$$p_5 = p_2 - \Delta p_{\mathrm{HEX},c} \tag{5.4}$$

5-3 Working fluid temperature increases through a combustion process. The mass of the burned fuel is added to the working fluid.

$$T_3 = T_5 + \frac{\dot{m}_f \, \eta_{comb} \, LHV}{\dot{m}_3 \, c_{p_{5,3}}} \tag{5.5}$$

$$p_3 = p_5 - \Delta p_{comb} \tag{5.6}$$

$$\dot{m}_5 = \dot{m}_3 + \dot{m}_f \tag{5.7}$$

3-4 Working fluid is expanded through the turbine.

$$T_4 = T_3 - T_3 \eta_{turb} \left[1 - \left(\frac{1}{PR_t} \right)^{\gamma - 1/\gamma} \right] \tag{5.8}$$

$$p_4 = \frac{p_3}{PR_t} \tag{5.9}$$

$$PR_t = \frac{p_3}{p_1 + \Delta p_{\mathrm{HEX},h}} \tag{5.10}$$

4-6 Working fluid flows through hot side of the recuperator, decreasing temperature and losing pressure.

$$T_6 = T_4 - \varepsilon \frac{\dot{m}_2 c_{p_{2,5}}}{\dot{m}_4 c_{p_{4,6}}} (T_4 - T_2) \tag{5.11}$$

$$p_6 = p_4 - \Delta p_{\text{HEX},h} \tag{5.12}$$

Power output and system efficiency are defined as:

$$P_{out} = \eta_{mech}\left[\dot{m}_3 c_{p_{3,4}}(T_3 - T_4)\right] - \dot{m}_1 c_{p_{1,2}}(T_2 - T_1) \tag{5.13}$$

$$\eta_{sys} = \frac{P_{out}}{\dot{Q}_{in}} = \frac{P_{out}}{\dot{m}_f LHV} \tag{5.14}$$

The main objective of the parametric study is to understand the impact of the different system design parameters on the required heat exchanger characteristics. To this purpose, a overall target system efficiency as well as a system power output were fixed. These fixed parameters are termed as target parameters.

The required mass flow to obtain the target power output can be calculated from the specific power of the gas turbine cycle. Given the definition of power output shown in 5.13, recuperator cold side mass is equal to:

$$\dot{m}_{c,i} = \frac{P_{out}}{c_{p_{3,4}}(T_3 - T_4) \; - c_{p_{1,2}}(1 + \dot{m}_f)(T_2 - T_1)} \tag{5.15}$$

The required effectiveness can be calculated by using the target system efficiency and turbine inlet temperature. First, the required thermal power from the combustor is calculated:

$$\dot{Q}_{in,eff} = \frac{P_{out}}{\eta_{comb}\eta_{sys}} \tag{5.16}$$

The target recuperator outlet temperature can then be obtained:

$$T_5 = T_4 - \frac{\dot{Q}_{in,eff}}{\dot{m}_5 c_{p_{5,4}}} \tag{5.17}$$

Once the recuperator cold side outlet temperature T_5 is known, Equation 5.3 can be used to obtain the required recuperator effectiveness.

Figure 5.2 shows a schematic view of the workflow of the parametric study, where the relationship between all previous aspects is seen.

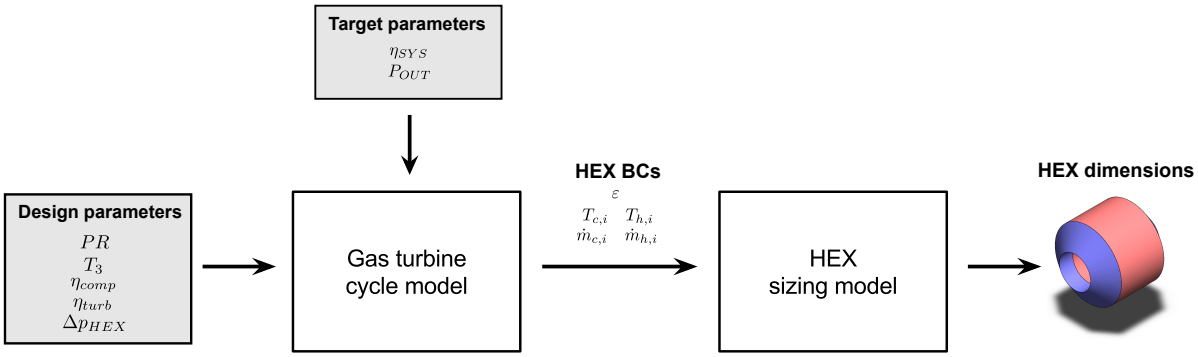

Figure 5.2: Schematic for parametric study components

[1] Double subscripts indicate average properties between two flow stations.

5.1.2. Parametric study design space

The design parameters varied in the sensitivity are shown in Table 5.1. The total number of different heat exchanger geometries obtained is 540.

Table 5.1: Independent gas turbine cycle design parameters

Parameter [Unit]	Symbol	Min.	Max.	Number of levels
Compressor pressure ratio [-]	PR_c	2.5	5	6
Turbine inlet temperature [K]	T_3	1000	1300	4
Compressor isentropic efficiency [-]	η_{comp}	0.77	0.83	3
Turbine isentropic efficiency [-]	η_{turb}	0.80	0.86	3
Overall recuperator pressure losses [-]	Δp_{HEX}	0.03	0.10	3

Additional assumptions for losses and efficiencies of the gas turbine cycle are shown on Table 5.2. All of these parameters are kept constant in the parametric study.

Table 5.2: Additional assumptions for losses and efficiencies

Parameter	Symbol	Value
Combustion pressure losses [-]	Δp_{comb}	0.02
Combustion efficiency [-]	η_{comb}	0.98
Mechanical (Bearing) efficiency [-]	η_{mech}	0.98
Ambient heat losses [W]	$\dot{Q}_{amb}$	$\dot{Q}_{in}$

The design variable bounds and constraints for the this analysis were set as follows:

The selection of this bounds were made based on the packaging requirements that have been preliminary set for the current design. Refinement of the design space delimitations is easily implemented when detailed information of the application becomes available.

In addition to the set of design parameters shown in Table 5.1, 8 different heat transfer surface geometries will be analyzed, 6 cross-corrugated geometries and 2 cross-wavy. The heat transfer and pressure loss correlations used in the parametric study were published by Utriainen [23]. The set of 8 heat transfer surface geometries feature the same hydraulic diameter. The Nusselt number and Fanning friction factor correlations have the following linear form:

$$Nu = C_1 + C_2 Re \qquad fRe = C_3 + C_4 Re \tag{5.18}$$

The main design parameters of the 8 heat transfer geometries are shown in Table 5.4. The acronym used to indicate the different test cases varies depending on the characteristics of the recuperator heat transfer surface, which can be of the CC and CW type. The figures after the abbreviation refer to pitch-to-height ratio and the phase angle between corrugated plates. In case of the first geometry in Table 5.4 the pitch-to-height

Table 5.3: Selection of design variable bounds and constraints for 30 kW application

Design variable	Initial Value	Lower/Upper Bounds
HEX Length (x_1)	0.20	[0.06, 0.42]
C/B Ratio (x_2)	0.88	[0.4,1.3]
C (x_3)	0.11	[0.022,0.25]
Inner Diameter (x_4)	0.170	[0.12,0.28]
Maximum OD (from g_3)	0.45	

ratio is 2.20 and the phase angle is 60°. In the case of a CW surface, the first number identifies the corrugation pitch and the second the shape of the waviness see [20].

Table 5.4: Heat transfer surface geometric characteristics

Type	Name	Pitch [mm]	Height [mm]	P/H [-]
CC	CC2.2-60	2.36	1.07	2.22
CC	CC2.2-75	2.36	1.07	2.22
CC	CC3.1-60	2.86	0.93	3.06
CC	CC4-45	3.48	0.87	4.00
CC	CC4-60	3.48	0.87	4.00
CC	CC4-75	3.48	0.87	4.00
CW	CW3-Z8	1.38	2.28	0.61
CW	CW3-Z3	1.38	2.28	0.61

The corresponding Nusselt number and Fanning friction factor coefficients are shown in Table 5.5. The coefficients for the CC surfaces originate from the experimental work of Stasiek et al. [44], while the CW coefficients were taken from Utriainen [20]. The reported data was fitted by Utriainen using the linear expression shown in Equation 5.18, which showed a good correlation to the data with R^2 values above 98% for all the surfaces. The fitting was done using only the reported data for $Re \leq 1000$, namely only for the laminar regime. The lowest Reynolds number at which transition occurred in the experimental data set was observed close to 1000, for a corrugation angle of 75°. The author also reported that transition occurred at higher Reynolds number when the corrugation angle was decreased. Notice that the typical Re is generally low given the small hydraulic diameter of the channels of this type of HEX.

Table 5.5: Heat transfer and pressure loss correlations

		Nu		fRe	
Type	Name	C_1	C_2	C_3	C_4
CC	CC2.2-60	6.2884	1.65E-02	28.302	3.95E-02
CC	CC2.2-75	8.8038	2.31E-02	38.761	5.41E-02
CC	CC3.1-60	5.0307	1.32E-02	49.529	6.92E-02
CC	CC4-45	2.9241	7.66E-03	21.318	2.95E-02
CC	CC4-60	3.8988	1.02E-02	42.453	5.93E-02
CC	CC4-75	6.1107	1.48E-02	85.639	0.1362
CW	CW3-Z3	20.5256	2.31E-02	51.727	0.2524
CW	CW3-Z8	1.8194	3.88E-03	26.172	3.13E-02

5.2. Parametric study employing the CC 2.2-60 geometry

In this section, the impact of the main system design variables on the recuperator design for the geometry CC 2.2-60 is first analyzed.

5.2.1. Design space feasibility

Figure 5.3 shows the target recuperator effectiveness obtained from Equations 5.17 and 5.3 as a function of gas turbine cycle parameters. The plot shows all the design cases considered in the parametric study, highlighting in red those that resulted in a non-feasible recuperator. A design solution is deemed infeasible if:

- The required effectiveness is above 1, shown Figure 5.3 using dotted red line.
- The targeted heat exchanger effectiveness or pressure losses are not compatible with the constraints imposed by the application. For example, a higher frontal area leads to lower flow speed and lower

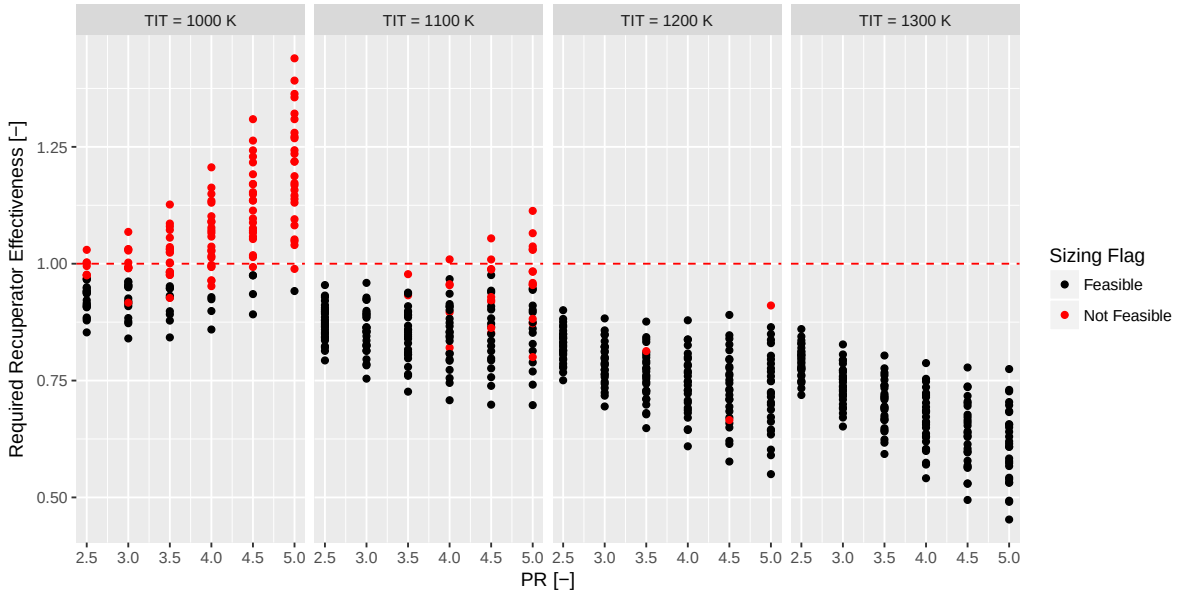

Figure 5.3: Required recuperator effectiveness of feasible and unfeasible design operating points

pressure losses but it can result in unfeasibly high outer diameter of the recuperator. Similarly, a too high target effectiveness is achievable only through a very large recuperator, which is not feasible within the design space.

The fact that some design parameter combinations results in unfeasible recuperator designs is completely dependent on the boundary conditions of the optimization problem. This underlines the importance of properly selecting constraints values in order to fully utilize the design space.

5.2.2. Single design point geometry

Before analyzing the trends that result from the variation of the different gas turbine design parameters, it is useful to review the geometry of a single set of design parameters. This set was selected due to its similarity with Capstone's C30 variant [8], implying that the required TIT and component efficiencies are achievable under the current state-of-art. The GT cycle has the following values for the design parameters:

Table 5.6: Independent and dependent design point cycle parameters

Parameter [Unit]	Symbol	Value
Compressor pressure ratio [-]	PR_c	3.5
Turbine inlet temperature [K]	T_3	1100
Compressor isentropic efficiency [-]	η_{comp}	0.77
Turbine isentropic efficiency [-]	η_{turb}	0.83
Overall recuperator pressure losses [-]	Δp_{HEX}	0.03
Target recuperator effectiveness [-]	ε	0.856
Cold side mass flow [kg/s]	$\dot{m}$	0.276
Hot side mass flow [kg/s]	$\dot{m}$	0.278
Cold side inlet temperature [K]	T_2	449
Hot side inlet temperature [K]	T_4	868

The resulting recuperator dimensions are shown in Figure 5.4. The left plot shows the frontal face of the annular recuperator, while the right plot shows the dimensions of a flat unitary cell (without the involute profile).

Table 5.7 shows relevant parameters for the resulting recuperator design.

Table 5.7: Relevant parameters for sample recuperator design

Parameter [Unit]	Symbol	Value
Inner diameter [m]	d_i	0.2800
Outer diameter [m]	d_o	0.3863
Crossflow section inlet width [m]	A	0.0158
Counterflow section length [m]	B	0.1101
Counterflow section height [m]	C	0.0633
Recuperator length [m]	L_{HEX}	0.1418
Recuperator volume [m^3]	V_{HEX}	0.0070
Recuperator material mass [kg]	m_{HEX}	11.1663
Number of unitary plates [-]	N_{plates}	380

From the resulting heat exchanger configuration a number of observations can be made:

- The shape of the crossflow section is completely determined by the constraint on the area ratio A/C, resulting in a value of 0.25. This is because the effectiveness of the crossflow section tends to be lower than that of the counter flow section. Thus, the optimizer tries to minimize the value of A. Moreover, the smaller the A/C ratio the higher the cross section of the counterflow part of the recuperator. This is beneficial to lower the pressure losses.
- The inner diameter d_i, a design variable, is also limited by its upper bound defined in the sizing model setup.
- 95% of the pressure losses occur on the gas side. This due to the adoption of the same hydraulic diameter for both the HP and LP streams. A better distribution of pressure losses by using independent hydraulic diameters on the gas and air side may lead to a smaller package for the same boundary conditions.

- The high number of unitary cells is caused by the large inner diameter, due to a larger length (i.e perimeter) divided in a constant plate thickness. This is not desirable for the heat exchanger design since the manufacturing process will involve a higher number of parts.

The selection of this particular recuperator design follows the definition of a set of GT cycle parameters that has been already implemented on a recuperated GT. However, this does not imply that the design referenced in Table 5.7 is in any way the optimal recuperator for the application at hand. The implications of determining an optimal recuperator geometry will be discussed in Section 5.4.

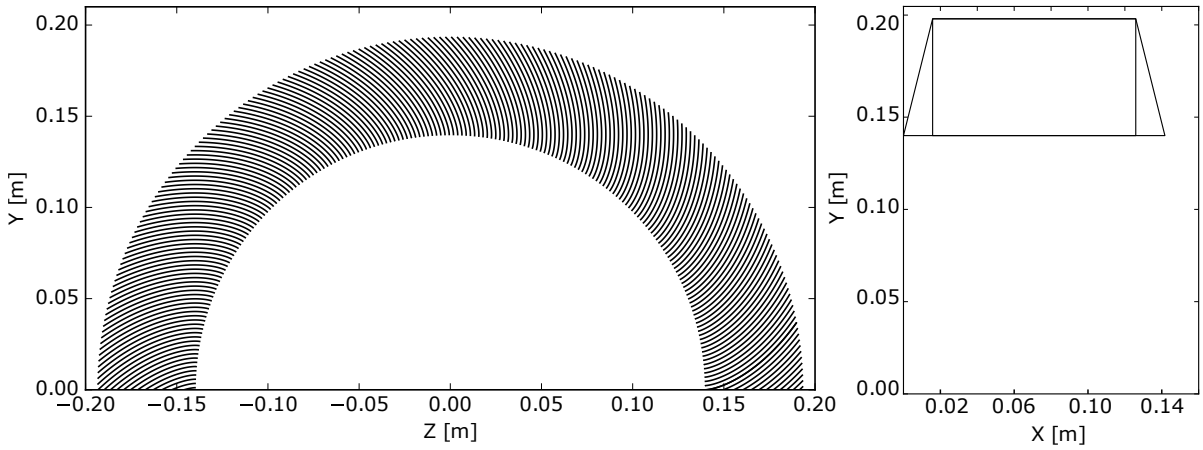

Figure 5.4: Resulting recuperator geometry for reference design cycle

5.2.3. Parameter impact on target heat exchanger effectiveness

In the current Section, the impact of the different design parameters on the required effectiveness can be now analyzed.

The following figures do not report design solutions for a TIT of 1000 K, since most of them were unfeasible. Figure 5.5 shows the target recuperator effectiveness as a function of pressure ratio PR, turbine inlet temperature TIT, as well as compressor and turbine isentropic efficiencies η_{comp},η_{turb}. For this exercise, the pressure losses throughout the recuperator are equal to 6% of the inlet pressure for each stream.

The following conclusions can be drawn from Figure 5.5:

- At a fixed PR, an increase in TIT, η_{comp} and η_{turb} always lead to a lower required recuperator effectiveness. This is mainly driven by the fact that the required thermal duty reduces if the conversion efficiency of the gas cycle increases.

- Cold inlet temperature of the recuperator increases with pressure ratio, while the opposite trend occurs for the inlet temperature of the hot fluid. The rate of change of these temperatures is dependent on the component efficiencies of compressor and turbine.

Figure 5.6 shows the effect of recuperator pressure loss on the recuperator target effectiveness. By increasing the allowable pressure loss, the pressure ratio of the turbine is reduced, consequently reducing the power output of the turbine. This will reduce the single cycle efficiency, which has to be compensated by a higher effectiveness of the recuperator. Figure 5.6 is shown at $PR = 3$, since the magnitude of the recuperator effectiveness change is very similar across different pressure ratios. The same can be drawn for the rest of the design parameters (TIT, η_{comp} and η_{turb}) shown in the Figure.

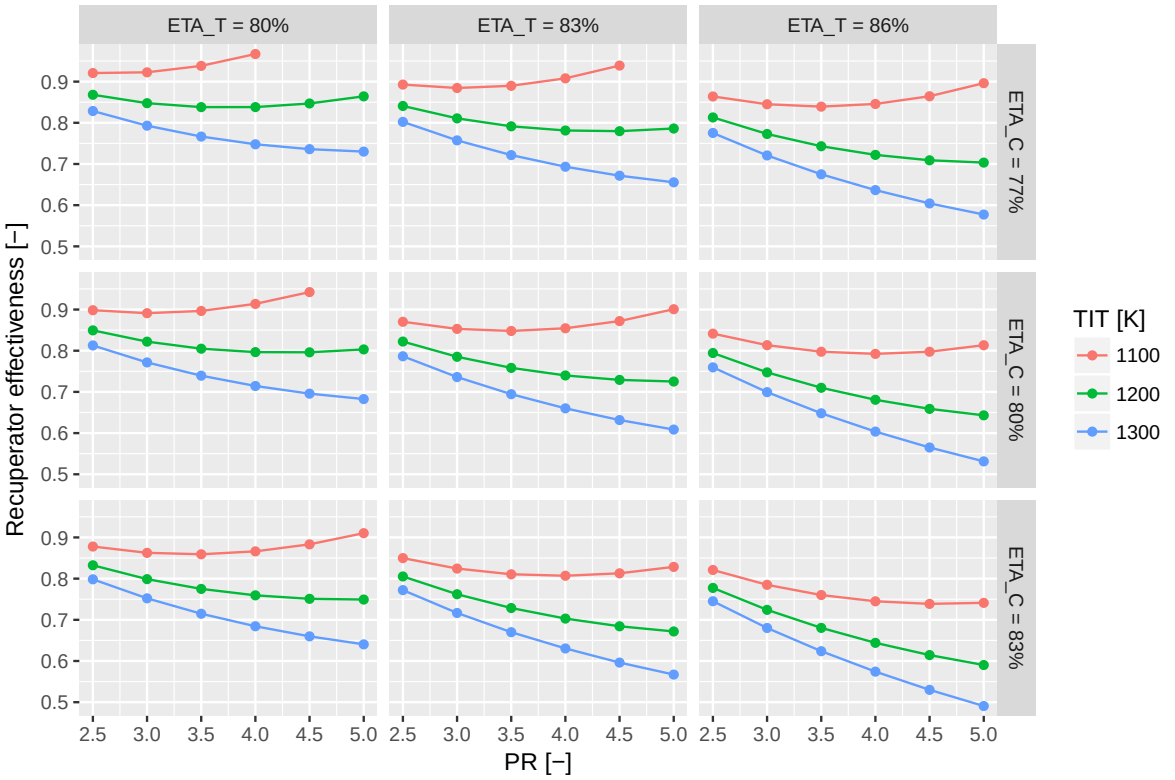

Figure 5.5: Target heat exchanger effectiveness as a function of gas turbine cycle design parameters

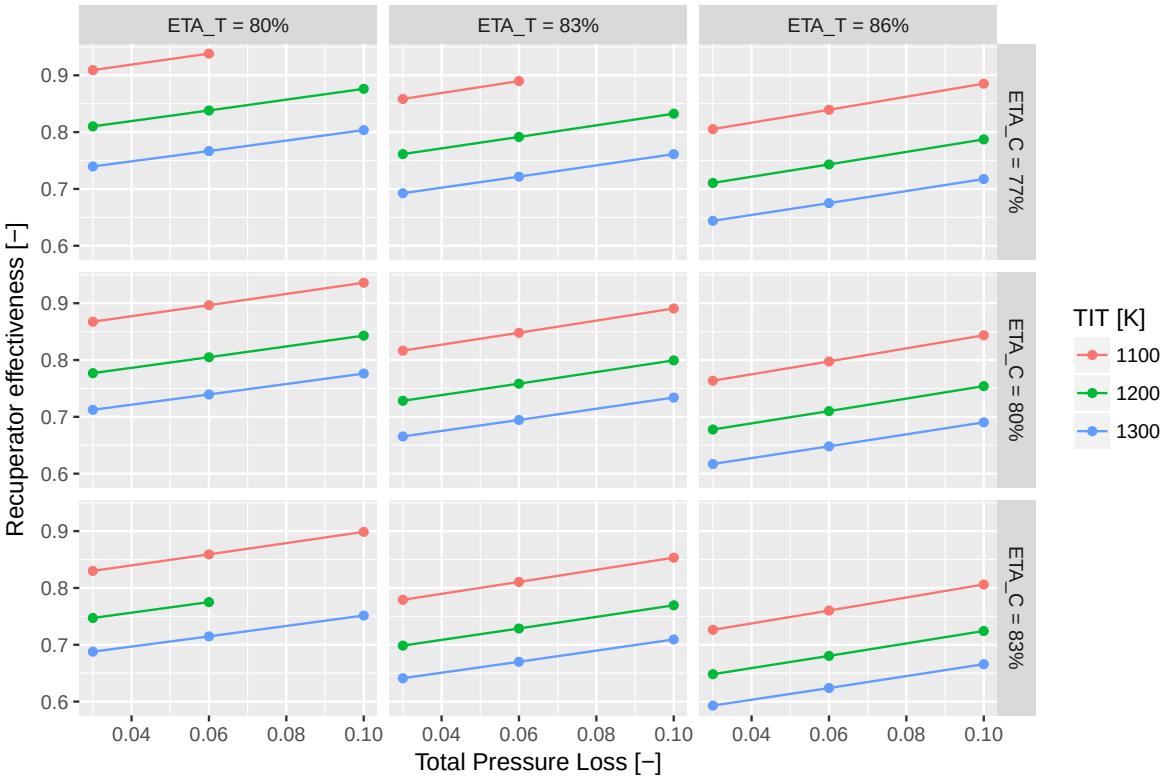

Figure 5.6: Target heat exchanger effectiveness as a function of total recuperator pressure loss for $PR = 3$

5.2.4. Parameter impact on heat exchanger size

The most obvious figure of merit to evaluate the effect of the GT cycle parameters on the recuperator size is the overall volume of the HEX. This parameter has the largest impact on the feasibility of the concept since it is closely related to the price and weight of the component.

Figure 5.7 shows the resulting recuperator volume as a function of different gas turbine cycle design parameters. All the reported design solutions have a relative pressure drop in the cold and hot stream equal to 6% of the inlet pressure. Again, the solutions with a TIT of 1000 K are not shown in the Figure because most of them are not feasible. As expected, the resulting recuperator volume increases exponentially at high target effectiveness values.

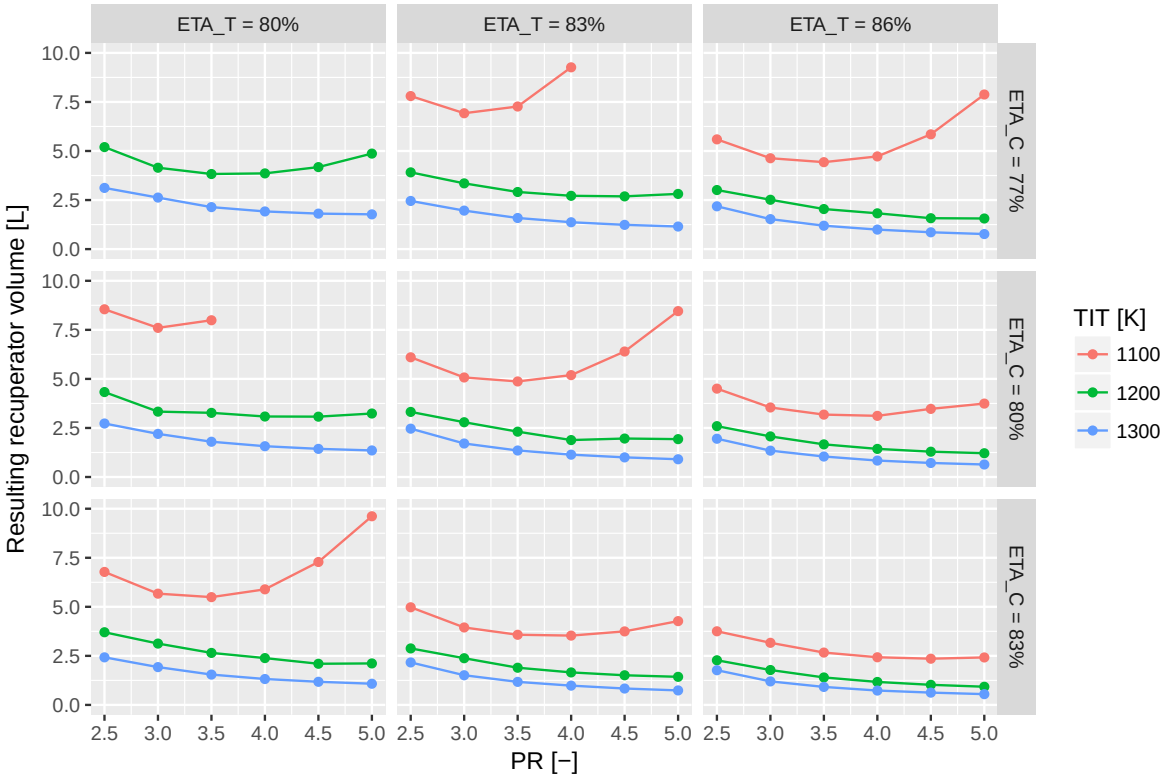

Figure 5.7: Resulting heat exchanger volume as a function of gas turbine cycle design parameters

From the current parametric analysis, it is difficult to isolate the influence of the required system mass flow and the targeted recuperator effectiveness on the recuperator volume. This is mainly due to the fact that specific power and simple cycle efficiency are closely related to the selected gas turbine design parameters. From the HEX design theory discussed in Section 3.2.1, it is expected that the recuperator volume increases linearly with mass flow (i.e. thermal duty $\dot{Q}$) for a given effectiveness level. The volume of the recuperator increases exponentially with effectiveness, as it can be inferred from the P-NTU relationships shown before.

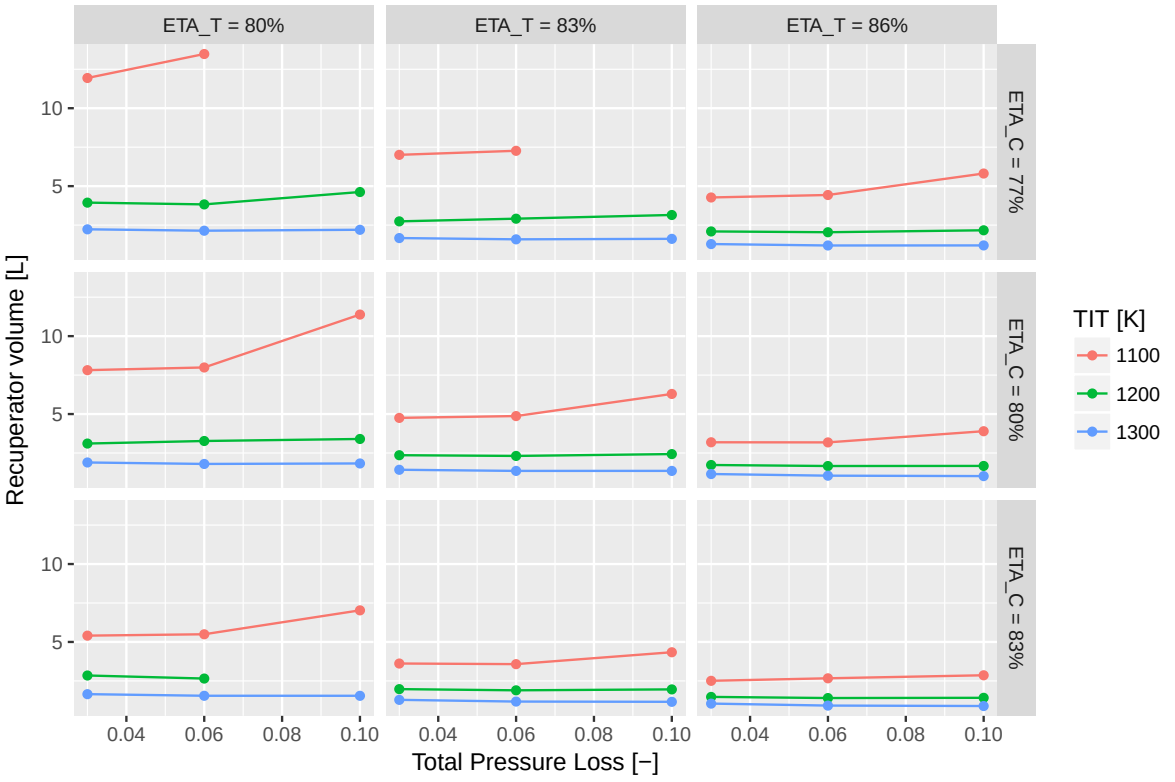

Figure 5.8: Resulting heat exchanger volume as a function of total pressure loss for a single PR

Figure 5.8 shows recuperator volume as a function of total pressure loss for different parameter combinations at a constant pressure ratio of 3.5. One interesting outcome that is apparent in this Figure, is that the increase in system pressure loss leads to a larger recuperator, while for a given fixed target effectiveness, increasing the allowable pressure losses always reduces recuperator volume. An increase in Reynolds number and consequently pressure losses, is caused by the reduction in frontal area. This phenomenon can be identified in Figure 5.9, which shows the resulting recuperator annular frontal area versus allowable pressure losses.

In this case, that higher pressure losses penalize cycle efficiency and they have to be compensated by a higher recuperator effectiveness. The required heat transfer area thus increases in spite of the more favorable heat transfer coefficients due to the higher speed of the fluids in the HEX. Furthermore, the impact in the recuperator volume by the system pressure losses varies with system mass flow. This fact can be identified by comparing the subplots with low component efficiencies with subplots with high component efficiencies in Figure 5.8. Figure 5.10 illustrates how the impact different pressure losses in recuperator volume increases with system mass flow.

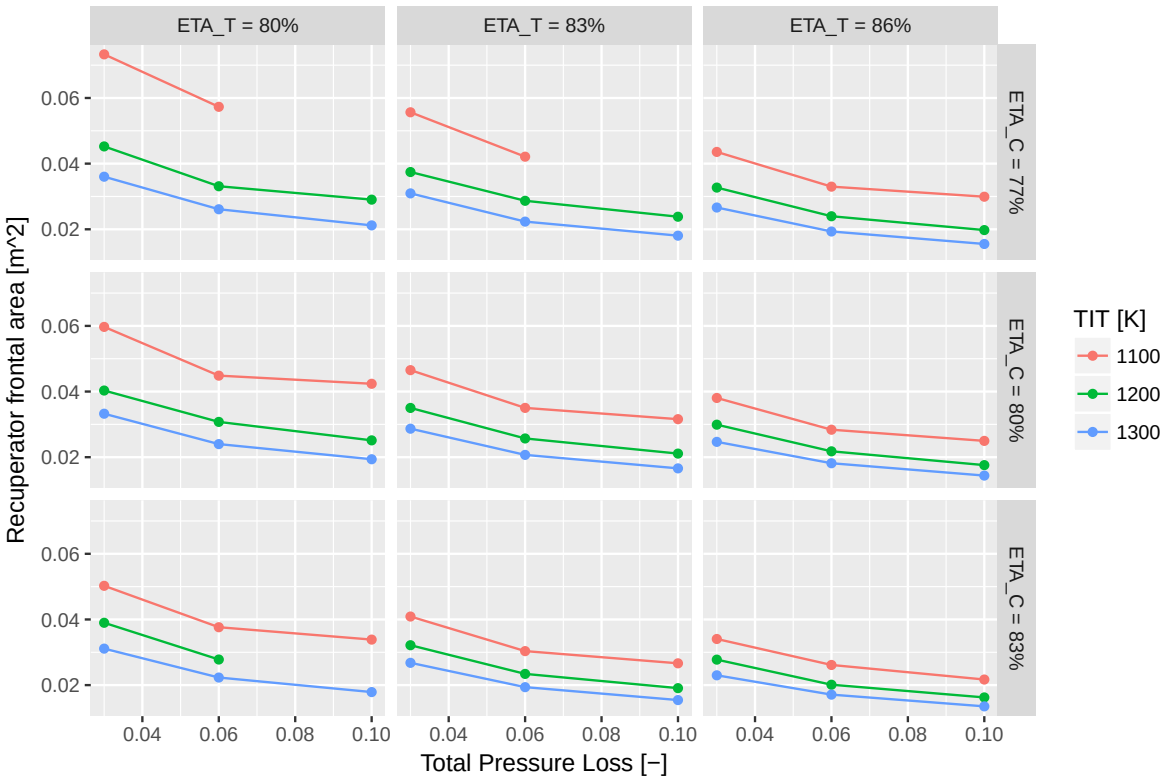

Figure 5.9: Resulting heat exchanger frontal area as a function of total pressure loss for a single PR

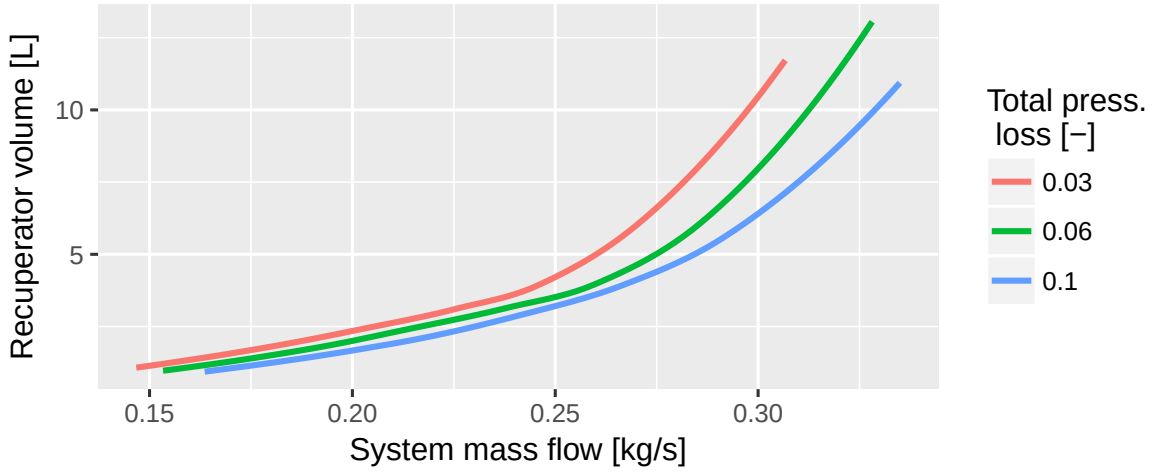

Figure 5.10: Heat exchanger volume as a function of system mass flow for different pressure losses

5.2.5. Recuperator weight and cost estimations

One of the advantages of employing a gas turbine as a range extender in comparison to other prime mover concepts, is the more favorable power-weight ratio. For this reason, the resulting recuperator weight plays an important role on determining which design is more suited for the range extender application.

It is important to highlight the limitations of the current procedure used to estimate the recuperator weight. Only the weight of the raw material of the recuperator is being estimated, based on the required heat transfer area of each recuperator section, the density of the required alloy and assuming a constant plate thickness. In reality, the plate thickness will be determined by the structural requirements of the recuperator, which in turn depend on the design specifications considered during the thermal design. The recuperator weight estimation could be improved by implementing preliminary mechanical stress calculations based on the pressure and temperature at which the unit is operating.

The input parameters used in the weight calculation are outlined in Table 5.8. Density values for stainless steel 347 and Inconel 625 are shown, since these were the two alloys considered in the analysis.

Table 5.8: Assumed input parameters for material volume and mass calculations [24, 25]

Parameter [Unit]	**Symbol**	**Value**
Primary surface plate thickness [mm]	$\delta_{\text{w,PS}}$	0.1
Fin thickness [mm]	$\delta_{\text{w,FIN}}$	0.06
Stainless steel 347 density [kg/m^3]	ρ_{SS347}	7970
Inconel 625 density [kg/m^3]	ρ_{IN625}	8440

Unit cost is a direct consequence of the recuperator mass, since at the moment this is estimated only based on the raw material costs. Also manufacturing will contribute to the cost of the recuperator, but it is difficult to how manufacturing costs do vary depending on the fins type or the HEX structure, which of the recuperator parameters would reduce manufacturing costs. The detailed design or even the construction of several prototypes are needed before a clear trend between manufacturing costs and HEX characteristics can be identified.

Since the cost of materials can vary significantly over time, the cost analysis in the parametric study was done in a relative basis,allowing to highlight the importance of material selection. The price of the stainless steel 347 is used as a reference value while the Inconel 625 is assumed five times more expensive than stainless steel [21]. The actual price ratio between these materials is subject to a lot of factors, but it has limited range of variation, which do not affect the conclusions of the present analysis.

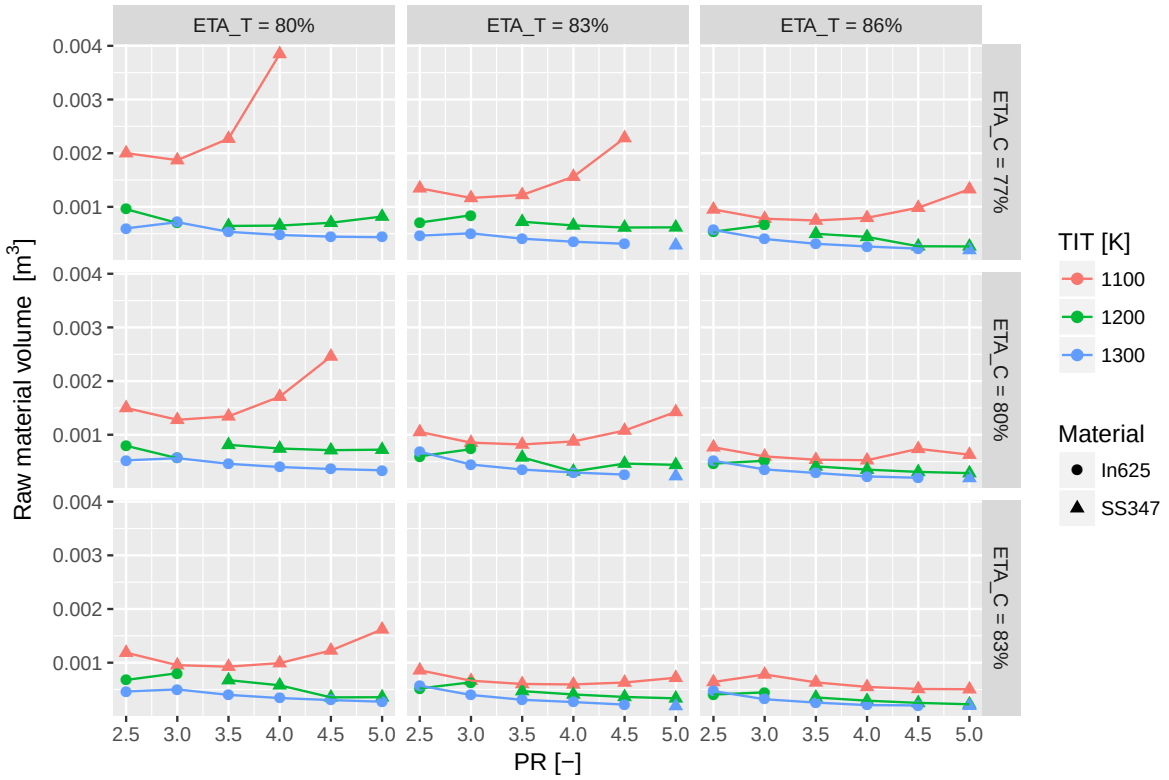

Figure 5.11: Heat exchanger material volume as a function of gas turbine cycle design parameters

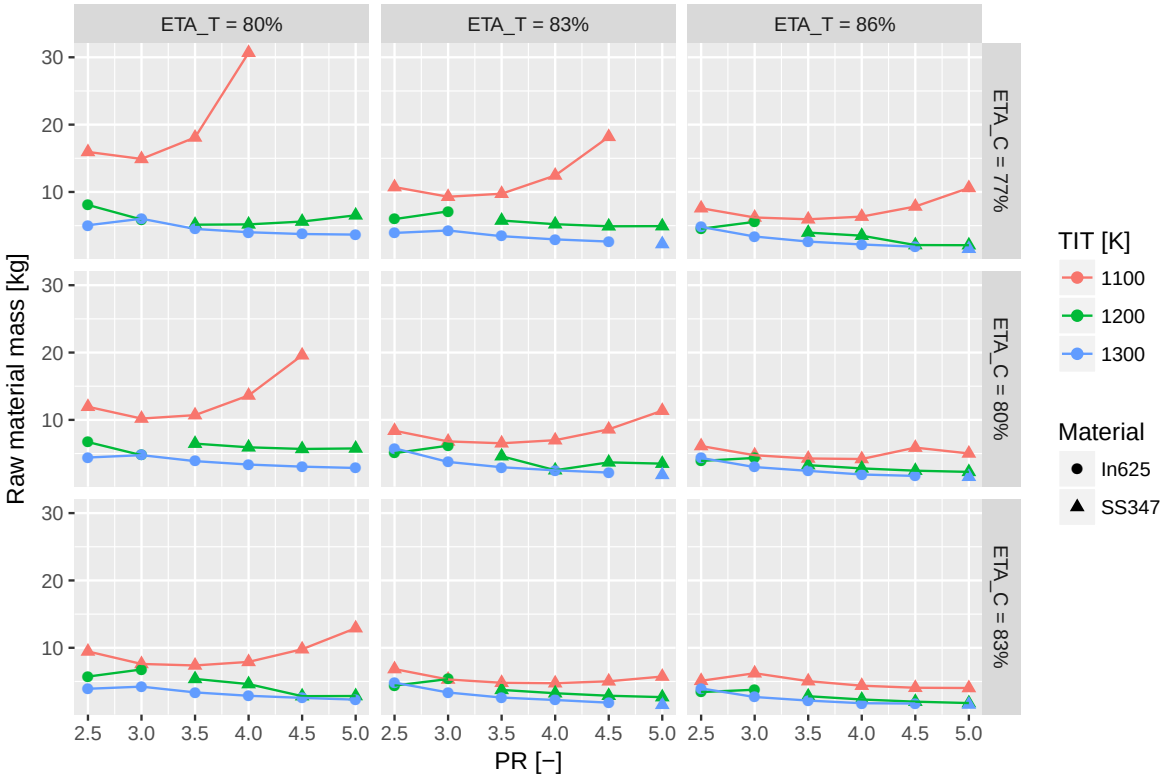

Figure 5.12: Heat exchanger weight as a function of gas turbine cycle design parameters

Figure 5.11 shows the resulting material volume of the recuperator as a function of different gas turbine

design parameters. When comparing this Figure with that for the recuperator volume, it can be noticed that there are small step changes in the trends for a given TIT. These small variations are caused by large step changes in outer and inner diameters seen in Figures 5.13, 5.14. This is caused by the non linear relationship of the diameters and the involute profile discussed in Appendix A.

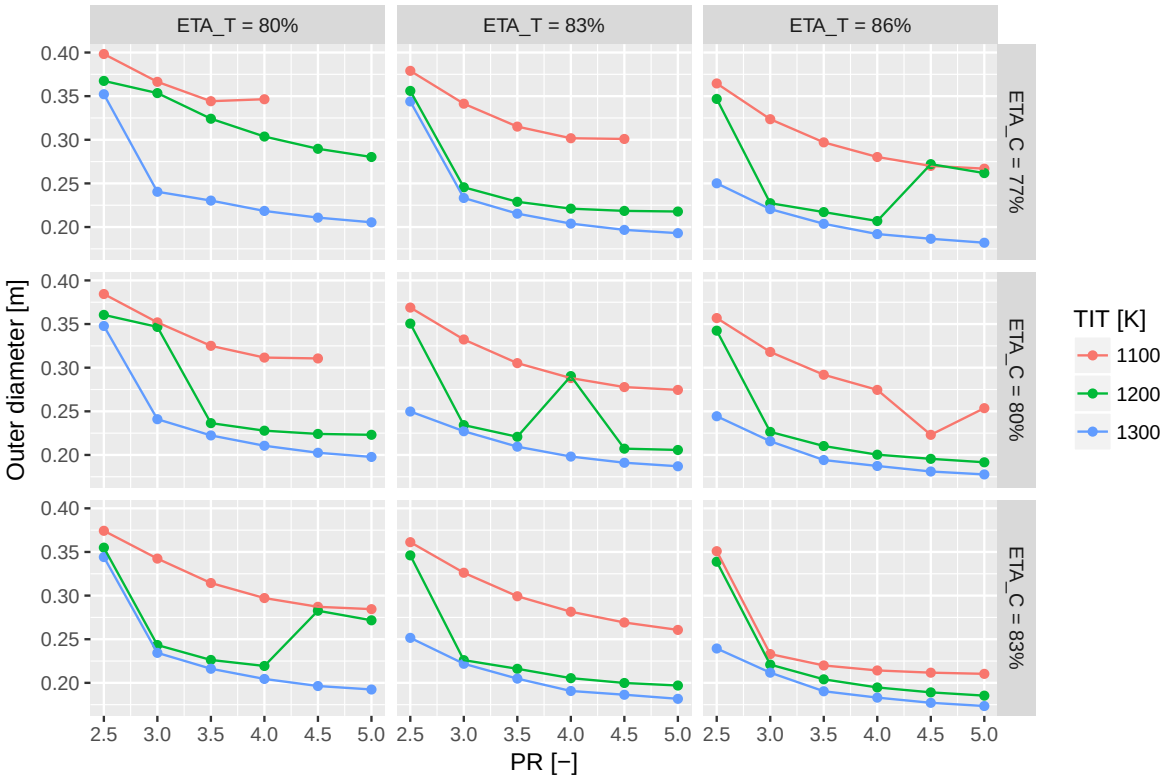

Figure 5.13: Recuperator outer diameter as a function of gas turbine cycle design parameters

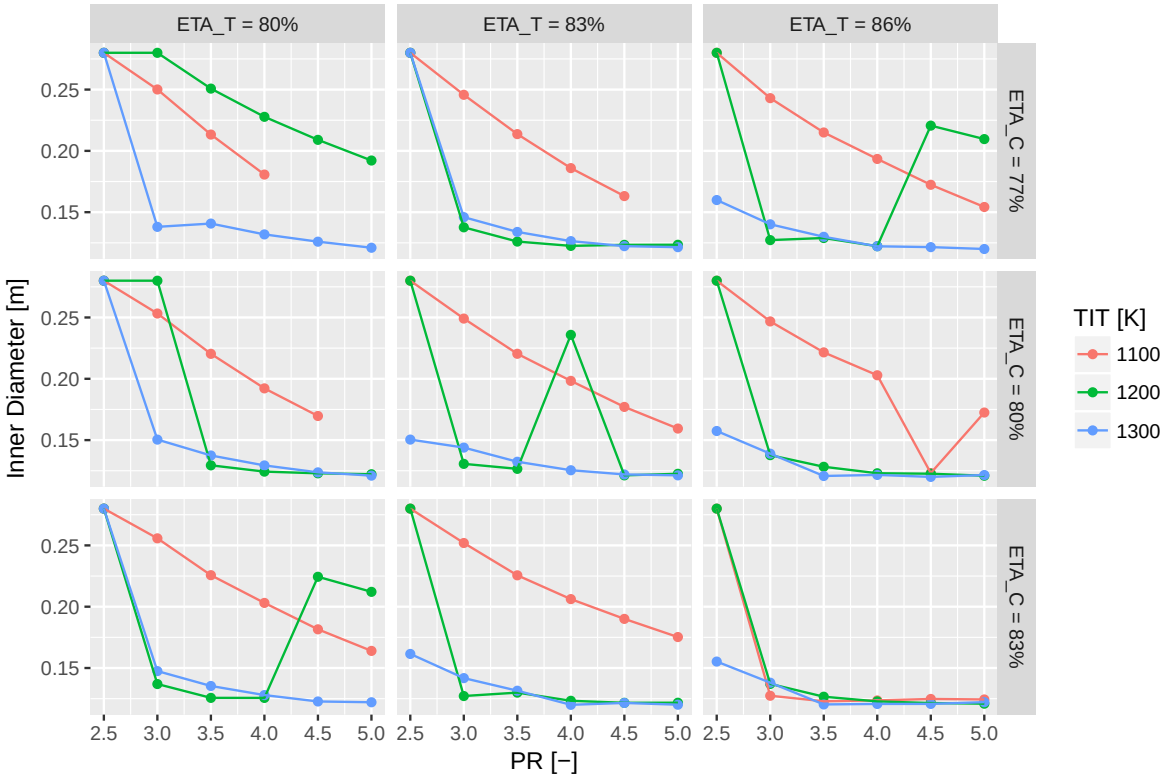

Figure 5.14: Recuperator inner diameter as a function of gas turbine cycle design parameters

Figure 5.15 shows the calculated relative price of the recuperator based on the resulting material volume,

as well as the type of material requirement based on the hot side inlet temperature. The reference value for the temperature limits of the SS347, 650 °, put forth by McDonald [21] was used to determine the material requirement for the analyzed recuperator design.

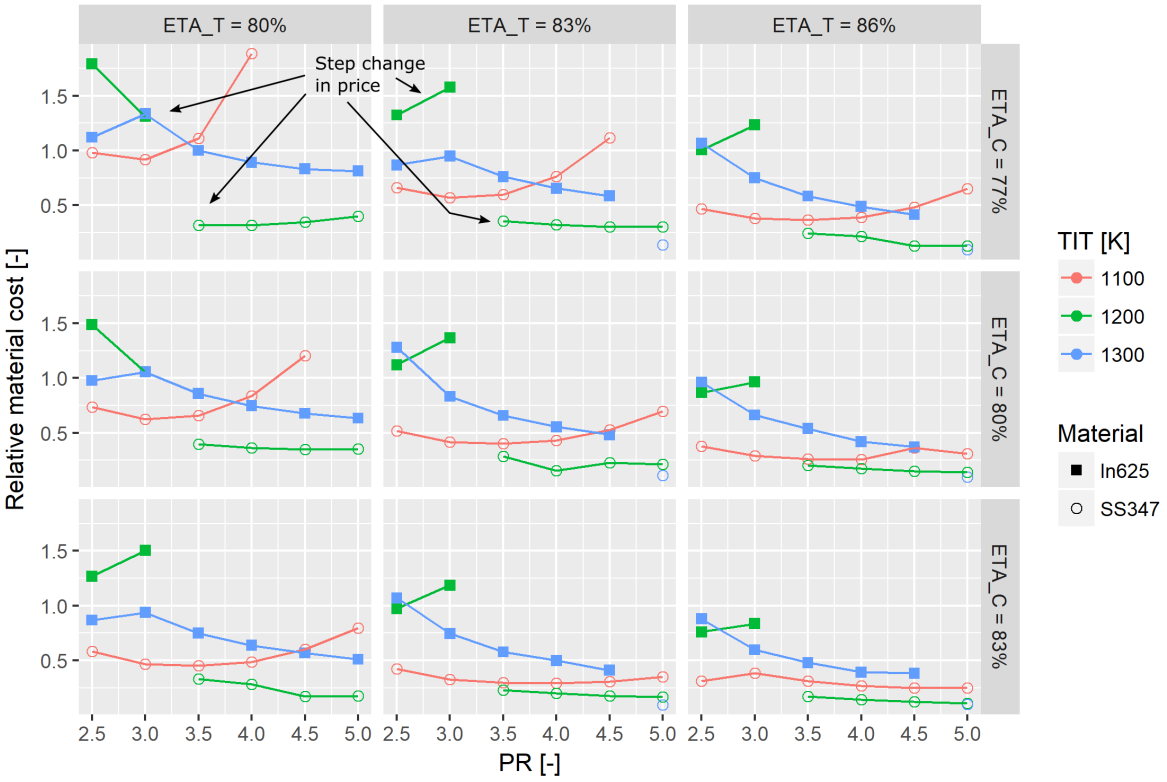

Figure 5.15: Relative material price as a function of gas turbine cycle design parameters

Important conclusions can be drawn from the influence of different design parameters in the recuperator price. The main drivers of materials costs are the selected pressure ratio and the turbine inlet temperature, due to the fact that these two parameters have the largest impact on turbine exhaust temperature. A good example of the influence of these parameters can be seen facet located in the upper left corner of Figure 5.15.

Table 5.9: Impact of pressure ratio at fixed design parameters in resulting recuperator volume and price

Pressure Ratio [-]	**Gas inlet temp.** [^{o}C]	**HEX volume** [m^3]	**Relative price** [-]
2.5	749.16	5.19	1.790
3.0	715.73	4.14	1.310
3.5	688.58	3.82	0.315
4.0	665.86	3.85	0.318
4.5	646.42	4.18	0.344
5.0	629.48	4.86	0.401
Design parameters: TIT = 1200 K, η_{comp} = 0.77, η_{turb} = 0.8, Δp_{HEX} = 0.06			

Table 5.9 shows the change in recuperator volume and recuperator relative price as a function of pressure ratio for fixed values of TIT, compressor and turbine efficiencies as well as overall pressure losses. In Table 5.9, the observed step change (highlighted in gray) in recuperator price is observed when the pressure ratio of the system is increased from 3 to 3.5. The increased pressure ratio allows to reduce the turbine exhaust temperature to a level that is compatible with the use of stainless steel.

The assumption done about the material requirements of the heat exchanger has clear limitations, since it only uses the temperature of the hot side inlet to select the recuperator material. Other important factors

come into play when determining the required material to guarantee structural integrity, such as flow pressures, thermal gradients as well as expected lifetime and number of cycles. Even though the limitations form the current assumptions are clear, it still highlights the fact that the selection of gas turbine design parameters could be driven in order to meet the required boundary conditions for applying a lower grade material such as stainless steel 347 and keep unit material costs lower.

5.3. Parametric study: heat transfer surface geometry comparison

The comparison presented in this section has two objectives: compare the characteristics of the recuperator and analyze the effect of the main design parameters when different types of heat transfer surfaces are adopted.

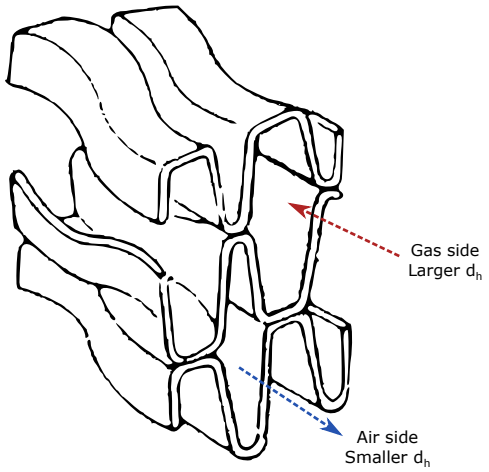

Figure 5.16: Hydraulic diameter difference in cross-wavy surfaces

The heat transfer surfaces analyzed are listed in Tables 5.4 and 5.5. It is a total of 8 different surface geometries, out of which 6 are of the cross corrugated type, while 2 are of the cross wavy type. Keep in mind that, in order to maintain consistency with the published correlations, the geometries with a CC surface are assumed to have the same hydraulic diameter on both cold and hot sides, while those with a CW surface used the same hydraulic diameter for the cold side as the CC cases (1.54 mm), while the gas side features a 42% larger hydraulic diameter (2.2 mm). This is achieved by the corrugation depth of the plate, as exemplified in Figure 5.16.

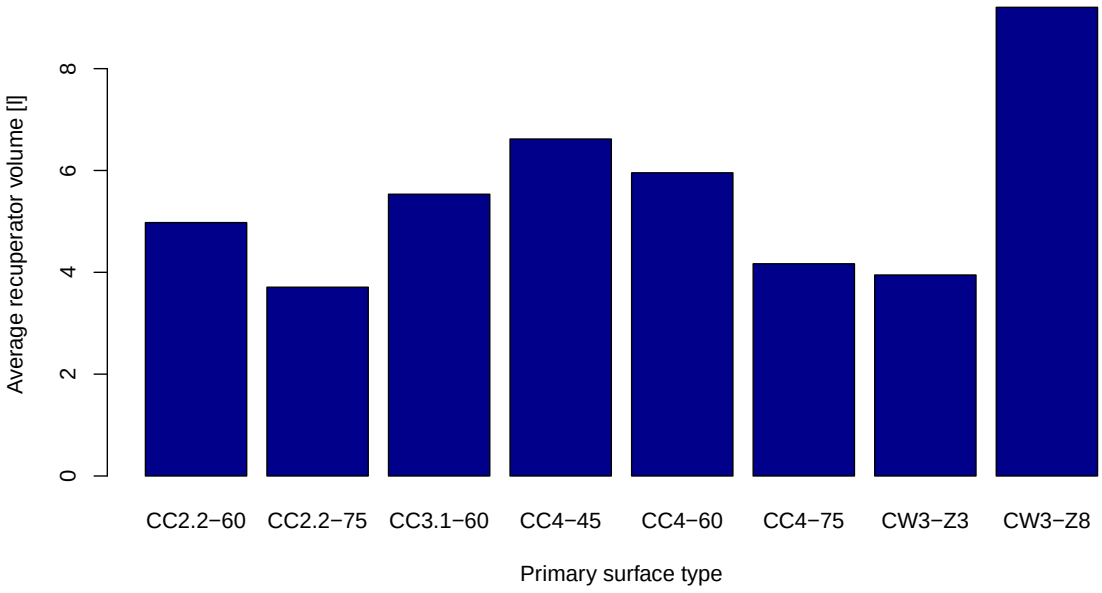

Figure 5.17: Average recuperator volume for each heat transfer surface geometry

Figure 5.17 shows the average recuperator volume for each of the heat transfer surfaces used in the analysis. From this comparison, it is clear that the type of heat transfer surface has a very large impact on the resulting recuperator geometry. Furthermore, this difference can be seen between surfaces of the same type (i.e. CW), which highlights the influence of parameters such as pitch-to-height ratio and phase angle.

Another aspect to highlight, is that a low heat transfer surface performance may lead to a design that does not meet the packaging constraints such as the limitations on outer diameter or recuperator length. Table 5.10 shows the percentage of design points that resulted in feasible recuperator design for the current set of specifications and constraints. By comparing Figure 5.17 and Table 5.10 it is clear that adoption of a heat transfer surface with a lower fluid-dynamic performance will make the design of a compact recuperator more challenging.

Table 5.10: Percentage of feasible points in design space for each surface geometry

	CC2.2-60	**CC2.2-75**	**CC3.1-60**	**CC4-45**	**CC4-60**	**CC4-75**	**CW3-Z3**	**CW3-Z8**
Feasible solutions [%]	78	69	58	47	55	59	55	19

Furthermore, the effect of main design parameters on recuperator geometry was compared for the different surface geometries. This was done in order to identify possible beneficial interactions between design parameters and different surface geometries. Figure 5.18 shows the effect of increasing turbine efficiency on recuperator volume. The Figure shows that the effect of the change in η_T is very similar in relative terms between all of the surfaces. Note that surface CW3-Z8 is not part of the plotted geometries due to the low number of feasible solutions. The same conclusions were drawn for other parameters such as TIT, compressor efficiency and overall pressure losses. These plots are shown in Appendix C. From this comparison it can be stated that the modification of design parameters to achieve a different recuperator geometry can be done using a similar approach, regardless of the type of surface being employed.

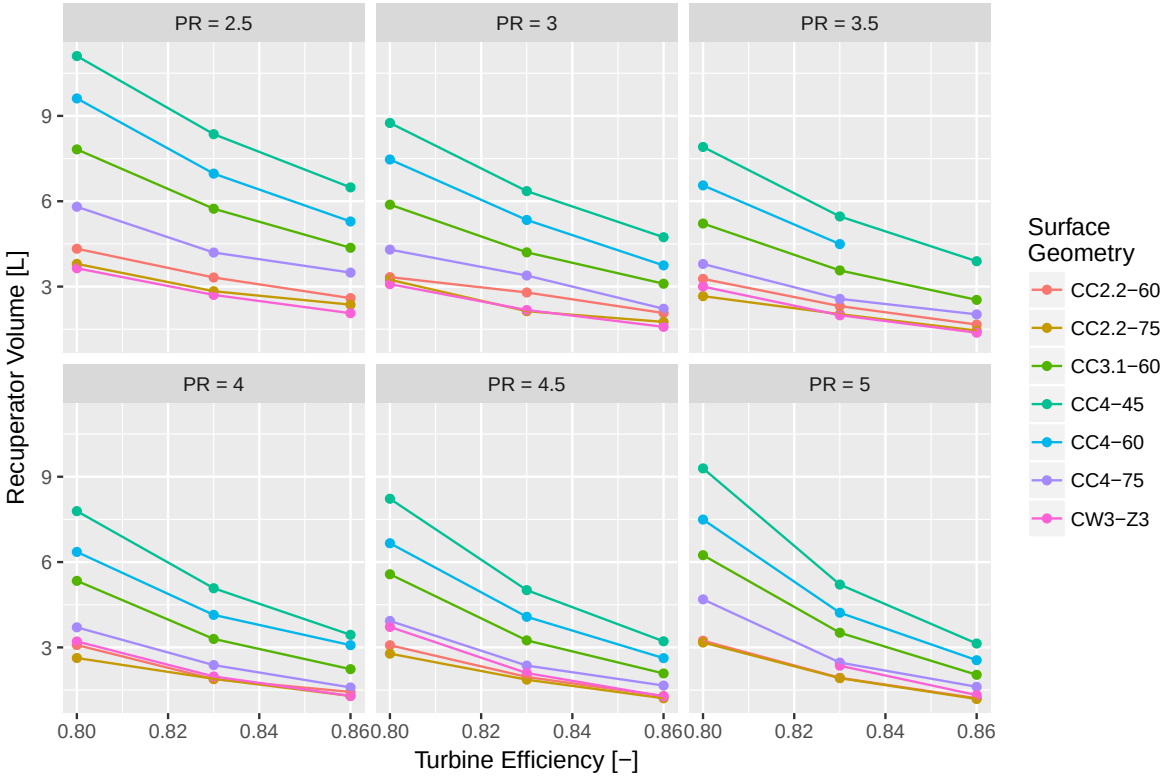

Figure 5.18: Comparison for different surface geometries of effects of modifying turbine efficiency on recuperator volume for constant $\Delta p_{total} = 0.06$, $TIT = 1200$ and $\eta_C = 0.8$

5.4. Discussion on optimal solutions in the design space

By reviewing the defined design space for the recuperator design, a large number of heat exchanger geometries has been obtained. The selection of the best gas turbine design characteristics in terms of the recuperator requirements is not trivial. In virtually all of the cases, the highest component efficiencies, turbine inlet temperature and pressure ratio lead to the smallest recuperator. This is expected from GT cycle parameters such as specific power and efficiency. In addition to that, the increase in all of this parameters simultaneously may not be achievable. The real benefit of this approach is to identify parameters that may have a large impact on the recuperator design when starting from a base design. Two examples of notable trends are discussed below:

- The cost of a recuperator can be reduced by a large margin if the required PR for obtaining temperatures compatible with lower grade materials is identified. An example of this large impact is shown in Table 5.9. The benefit of increasing PR beyond this point is negligible in comparison to the large step identified after a lower grade material is used.
- The relationship of allowable pressure loss, frontal area and volume is also interesting. The application may require a certain limitation in terms of packaging that can be achieved by increasing pressure losses. If the loss in specific power is compensated with a larger system mass flow, the resulting recuperator volume remains the same, while reducing the frontal area.
- For a given set of turbine inlet temperature and component efficiencies, an optimal pressure ratio can be identified in terms of recuperator volume

6

Investigation of fluid-dynamic performance of the selected CC plate by CFD

This chapter addresses the numerical analysis of the thermal and hydraulic performance of a heat transfer surface geometry. Section 6.1 discusses the model setup and boundary conditions for the numerical analysis. Finally Section 6.2 covers the comparison between the CFD results and the reference experimental data.

The sensitivity analysis described in Chapter 5 has shown that the most promising heat transfer surface for the recuperator is of the CC type with a pitch to height ratio of 2.2 and a phase angle of 60 degrees. However, this result strongly depends on the empirical heat transfer and pressure drop correlations available in the literature for such a type of heat transfer surface. At the current stage of the research, the validity or interpretation errors of these correlations is unknown and can be assessed only by a CFD study, such as the one here presented.

The experimental data used as a reference for the CFD study was published by Stasiek [44], who investigated the fluid-dynamic performance of channels made with corrugated plates of different shapes. The experiments were carried out in a wind tunnel, which allowed to change the inlet flow conditions to the test section. Reynolds number range covered varies from 500 to 5000. The corrugated plate forming the top part of the channel was kept at a constant temperature by a water bath. was instrumented by pressure taps to measure the pressure drop along the plate, while the temperature distribution was measured by a thermographic camera. The corrugated plates were sufficiently long in order to account for entrance effects. The published heat transfer and pressure loss correlations were generated using measurements in a section of the plates were the flow was deemed as fully developed. The corrugation phase angle was modified by changing the orientation of the bottom plate in relation to the top plate. Three values of pitch to height ratio were analyzed.

6.1. Model setup and boundary conditions

The current section describes development of the model, including the geometry, the selection and modeling of the boundary conditions.

6.1.1. Computational mesh and numerical setup

The complete heat transfer surface geometry was reduced to a periodic section, in order to decrease the computational requirements for the simulation. This assumption is in line with the observed phenomena in the reference experimental setup, which observed periodic flow behavior after a certain number of corrugations.

Figure 6.1 shows the mesh construction. The unitary cell is obtained by dividing the corrugated plates into periodic geometry sections. Then, the fluid dynamic behavior of the unitary cell can be, to a first approximation, extended to that of the whole recuperator. The inlet cells where entrance effects are observed, can then be ignored since they are a small amount compared to the number of cells where the periodic phenomenon is occurring.

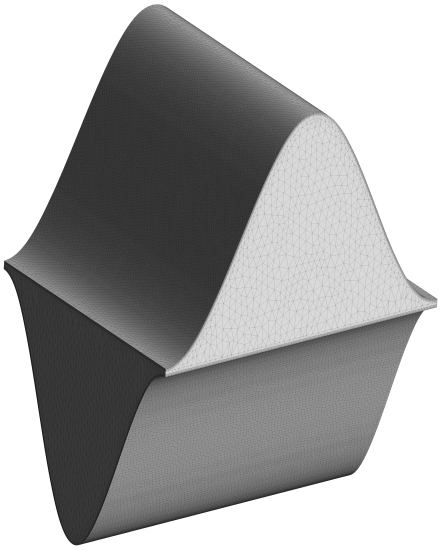

Figure 6.1: Meshed periodic element for the simulated CC 2.2-60 geometry

A grid independence study was performed at a single Reynolds number in order to understand the effect of the mesh size on the parameters of interest. Three different mesh sizes were considered, coarse grid of 875,000 elements, a medium grid of 1,250,000 and a fine grid of 1,625,000. The change in Nu and f from the coarse grid to the medium grid was 11% and 5% respectively. The change in Nu and f from the medium grid to the fine grid was 1% and 0.5% respectively. The medium grid was then deemed sufficiently accurate for the analysis.

6.1.2. Flow regime modeling

To generate the heat transfer and pressure loss correlations of the selected geometry, ANSYS CFX was used to perform the CFD study. The flow is modeled using three different approaches :

- Laminar regime (i.e. no turbulence model)
- Turbulent regime - Standard $k-\varepsilon$ model [60].
- Turbulent regime Shear Stress Transport model [61].

Since the dependency between Re number and flow regime is unknown for the geometry of interest, both the laminar and turbulent case have to be considered in the simulations. Regarding the turbulent case, two different models were used due to the high uncertainty associated with RANS simulations when modeling heat transfer in turbulent regime.

6.1.3. Boundary conditions

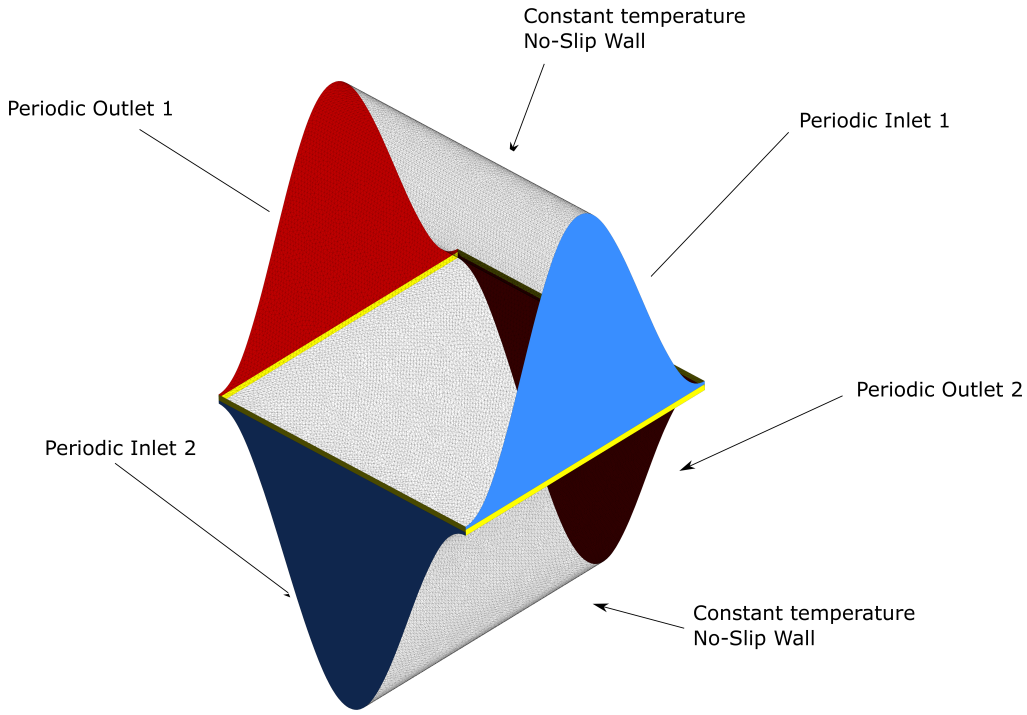

Figure 6.2: Boundary conditions of the CFD model

As shown in Figure 6.2,the boundary conditions for the model are:

- Constant temperature on the upper and lower no-slip walls. These walls represent the boundary between the hot and the cold fluid in the heat exchanger.

- Periodic inlet and outlet walls. Periodicity was defined at two inlet and outlet faces (top and bottom). Energy and pressure sinks were added to the outlet boundaries in order to define inlet and outlet as periodic surfaces.

The assumption of constant temperature on the solid walls of the simulation domain is only partially motivated by the fact that the test setup, on the side of the heat transfer surface geometry was kept at a constant temperature using a water bath. The reason is that the actual temperature distribution on the walls of the unitary cell cannot be determined without simulating at least two adjacent channels of the HEX, one with the hot stream, and the other one with the cold fluid. The computational cost of these simulations is not compatible with the resources available in this project. Due to the low velocities in the analysis, the flow was assumed as incompressible. The fluid was modeled as dry air with constant thermodynamic properties at 375K. All surfaces were assumed as smooth.

To investigate different Reynolds numbers in the simulations, the magnitude of the pressure sink at the boundaries was varied. This results in an increase of the mean flow velocity through the unitary cell. 6 different magnitudes of pressure sinks were used to obtain a range of Reynolds numbers from approximately from 200 to a 1000. Fixed magnitudes for the pressure sinks where used, but the resulting Re varied slightly between the different model setups. The small difference is noticeable when the results are compared in Figures 6.3 and 6.4 (Re values in the x-axis are slightly different.)

6.2. Heat transfer surface performance

Figures 6.4 and 6.3 show the comparison of the resulting heat transfer and pressure loss numerical predictions with the correlation obtained from the experimental data.

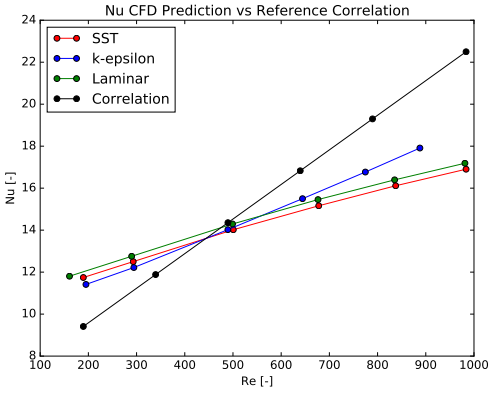

Figure 6.3: Comparison of predicted Nu versus the reference correlation

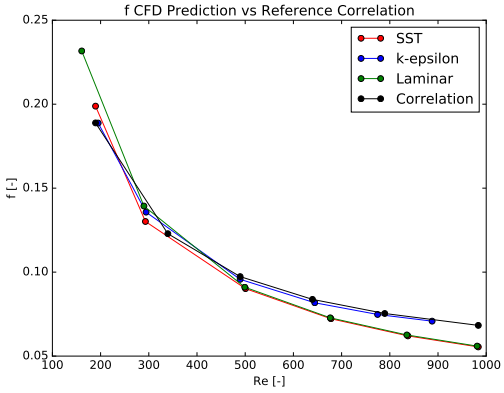

Figure 6.4: Comparison of predicted f versus the reference correlation

The relative difference of between the numerical simulation and reference data is summarized below:

Table 6.1: Resulting errors of CFD analysis vs experimental correlation

	k-epsilon		**SST**		**Laminar**	
	Min Re	**Max Re**	**Min Re**	**Max Re**	**Min Re**	**Max Re**
Nu error	0.168	-0.168	0.199	-0.331	0.243	-0.307
f error	0.022	-0.008	0.050	-0.231	0.070	-0.222

From Figure 6.3 it can be seen that all of the numerical results show a different with Re number with respect to the reference experimental data. $k-\varepsilon$ model exhibits the highest slope of the Nu versus Reynolds number. It can also be observed that Nu is over-predicted at low Re, while it is underpredicted at high Re. The laminar simulation shows a very similar behavior to the SST model, which is explained by the $k-\omega$ formulation used by the SST model. Regarding the friction factor, all the simulation setups show a better prediction at low Reynolds numbers, while the error starts to increase with higher Re.

By analyzing both the accuracy of the heat transfer and pressure loss predictions, a number of hypothesis for the causes of the discrepancies can be proposed. The fact that the pressure loss predictions are accurate at low Reynolds numbers may suggest that the flow is fully laminar at those conditions. This is also supported by the similar behavior of the laminar and turbulence model setups. At the higher range of Reynolds numbers analyzed, the pressure loss is underpredicted, which may suggest that the flow is transitional.

None of the simulation setups shows very good agreement with the reference data. This could indicate that some of the assumptions taken when defining the model boundary conditions, do not represent well the actual conditions along the heat transfer surface. It is worth noting that in published research on numerical simulation of heat transfer surfaces [36], a discrepancy between experiments and simulations is often observed regardless of the turbulence modeling and boundary condition selected.

Finally, it is important to stress that the largest discrepancies between the simulations and experimental correlation occur at the lower and upper end of the analyzed Reynolds number ranges. The median Reynolds number value for all the heat exchanger sizing analysis is 320 and 780 for the air and gas sides respectively. Even though the numerical analysis does not provide highly accurate predictions, the discrepancy with the experimental correlation remains small, thus indicating indicate that this setup could be used to quantify the performance of new geometries.

7

Summary and conclusions

The objective of this work was the preliminary design of a recuperator for a range extender for a hybrid electric vehicle (HEV), based on a small-scale recuperated gas turbine. Besides demonstrating that feasible solutions within the delimited design space exist, the design effort highlighted the importance of the interaction of the performance targets, gas cycle parameters and required recuperator geometry.

After reviewing a comprehensive list of publication covering the development of small scale gas turbine recuperators, a base configuration for the recuperator was identified. The selection of these design features is key to achieving the particular targets of a low-cost lightweight recuperator for a micro gas turbine for use in range extended vehicles. This is a primary surface HEX with an annular structure which can be subdivided in 3 main sections: 2 with a cross-flow arrangement and a main one of the counterflow type.

After the selection of the base configuration a sizing model, which was validated using the performance data of a gas turbine recuperator featuring a topology similar to that considered in the present study. Even though some information about the heat transfer surface geometry was missing from the reference data, the developed model appears to be sufficiently accurate for a preliminary design. The model was then used to illustrate that a number of recuperator geometries were feasible within the analyzed design space of gas turbine parameters and geometric constraints. Furthermore, a sensitivity analysis was performed by varying the main design parameters of the gas turbine cycle. The results indicate that a true optimization of the system requires an integrated design and simultaneous optimization of the gas cycle and its components. The analysis shows also that increasing the specific power or the simple cycle efficiency lead to smaller and lighter recuperator. It was also clear that the characteristics of the selected heat transfer surface have a very large impact on the resulting volume of the recuperator. A difference between surface geometry sensitivity to cycle design parameters was not observed in the generated recuperator designs. The parametric analysis underlined the importance of integral design of a recuperator, by showing examples of small (or even counter intuitive) changes in GT design parameters that have a large beneficial impact on recuperator geometry and cost.

Finally, a CFD study was performed to verify that the reliability of the heat transfer and pressure drop correlations for the CC surface that appears to have the most promising performance. The predictions of pressure loss show high agreement with the experimental correlation if Reynolds number is below 500, while a discrepancy as high as 23% is found for a Reynolds number of 1000. This may indicate that the flow is showing becoming transitional. The trend of the Nu vs Re predicted by CFD has a weaker dependency on the Re, if compared to that of the empirical correlation. This suggests that the chosen boundary conditions and model setup are not fully representative of the actual conditions in the heat transfer device.

7.1. Answers to the initial research questions

1.- Which are heat exchanger topologies suitable for the recuperator?

From the different concepts reviewed in the literature study, it is clear that a primary surface recuperator with an annular configuration is the most promising solution to fulfill the design requirements of the system.

2.- What is the required size of the recuperator for a 30kW range extender with an efficiency of 30%?

When a set of state of the art GT design parameters is implemented, it is shown that a recuperator with an effectiveness of 85.6% and an overall relative pressure loss of 3% is a feasible design within the constraints of the application at hand.

3.- What is the impact of gas turbine cycle parameters on the recuperator geometry?

The impact of the different gas turbine design parameters can be summarized by using two intermediate cycle parameters: specific power ans simple cycle efficiency. By using a fixed power output and target system efficiency, the required heat exchanger effectiveness as well as operating mass flow changed with every set of gas turbine design parameters. Maximizing specific power results in a reduction of recuperator volume through means of lowering the mass flow of the system. On the other hand, the increased simple cycle efficiency resulted in a lower requirement for recuperator effectiveness in order to reach the same fixed system efficiency. The main challenge in terms of heat exchanger design when maximizing these parameters, is the hot side inlet temperature. A high gas side inlet temperature leads to higher grade materials, which are not beneficial for the low cost objectives of the GTRE concept.

4.- Are the correlations used in the heat exchanger sizing reliable?

The numerical analysis performed for one of the heat transfer surface geometries shows reasonable agreement between the reference experimental correlation and the predicted performance. Pressure loss predictions were fairly accurate for low Reynolds numbers range, showing a larger discrepancy at higher Reynolds numbers. Improving the CFD model may result in increased confidence in both the experimental correlation and a refined numerical approach.

7.2. Recommendations for further research

Some future steps in the development of a GTRE recuperator identified in this project are the following:

- Coupling the recuperator sizing model with GT design methods that successfully capture the interaction between parameters such as mass flow, pressure ratio and isentropic efficiency.
- The development of reliable heat transfer and pressure loss correlations for surface geometries is key to increase the accuracy of the preliminary sizing model. The current project used published correlations obtained through experiments, but the development efforts would benefit from a test setup to obtain correlations for any surface geometry.
- Validation of numerical model may open the possibility of geometry optimization that could lead to significant improvements.
- Particular attention should be devoted to develop a recuperator concept that is compatible with large volume manufacturing which is key to the successful deployment of the present GTRE recuperator to the automotive market.
- Alternative approaches to heat exchanger production such as ceramic cores or additive manufacturing were not the focus of this work, mainly due to the uncertainties related to their application in a low-cost, large quantity automotive environment. Special attention should be placed in these technologies in case a substantial development lowers production costs.

A

Description of method to obtain plate involute profile

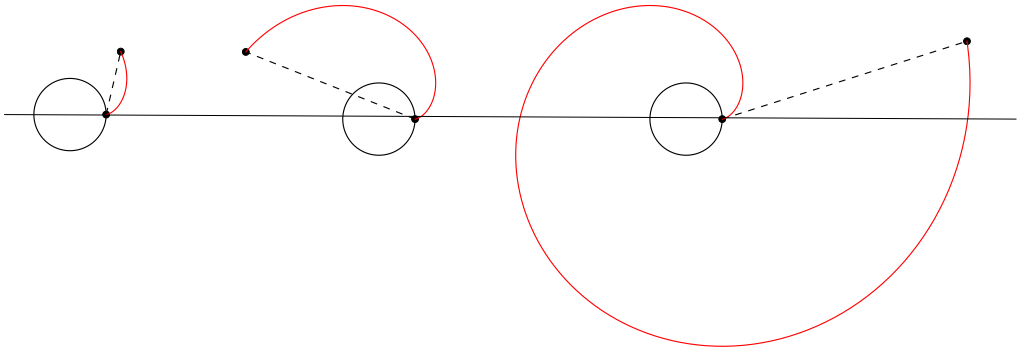

Figure A.1: Involute of a circle

Since the unitary cells of the heat exchanger are curved (seen in Figure 3.1), an assumption has to be done in order to obtain the recuperator outer diameter. A defined curve profile is needed in order to translate the dimensions of the flat unitary plate into the final annular construction. The curve chosen to define this profile is the involute (also known as evolvent) of a circle. An involute is defined as a curve obtained from another defined curve by attaching a string to it and tracing its free end as it is unwound. The equations describing the curve of the involute are:

$$x = r(\cos\theta + \theta\sin\theta) \tag{A.1}$$

$$y = r(\sin\theta - \theta\cos\theta) \tag{A.2}$$

$$A_{inv} = \frac{r}{2}\theta^2 \tag{A.3}$$

where A is the arc length of the involute curve, and r is the radius of the inner circle with diameter d_i used in the profile of the involute. By establishing the length of the flat unitary cell, the x and y coordinates can be obtained, which leads to determining the outer diameter of the annular heat exchanger. The outer diameter d_o of the resulting recuperator is given by:

$$d_o = d_i + 2\sqrt{x^2 + y^2} \tag{A.4}$$

B

Table of reported performance data used for model validation

The following data used for model validation purposes was reported by Capstone in a DOE project report. [8]

No. of plates	**Fins/Meter [-]**	**C [m]**	**B [m]**	**A [m]**	**ID [m]**	**OD [m]**	**Reference Δp [%]**	**Reference ε [%]**
223	511.8	0.265	0.222	0.041	0.449	0.800	2.32	89.1
223	551.2	0.258	0.201	0.052	0.449	0.793	2.32	89.1
223	590.6	0.255	0.180	0.062	0.449	0.791	2.32	89.1
223	657.5	0.255	0.148	0.079	0.449	0.791	2.32	89.1
237	511.8	0.248	0.224	0.040	0.477	0.813	2.32	89.1
237	551.2	0.241	0.202	0.051	0.477	0.807	2.32	89.1
237	590.6	0.239	0.180	0.062	0.477	0.805	2.32	89.1
237	657.5	0.239	0.148	0.078	0.477	0.805	2.32	89.1
250	511.8	0.233	0.226	0.040	0.503	0.826	2.32	89.1
250	551.2	0.227	0.203	0.051	0.503	0.820	2.32	89.1
250	590.6	0.226	0.181	0.062	0.503	0.819	2.32	89.1
250	657.5	0.226	0.149	0.078	0.503	0.819	2.32	89.1
260	511.8	0.223	0.227	0.039	0.523	0.837	2.32	89.1
260	551.2	0.218	0.204	0.051	0.523	0.831	2.32	89.1
260	590.6	0.216	0.182	0.062	0.523	0.830	2.32	89.1
260	657.5	0.217	0.149	0.078	0.523	0.831	2.32	89.1
270	511.8	0.214	0.228	0.039	0.544	0.848	2.32	89.1
270	551.2	0.209	0.204	0.050	0.544	0.843	2.32	89.1
270	590.6	0.208	0.182	0.062	0.544	0.841	2.32	89.1
270	657.5	0.209	0.149	0.078	0.544	0.842	2.32	89.1

C

Additional plots of main design parameter effects for different surface geometries

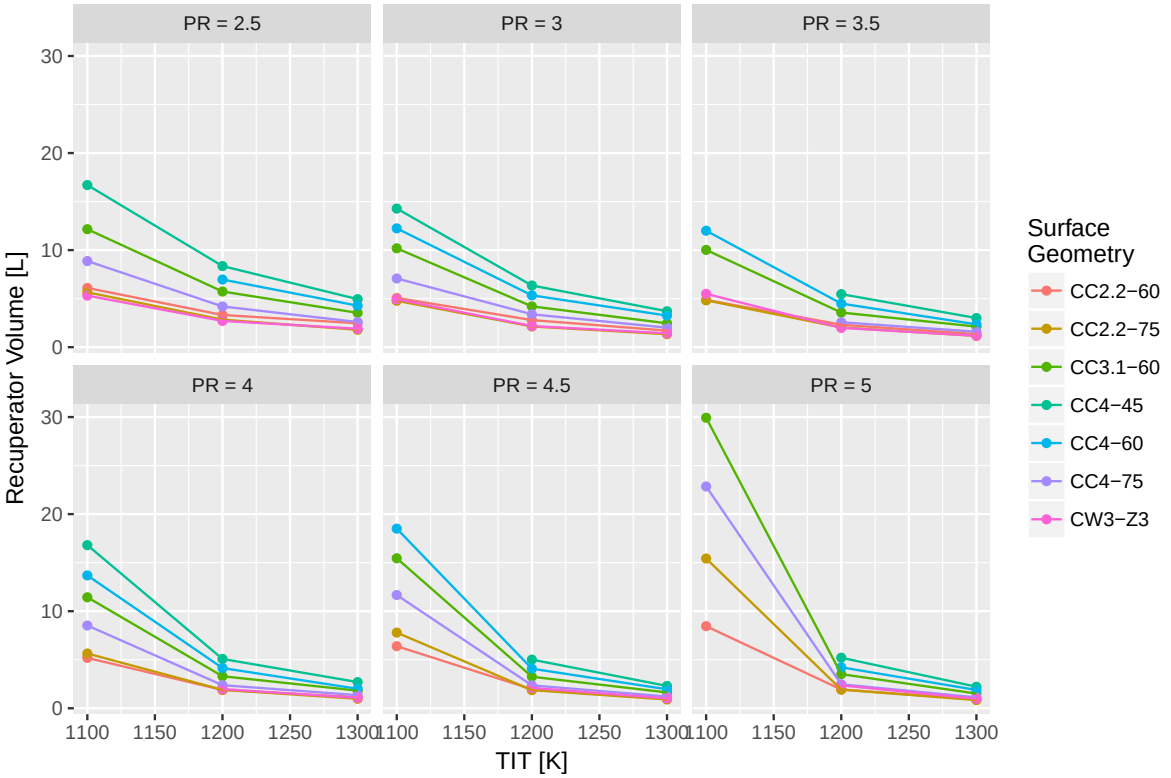

Figure C.1: Comparison for different surface geometries of effects of modifying turbine inlet temperature on recuperator volume for constant $\Delta p_{total} = 0.06$, $\eta_T = 0.83$ and $\eta_C = 0.8$

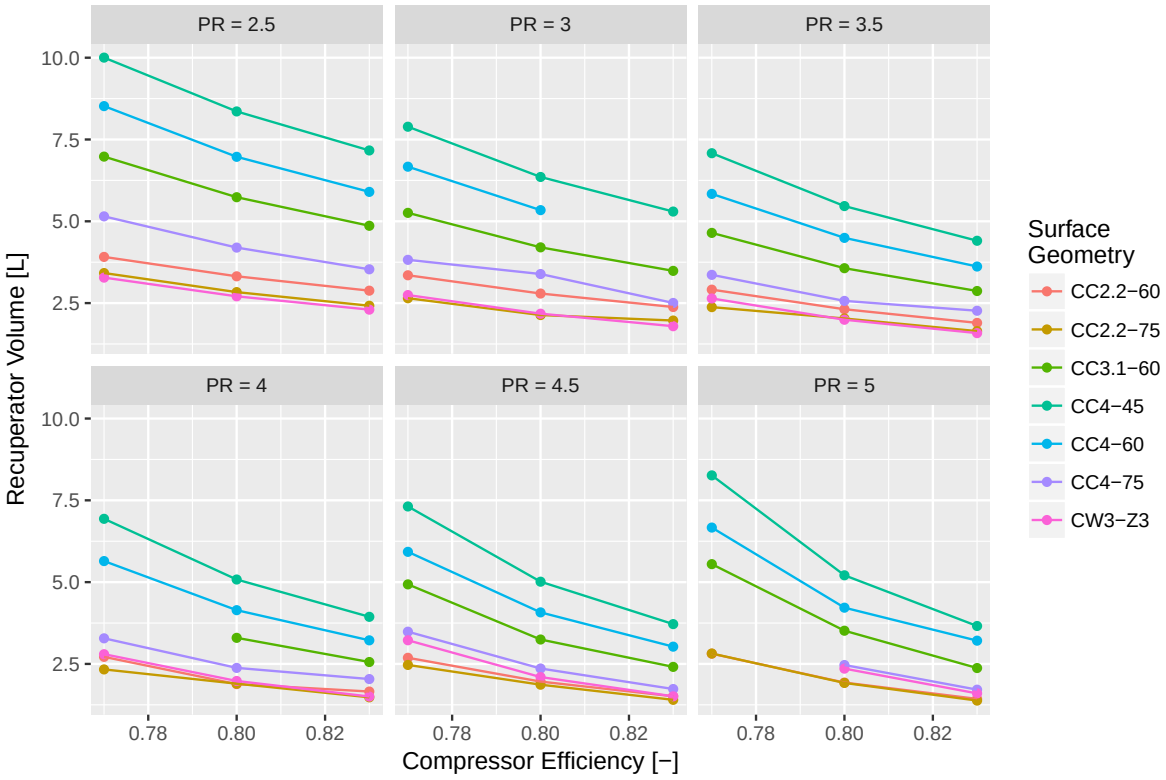

Figure C.2: Comparison for different surface geometries of effects of modifying compressor efficiency on recuperator volume for constant $\Delta p_{total} = 0.06$, $\eta_T = 0.83$ and $TIT = 1200$

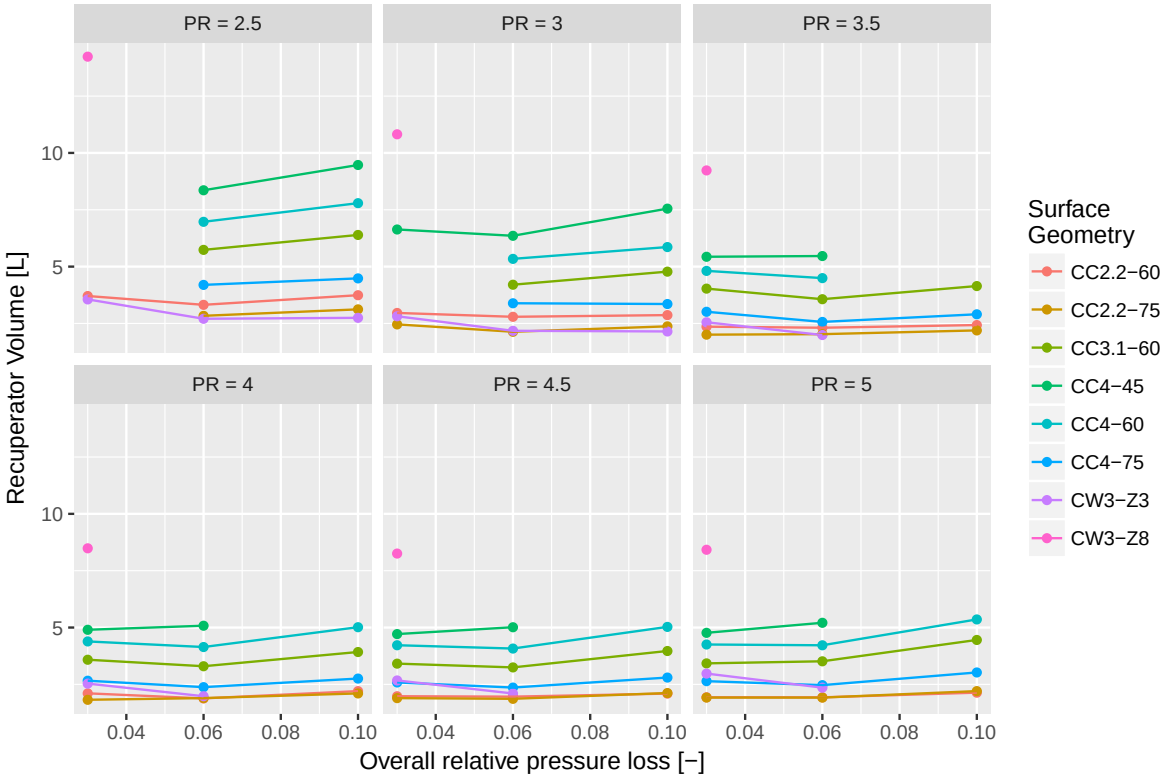

Figure C.3: Comparison for different surface geometries of effects of modifying overall pressure loss on recuperator volume for constant $TIT = 1200$, $\eta_T = 0.83$ and $\eta_C = 0.8$

Bibliography

[1] Amsterdam Roundtables Foundation, "Electric vehicles in europe: gearing up for a new phase?" 2014.

[2] M. Coffman, P. Bernstein, and S. Wee, "Factors affecting ev adoption: a literature review and ev forecast for hawaii." Hawaii, 2015.

[3] Wang Q., Zeng M., Ma T., Du X., and Yang J., "Recent development and application of several high-efficiency surface heat exchangers for energy conversion and utilization," *Applied Energy*, vol. 135.

[4] V. Kadambi, S. Etemad, and L. Russo, "Primary Surface Heat Exchanger for a Ground Vehicle Gas Turbine," *SAE Technical Paper*.

[5] E. L. Parsons, "Development, Fabrication and Application of a Primary Surface Gas Turbine Recuperator," *SAE Technical Paper*.

[6] M. Ward and L. Holman, "Primary Surface Recuperator for High Performance Prime Movers," *SAE Technical Paper*.

[7] B. Treece, P. Vessa, and R. McKeirnan, "Microturbine Recuperator Manufacturing and Operating Experience," in *Turbo Expo 2002, Volume 1*. ASME International, 2002.

[8] Capstone Turbine Corporation. (2008) Final Technical Report: Advanced Micro Turbine System. [Online]. Available: https://www.osti.gov/scitech/servlets/purl/975026

[9] J. I. Oswald, D. A. Dawson, and L. A. Clawley, "A New Durable Gas Turbine Recuperator," in *Turbo Expo 1999, Volume 2*. ASME International, jun 1999.

[10] H. Antoine and L. Prieels, "The ACTE Spiral Recuperator for Gas Turbine Engines," in *Turbo Expo 2002, Volume 1*. ASME International, 2002.

[11] G. Lagerström and M. Xie, "High Performance and Cost Effective Recuperator for Micro-Gas Turbines," in *Turbo Expo 2002, Volume 1*. ASME International, 2002.

[12] C. F. McDonald, "Low-cost compact primary surface recuperator concept for microturbines," *Applied Thermal Engineering*, vol. 20, no. 5.

[13] J. Kesseli, T. Wolf, J. Nash, and S. Freedman, "Micro, Industrial, and Advanced Gas Turbines Employing Recuperators," in *Turbo Expo 2003, Volume 3*. ASME International, 2003.

[14] R. A. Proeschel, "Proe 90™Recuperator for Microturbine Applications," in *Turbo Expo 2002, Volume 1*. ASME International, 2002.

[15] A. Clay and G. D. Tansley, "Exploration of a simple, low cost, micro gas turbine recuperator solution for a domestic combined heat and power unit," *Applied Thermal Engineering*, vol. 31.

[16] B.-J. Tsai and Y. Wang, "A novel Swiss-Roll recuperator for the microturbine engine," *Applied Thermal Engineering*, vol. 29.

[17] B. Zohuri, "Heat exchanger types and classifications," in *Compact Heat Exchangers*. Springer, 2017, pp. 19–56.

[18] R. K. Shah and D. P. Sekulic, "Fundamentals of heat exchanger design," Hoboken, NJ, 2003. [Online]. Available: http://dx.doi.org/10.1002/9780470172605

[19] S. Freund and S. Kabelac, "Investigation of local heat transfer coefficients in plate heat exchangers with temperature oscillation ir thermography and cfd," *International Journal of Heat and Mass Transfer*, vol. 53, no. 19, pp. 3764–3781, 2010.

[20] E. Utriainen and B. Sundén, "A numerical investigation of primary surface rounded cross wavy ducts," *Heat and Mass Transfer*, vol. 38, no. 7, pp. 537–542, Aug. 2002. [Online]. Available: https://doi.org/10.1007/s002310100243

[21] C. F. McDonald, "Recuperator considerations for future higher efficiency microturbines," *Applied Thermal Engineering*, vol. 23, no. 12.

[22] G. Nellis and S. Klein, *Heat Transfer*. Cambridge: Cambridge University Press, 2012.

[23] E. Utriainen and B. Sundén, "Evaluation of the cross corrugated and some other candidate heat transfer surfaces for microturbine recuperators," *Journal of Engineering for Gas Turbines and Power*, vol. 124, no. 3, pp. 550–560, 2002.

[24] C. Y. Ho and T. K. Chu, "Electrical resistivity and thermal conductivity of nine selected aisi stainless steels," Tech. Rep., 1977.

[25] K. D. Maglic, N. L. Perovic, and A. M. Stanimirovic, "Calorimetric and transport properties of Zircalloy 2, Zircalloy 4, and Inconel 625," *International journal of thermophysics*, vol. 15, no. 4, 1994.

[26] Organisation for Economic Cooperation and Development - International Energy Agency, "Global ev outlook 2017 : Two million and counting." 2017. [Online]. Available: http://dx.doi.org/10.1787/9789264278882-en

[27] J. Stark, R. Klementschitz, C. Link, C. Weiss, B. Chlond, N. Mallig, R. Trigui, T. Franke, M. Baumann, L. Brethauer, P. Jochem, and M. Gunther, "Electric vehicles with range extenders: Evaluating the contribution to the sustainable development of metropolitan regions," *J. Urban Plann. Dev. Journal of Urban Planning and Development*, vol. 144, no. 1, 2018.

[28] C. F. McDonald and C. Rodgers, "Small recuperated ceramic microturbine demonstrator concept," *Applied Thermal Engineering*, vol. 28, no. 1.

[29] K. Darrow, R. Tidball, J. Wang, and A. Hampson, "Catalog of chp technologies," *US Environmental Protection Agency, Washington, DC*, p. 2, 2015.

[30] A. S. Kosoi, O. S. Popel', V. N. Beschastnykh, Y. A. Zeigarnik, and M. V. Sinkevich, "Small gas-turbine units for the power industry: Ways for improving the efficiency and the scale of implementation," *Thermal Engineering*, vol. 64, no. 10, pp. 723–728, Oct 2017. [Online]. Available: https://doi.org/10.1134/S0040601517100068

[31] D. J. Gelman and T. L. Perrot, "Advanced heat engines for range extender hybrid vehicles," *SAE Technical Paper*, 1993.

[32] C. F. McDonald, "Gas turbine recuperator renaissance," *Heat Recovery Systems and CHP*, vol. 10, no. 1.

[33] D. G. Wilson, "Regenerative Heat Exchangers for Microturbines and an Improved Type," in *Turbo Expo 2003, Volume 3*. ASME International, 2003.

[34] D. Wilson, "Low-leakage and high-flow regenerators for gas turbine engines," *Proceedings of the Institution of Mechanical Engineers, Part A: Journal of Power and Energy*, vol. 207, no. 3, pp. 195–202, 1993.

[35] C. Soares, *Microturbines*. Amsterdam; Boston: Elsevier/Butterworth-Heinemann, 2007.

[36] G. Xiao, T. Yang, H. Liu, D. Ni, M. L. Ferrari, M. Li, Z. Luo, K. Cen, and M. Ni, "Recuperators for micro gas turbines: A review," *Applied Energy*, vol. 197, pp. 83–99, 2017.

[37] C. F. McDonald, "Recuperator Development Trends for Future High Temperature Gas Turbines," in *IGTI 1975 , Volume 1A*. ASME International, mar 1975.

[38] H. F. Jen, "Primary Surface Recuperator for Vehicular Gas Turbine," *SAE Technical Paper*.

[39] Capstone Turbine Corporation. (2015) Combined heat and power systems technology development and demonstration: 370 kw high efficiency microturbine. [Online]. Available: https://www.osti.gov/servlets/purl/1224801

[40] H. Antoine and L. Prieels, "Aero-Thermal Optimisation of a Spiral Primary Surface Recuperator: Modelling and Testing," in *Turbo Expo 2007, Volume 3*. ASME International, 2007.

[41] S. Förster and M. Kleemann, "Compact Metallic and Ceramic Recuperators for Gas Turbines," in *IGTI 1978, Volume 1A*. ASME International, apr 1978.

[42] H.-Y. Shih and Y.-C. Huang, "Thermal design and model analysis of the Swiss-roll recuperator for an innovative micro gas turbine," *Applied Thermal Engineering*, vol. 29.

[43] L. Zhang and D. Che, "Turbulence models for fluid flow and heat transfer between cross-corrugated plates," *Numerical Heat Transfer, Part A: Applications*, vol. 60, no. 5, pp. 410–440, 2011.

[44] J. Stasiek, M. Collins, M. Ciofalo, and P. Chew, "Investigation of flow and heat transfer in corrugated passages - i. experimental results," *International Journal of Heat and Mass Transfer*, vol. 39, no. 1, pp. 149–164, 1996.

[45] M. Ciofalo, J. Stasiek, and M. Collins, "Investigation of flow and heat transfer in corrugated passages - ii. numerical simulations," *International Journal of Heat and Mass Transfer*, vol. 39, no. 1, pp. 165–192, 1996.

[46] M. P. Bond, "Plate heat exchangers for effective heat transfer," *Chemical Engineer*, pp. 162–7, 1981.

[47] A. Muley and R. M. Manglik, "Experimental study of turbulent flow heat transfer and pressure drop in a plate heat exchanger with chevron plates," *Journal of Heat Transfer*, vol. 121, no. 1, pp. 110–117, Feb. 1999. [Online]. Available: http://dx.doi.org/10.1115/1.2825923

[48] J. A. Stasiek, "Experimental studies of heat transfer and fluid flow across corrugated-undulated heat exchanger surfaces," *International Journal of Heat and Mass Transfer*, vol. 41, no. 6-7, pp. 899–914, 1998.

[49] E. Utriainen and B. Sundén, "Numerical analysis of a primary surface trapezoidal cross wavy duct," *International Journal of Numerical Methods for Heat & Fluid Flow*, vol. 10, no. 6, pp. 634–648, 2000.

[50] E. Utriainen and B. Sunden, "A Comparison of Some Heat Transfer Surfaces for Small Gas Turbine Recuperators," in *Turbo Expo 2001, Volume 3*. ASME International, jun 2001.

[51] A. Traverso and A. F. Massardo, "Optimal design of compact recuperators for microturbine application," *Applied Thermal Engineering*, vol. 25.

[52] W. J. Matthews, K. L. More, and L. R. Walker, "Primary surface recuperator alloy oxidation: A comparison of accelerated engine testing to field operation," *Journal of Engineering for Gas Turbines and Power*, vol. 133, no. 4, p. 042302, 2011.

[53] J. E. Grady and NASA Glenn Research Center, "A fully nonmetallic gas turbine engine enabled by additive manufacturing," 2015. [Online]. Available: http://purl.fdlp.gov/GPO/gpo59971

[54] W. M. Kays and A. L. London, *Compact Heat Exchangers*. Krieger Pub. Co., oCLC: 421526609.

[55] J. N. Sweet, E. P. Roth, and M. Moss, "Thermal conductivity of inconel 718 and 304 stainless steel," *International journal of thermophysics*, vol. 8, no. 5, pp. 593–606, 1987.

[56] A. B. Lambe and J. R. R. A. Martins, "Extensions to the design structure matrix for the description of multidisciplinary design, analysis, and optimization processes," *Structural and Multidisciplinary Optimization*, vol. 46, no. 2, pp. 273–284, 2012.

[57] D. Kraft, "A software package for sequential quadratic programming," *Forschungsbericht- Deutsche Forschungs- und Versuchsanstalt fur Luft- und Raumfahrt*, 1988.

[58] E. Jones, T. Oliphant, and P. Peterson, "SciPy: open source scientific tools for Python," 2014.

[59] T. Ma, L.-x. Du, N. Sun, M. Zeng, B. Sundén, and Q.-w. Wang, "Experimental and numerical study on heat transfer and pressure drop performance of cross-wavy primary surface channel," *Energy Conversion and Management*, vol. 125, pp. 80–90, 2016.

[60] W. Jones and B. Launder, "The prediction of laminarization with a two-equation model of turbulence," *International journal of heat and mass transfer*, vol. 15, no. 2, pp. 301–314, 1972.

[61] F. R. Menter, "Two-equation eddy-viscosity turbulence models for engineering applications," *AIAA journal*, vol. 32, no. 8, pp. 1598–1605, 1994.